



8-2010

Structural and metamorphic evolution of the west-central Newton window, eastern Inner Piedmont, Burke, Catawba, and Lincoln Counties, North Carolina

William George Gilliam
wgillia1@utk.edu

Follow this and additional works at: https://trace.tennessee.edu/utk_gradthes

 Part of the [Tectonics and Structure Commons](#)

Recommended Citation

Gilliam, William George, "Structural and metamorphic evolution of the west-central Newton window, eastern Inner Piedmont, Burke, Catawba, and Lincoln Counties, North Carolina. " Master's Thesis, University of Tennessee, 2010.
https://trace.tennessee.edu/utk_gradthes/798

This Thesis is brought to you for free and open access by the Graduate School at TRACE: Tennessee Research and Creative Exchange. It has been accepted for inclusion in Masters Theses by an authorized administrator of TRACE: Tennessee Research and Creative Exchange. For more information, please contact trace@utk.edu.

To the Graduate Council:

I am submitting herewith a thesis written by William George Gilliam entitled "Structural and metamorphic evolution of the west-central Newton window, eastern Inner Piedmont, Burke, Catawba, and Lincoln Counties, North Carolina." I have examined the final electronic copy of this thesis for form and content and recommend that it be accepted in partial fulfillment of the requirements for the degree of Master of Science, with a major in Geology.

Robert D. Hatcher, Jr., Major Professor

We have read this thesis and recommend its acceptance:

Christopher Fedo, Theodore Labotka

Accepted for the Council:

Carolyn R. Hodges

Vice Provost and Dean of the Graduate School

(Original signatures are on file with official student records.)

To the Graduate Council:

I am submitting herewith a thesis written by William George Gilliam entitled "Structural and metamorphic evolution of the west-central Newton window, eastern Inner Piedmont, Burke, Catawba, and Lincoln Counties, North Carolina." I have examined the final electronic copy of this thesis for form and content and recommend that it be accepted in partial fulfillment of the requirements for the degree of Master of Science, with a major in Geology.

Robert D. Hatcher, Jr.

Major Professor

We have read this thesis
and recommend its acceptance:

Christopher Fedo

Committee member

Theodore Labotka

Committee member

Accepted for the Council:

Carolyn R. Hodges

Vice Provost and Dean of the Graduate School

**STRUCTURAL AND METAMORPHIC EVOLUTION OF THE WEST-
CENTRAL NEWTON WINDOW, EASTERN INNER PIEDMONT, BURKE,
CATAWBA, AND LINCOLN COUNTIES, NORTH CAROLINA**

A Thesis

Presented for the

Masters of Science

Degree

The University of Tennessee, Knoxville

William G. Gilliam

August 2010

DEDICATION

This thesis is dedicated to my grandfather,
William Frank Gilliam.

ACKNOWLEDGMENTS

Completion of this thesis would not have been possible without the patience and support of many people. First and foremost I would like to thank my adviser Dr. Robert D. Hatcher, Jr. for the mentorship and financial support to complete this thesis. I am very grateful to have had the opportunity to work and map alongside such a passionate geologist. I would also like to thank my committee members, Drs. Theodore Labotka and Christopher Fedo, for their support and assistance in finishing this thesis. I would also like to thank Dr. Larry Taylor and Allen Patchen in the University of Tennessee Electron Microprobe Facility. Additional thanks are extended to Carl Merschat and Bart Cattanach for their insightful field review and feedback on my geologic map.

I would also like to thank my field partner and fellow Kentuckian, Heather Byars, for her insightful conversations about our field areas and her wonderful home cooking. I was a pleasure to map and learn with you. A special thanks is extended to Arthur Merschat for willingness to discuss Inner Piedmont geology with me. Additionally I would like to thank my former and current office mates, Brittany Davis, Phillip Derryberry, Chris Howard, Matt Huebner, and Mary (Varnell) Jubb for putting up with me. Nancy “Damama” Meadows, thank you for your patience, positivity, and for making me feel at home. I am forever grateful for your positive encouragement, thorough proofreading, and birthday celebrations.

My graduate experience would not have been possible without the patience, love, and support from my family. Special thanks to my wife Lyndci for all the love and support she has provided me while I finish my thesis. This would not have been possible without you. Thanks to my mom, Evelyn for the positive encouragement, love, and support throughout my academic career. Thank you all for believing in me. Last but not least I would like to thank my grandfather, William Frank Gilliam, for introducing me to geology through our many walks up the creek. Who knew it would manifest into this.

ABSTRACT

Rocks of the western and eastern Inner Piedmont, along with the eastern Blue Ridge, comprise the Neoacadian metamorphic core of the southern Appalachians. The composite Inner Piedmont consists of the eastern Tugaloo (western Inner Piedmont) and Cat Square (eastern Inner Piedmont) terranes, which are separated by the Brindle Creek fault. Geochronologic evidence established the Brindle Creek fault as a terrane boundary within the Inner Piedmont, separating terranes of Laurentian and mixed Laurentian/Avalonian (peri-Gondwanan) zircon suites. The Newton window exposes Tugaloo terrane rocks of the Tallulah Falls Formation in the footwall of the Brindle Creek thrust sheet.

Detailed geologic mapping in the western Newton window revealed structural and metamorphic similarities between rocks across the Brindle Creek fault. Peak metamorphism occurred contemporaneously with peak deformation, reaching upper amphibolite facies across both terranes. Peak Neoacadian metamorphism occurred between 360 and 345 Ma. Electron microprobe analyses of Cat Square terrane core and rim garnet-biotite and garnet-plagioclase pairs indicate an average temperature and pressure of 620° C, 3.6 kbar and 710° C, 6.1 kbar, respectively. Temperature and pressure estimates from the lower Tallulah Falls Formation core and rim analyses yield conditions of 570° C, 4.1 kbar and 690° C, 5.9 kbar, respectively. The maximum burial depth for both Cat Square and Tugaloo terrane rocks is ~20 km. The range in metamorphic ages suggests subduction and accretion occurred at a rate of 1 kilometer per 1.75 million years.

Six deformational events shaped the western Newton window. D₁ features are limited to amphibolite boudins of the Tugaloo terrane. D₂ regional penetrative structures such as high-temperature foliations, mineral stretching lineations, and curved fold axes are the product of Neoacadian tectonism. The dominant S₂ foliation trends north-northwest and dips moderately to the west-southwest. North-northwest-trending L₂ mineral lineations parallel F₂ fold axes, creating a curved map pattern recording crustal flow in an ancient orogenic channel. D₃ resulted in open folding. The D₄ event produced regional open folds. D₅ and D₆ features occur as joints, cataclasis, and diabase intrusion.

TABLE OF CONTENTS

CHAPTER 1 INTRODUCTION.....	1
Geologic Setting.....	4
The Newton window/antiform.....	8
Regional structural framework and tectonics models.....	9
Metamorphism.....	11
Objectives.....	11
Methodology.....	11
 CHAPTER 2 LITHOLOGIC UNITS.....	 13
Introduction.....	13
Eastern Inner Piedmont Ashe-Tallulah Falls.....	17
Eastern Inner Piedmont Cat Square terrane.....	26
Cat Square sillimanite schist.....	26
Cat Square biotite gneiss.....	28
Walker Top Granite.....	31
Mesozoic features.....	35
Diabase dikes.....	35
Cataclasite.....	35
 CHAPTER 3 P–T ESTIMATES NEAR THE WESTERN NEWTON WINDOW.....	 41
Introduction.....	41
Timing of Metamorphism.....	46
Field and Petrographic Observations.....	47
Migmatite.....	50
Pegmatite.....	52
Pressure and Temperature Conditions.....	52
Analytical Methods.....	52
Survey of Geothermometers and Barometers.....	55

H3 Lower Tallulah Falls biotite gneiss/metagraywacke.....	56
LV284 Cat Square terrane biotite gneiss/metagraywacke.....	61
Results and Discussion.....	67
Summary.....	69
CHAPTER 4 STRUCTURAL EVOLUTION OF THE WESTER	
NEWTON WINDOW BASED ON MAP PATTERNS AND	
GEOLOGIC STRUCTURES.....	74
Introduction.....	74
Deformational Events.....	78
D ₁ Deformation.....	78
D ₂ Deformation.....	78
Foliations.....	78
Lineations.....	81
Folds.....	90
Faults.....	90
D ₃ and D ₄ Deformation.....	93
D ₅ and D ₆ Deformation.....	95
Map Patterns.....	95
Cross Section Interpretation.....	98
Western Newton Window Kinematic Overview.....	100
CHAPTER 5 CONCLUSIONS.....	105
REFERENCES CITED.....	107
APPENDIX I.....	113
VITA.....	142

LIST OF FIGURES

CHAPTER 1

Figure 1–1 Simplified tectonic map of the southern Appalachian Mountains.....	2
Figure 1–2 Simplified geologic map of the Cat Square terrane.....	3
Figure 1–3 Location map of Newton window.....	5
Figure 1–4 Tectonostratigraphy of the Appalachian Inner Piedmont.....	7

CHAPTER 2

Figure 2–1 Simplified geologic map showing locations of thins sections and photographs used in this chapter.....	14
Figure 2–2 Photos showing variations in topographic expression between sillimanite and biotite rich bedrock.....	16
Figure 2–3 Photo of lower Tallulah Falls biotite gneiss.....	19
Figure 2–4 Outcrop of lower Tallulah Falls biotite gneiss with leucosomes.....	21
Figure 2–5 Saprolitic exposure of lower Tallulah Falls biotite gneiss.....	22
Figure 2–6 Photo of lower Tallulah Falls hornblende-plagioclase gneiss at station R 130.....	23
Figure 2–7 Photo of lower Tallulah Falls hornblende-plagioclase gneiss at station R 50.....	24
Figure 2–8 Gondite interlayer in lower Tallulah Falls biotite gneiss.....	25
Figure 2–9 Outcrops of Cat Square terrane sillimanite schist.....	27
Figure 2–10 Cat Square terrane sillimanite schist at station H 1.....	29
Figure 2–11 Outcrop and saprolite of Cat Square terrane biotite gneiss.....	30
Figure 2–12 Cat Square terrane biotite gneiss from station LV 284.....	32
Figure 2–13 Walker Top granite outcrop and xenolith.....	33
Figure 2–14 Hand specimen and thin section of Walker Top Granite.....	34
Figure 2–15 IUGS classification of modal analyses of Walker Top Granite.....	37
Figure 2–16 Photos of Jurassic diabase dike and thin section.....	38
Figure 2–17 Photos of silicified cataclasite outcrop and thin sections.....	40

CHAPTER 3

Figure 3–1 Metamorphic domains depicting zones components of the southern Appalachian Blue Ridge and Inner Piedmont with shared tectonothermal event.....	42
Figure 3–2 Tectonothermal timeline for the Inner Piedmont.....	43
Figure 3–3 Metamorphic isograd map of the Inner Piedmont.....	44
Figure 3–4 Simplified geologic map and location map of thin sections, photographs, and samples used for calibration of metamorphic conditions.....	48
Figure 3–5 Cat Square and lower Tallulah Falls sillimanite.....	49
Figure 3–6 Migmatite in lower Tallulah Falls.....	51
Figure 3–7 Pegmatite at station LV 77.....	53
Figure 3–8 Back scatter electron photomicrograph of garnet in lower Tallulah Fall biotite gneiss at station H 3.....	57
Figure 3–9 X-ray map of Fe and Mg in sample H 3.....	60
Figure 3–10 X-ray map of Ca and Mn in sample H 3.....	62
Figure 3–11 Back scatter electron photomicrograph of garnet in Cat Square terrane biotite gneiss at station LV 284.....	63
Figure 3–12 X-ray map of Fe and Mg in sample LV 284.....	66
Figure 3–13 X-ray map of Ca and Mn in sample LV 284.....	68
Figure 3–14 Pressure temperature diagram for sample H 3 and LV 284.....	70
Figure 3–15 Metamorphic P-T estimates plotted for recent Inner Piedmont studies.....	72
Figure 3–16 Graph of rim and core temperature estimates versus distance from the Brindle Creek fault.....	73

CHAPTER 4

Figure 4–1 Index map of the eastern U.S. showing the location of the southern Appalachian Mountains and Inner Piedmont.....	76
Figure 4–2 S-C fabric and asymmetric garnets in Cat Square terrane sillimanite schist.....	79

Figure 4–3 Scatter and contoured equal area plot of poles to S_2 foliation.....	81
Figure 4–4 Compiled domain map of the Columbus Promontory, South Mountains, and Newton window areas.....	82
Figure 4–5 S_2 foliation form-line map	83
Figure 4–6 S_2 foliation map and form line map with stereo plots of poles to foliation.....	84
Figure 4–7 S_2 form-line and domain map with stereo plots of L_2 mineral lineations and F_2 fold axes.....	86
Figure 4–8 L_2 lineation photos.....	88
Figure 4–9 Equal area stereo plot of L_2 mineral lineations and F_2 fold axes.....	89
Figure 4–10 F_2 and F_3 folding.....	91
Figure 4–11 Composite scatter plot of L_2 mineral lineations and F_2 fold axes.....	92
Figure 4–12 Brindle Creek fault outcrop.....	94
Figure 4–13 Outcrop exposure of siliceous cataclasite.....	96
Figure 4–14 Simplified geologic map with cross-section lines.....	97
Figure 4–15 Cross sections across the map area.....	99
Figure 4–16 Patterns of S_2 and L_2 lineations in the northern Inner Piedmont.....	101
Figure 4–17 L_2 lineation map of study area.....	102
Figure 4–18 3D block diagram depicting the structure of part of the northern Inner Piedmont from Hendersonville, NC to the Sauratown Mountains window.....	103

LIST OF TABLES

CHAPTER 2

Table 2–1 Table of ages, terranes, rock types , and descriptions of rock units mapped in the study area.....15

Table 2–2 Modal analyses of lower Tallulah Falls hornblende-plagioclase gneiss from station R 130 and R 50, and biotite gneiss at station H 3.....20

Table 2–3 Modal analyses for Cat Square terrane Walker Top Granite.....36

CHAPTER 3

Table 3–1 Selected results from lower Tallulah Fall H 3 biotite gneiss microprobe analysis.....59

Table 3–2 Selected results from Cat Square terrane LV 284 biotite gneiss microprobe analysis.....65

CHAPTER 4

Table 4–1 Summary and relative timing of deformational events in the Inner Piedmont.....78

CHAPTER 1

INTRODUCTION

Rocks of the western and eastern Inner Piedmont, along with the eastern Blue Ridge, comprise the Neoacadian metamorphic core of the southern Appalachians (Fig. 1-1) (Osberg et al., 1989; Davis, 1993; Hatcher, 1993; Dennis and Wright, 1997a; Bream, 2003). The composite Inner Piedmont consists of the eastern Tugaloo (western Inner Piedmont) and Cat Square terranes (eastern Inner Piedmont), which are separated by the Brindle Creek fault (Davis, 1993; Giorgis, 1999; Williams, 2000; Bier, 2001; Mersch, 2003; Wilson, 2006; Gatewood, 2007; Byars, 2010) (Fig. 1-1). Geochronologic evidence has established the Brindle Creek fault is a terrane boundary within the Inner Piedmont, separating terranes of Laurentian and mixed Laurentian/Avalonian (peri-Gondwanan) zircon suites (Bream, 2003). The mixed provenance of the zircon suite, along with the striking differences in lithology, metamorphism, and plutonism, led to the distinction of the Cat Square (Fig. 1-2) terrane as a new Inner Piedmont tectonic terrane within the Inner Piedmont. Goldsmith et al. (1988) first mapped a broad, doubly plunging antiformal structure located in the eastern Inner Piedmont, which they subsequently called the Newton antiform (Fig. 1-2). This antiformal dome extends southwest from Statesville to Hickory and south into Lincolnton, North Carolina (Fig. 1-2). Goldsmith et al. (1988) previously identified an abrupt change from metapelites to large bodies of psammitic, amphibolite, and ultramafic rocks. Distinct lithologic differences between the core and limbs of the Newton antiform resulted in some unanswered questions concerning the origins of this transition: specifically, do they represent eastern Inner Piedmont basement? Preliminary geochronologic investigations of rocks occurring in the metapsammitic core of the Newton antiform by Mersch et al. (2005a) revealed a distinct detrital zircon assemblage indicative of Tugaloo terrane rocks (1.4, 1.2, 1.15, 1.0 Ga., Bream, 2003; Mersch et al., 2005a) and contained no

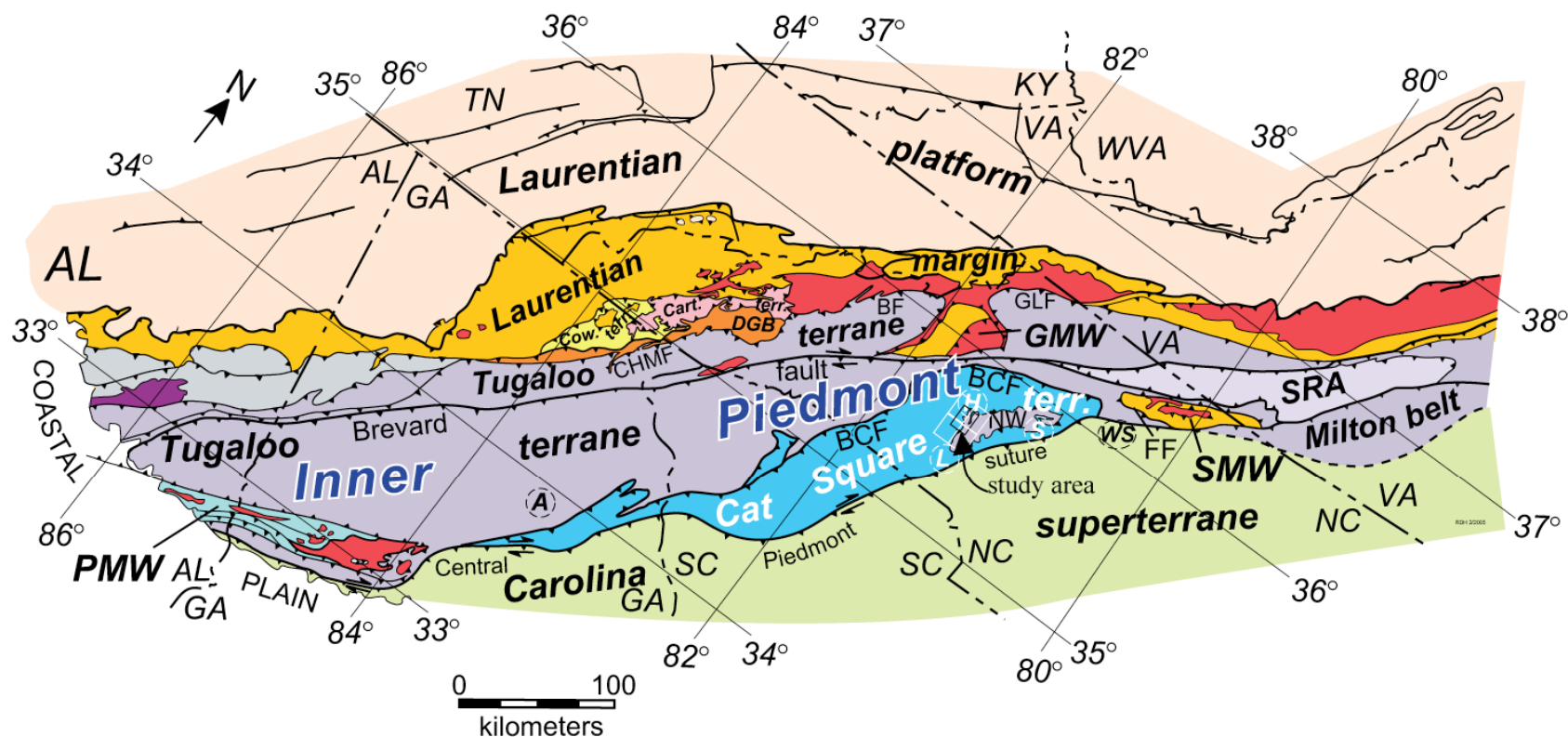


Figure 1–1. Simplified tectonic map of the southern Appalachians showing the location of the Inner Piedmont, and the Tugalo (lavendar) and Cat Square terrane (blue-green) terranes. Figure from Mershat and Hatcher (2008). Quadrangles used in this study are outlined in white, the black rectangle indicates the area of study. BCF-Brindle Creek fault. BF-Burnsville fault. Carr. terr.-Cartoogechaye terrane. CHMF-Chattahoochee-Holland Mountain fault. Cow. terr.-Cowrock terrane. DGB-Dahlonge gold belt. FF-Forbush fault. GLF-Gossan Lead fault. GMW-Grandfather Mountain window. NW-Newton window. SRA-Smith River allochthon. SMW-Sauratown Mountains window. PMW-Pine Mountain window. Towns circled in dashed lines: A-Athens. H-Hickory. L-Lincolnton. S-Statesville. WS-Winston Salem.

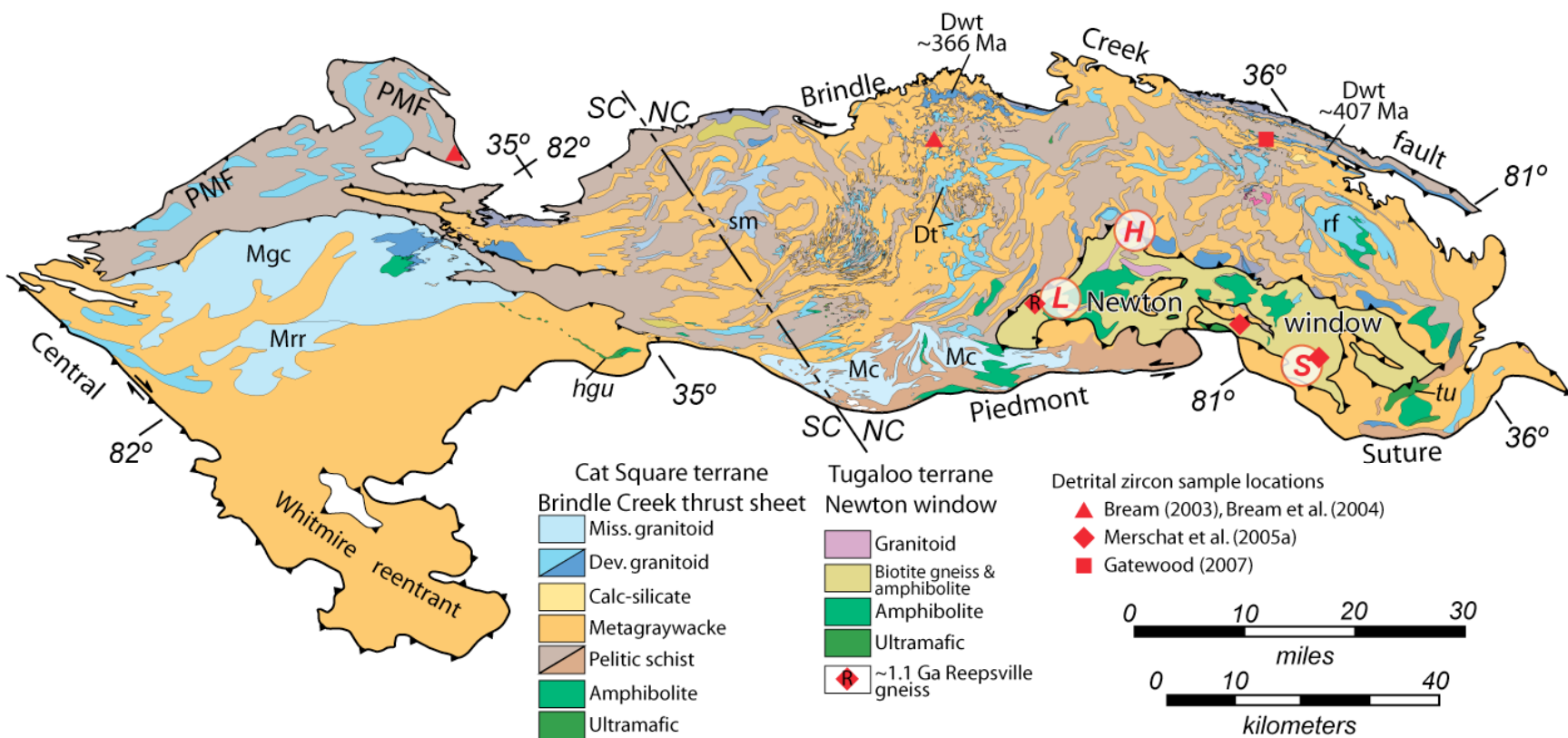


Figure 1-2. Simplified geologic map of the Cat Square terrane from its northern extent to near the Georgia-South Carolina border. Figure from Mersch and Hatcher (2008). Dt -Toluca Granite. Dwt-Walker Top Granite. hgu-Hammett Grove metaigneous mafic-ultramafic body. Mc-Cherryville Granite. Mgc-Gray Court Granite. Mrr-Reedy River Granite. PMF-Paris Mountain thrust sheet, a remnant of the original Brindle Creek thrust sheet that broke through as an out-of-sequence fault. rf-Rocky Face granite. sm-Sandy Mush granite. tu-Turnersberg ultramafic. H-Hickory. L-Lincolnton. S-Statesville.

zircons indicating Cat Square terrane (600, 500, and 430 Ma). These distinctions led Mersch et al. (2005a) to classify the Newton antiform as a window (Fig. 1-2).

GEOLOGIC SETTING

The Inner Piedmont extends approximately 700 km southwestward from the Sauratown Mountains window in north-central North Carolina to the Coastal Plain of Alabama, reaching a width of 100 km at its broadest extent (Fig. 1–2; Hatcher, 2002) and is one of the largest high-grade metamorphic terranes in the world. The eastern Inner Piedmont Cat Square terrane (Hatcher, 2002) is separated from the western Inner Piedmont by the Brindle Creek fault (Giorgis, 1999). Reconnaissance mapping by Goldsmith et al. (1988) (Fig 1–3) identified a boundary, although not previously indicated as a fault, throughout the Charlotte 1° x 2°-degree sheet. Giorgis (1999) was the first to identify the Brindle Creek fault based on the hanging wall truncation of a footwall synform. The Brindle Creek fault was further recognized to the northeast, in the Brushy Mountains (Kalbas, 2003; Mersch, 2003; Wilson, 2006; Gatewood, 2007), then truncating to the northeast against the border fault of the Davie County Mesozoic basin (Espenshade et al., 1975). In South Carolina the Brindle Creek fault is traceable between Greenville and Spartanburg (Nelson et al., 1998) and trends southwestward into west-central Georgia, and possibly into Alabama (Hatcher et al., 2007). To the east the Cat Square terrane is truncated by the exotic Carolina superterrane (Hatcher, 2002) along the central Piedmont suture.

Three distinct differences separate the Cat Square terrane from rocks of the eastern Tugalo terrane: 1) the absence of amphibolite; 2) ages and inheritance of detrital zircons; and 3) age and type of plutonism (Hatcher, 2002). Rocks of the Brindle Creek thrust sheet contain a Siluro-Devonian metagraywacke/biotite gneiss and sillimanite schist metasedimentary package intruded by catazonal Acadian plutons, such as the Walker Top (Giorgis, 1999; Mapes et al.

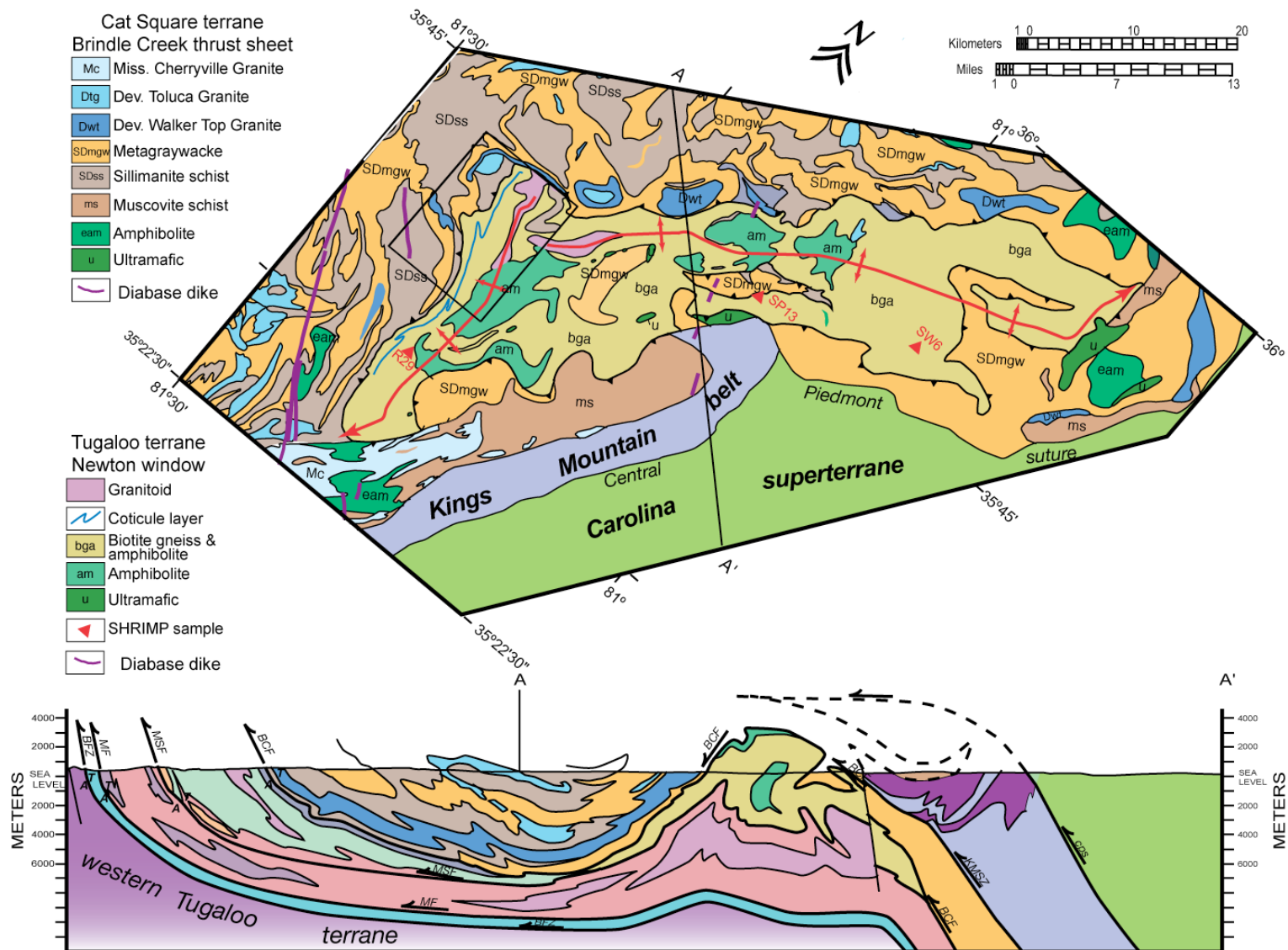


Figure 1-3. Location of the Longview, Hickory, Banoak, and Reepsville quadrangles with the study area superimposed. SHRIMP locations indicate the location of basement rocks in relation to the study area. Base map and cross section are modified after Goldsmith et al. (1988) and Hatcher and Mersch (2008).

2002; Bream, 2003) and Toluca Granites (Overstreet et al., 1963; Mapes et al., 2002) (Fig. 1–4a). Cat Square terrane metasedimentary rocks represent flysch facies eroded into the Cat Square basin. Large pods of amphibolite and ultramafic rocks are rare, but present in the Cat Square terrane, and represent portions of a relict ophiolite (Byars, 2010). The eastern Tugaloo terrane contains rocks of the Tallulah Falls and Poor Mountain Formations (Hatcher, 1993) (Fig. 1–4b) intruded by Ordovician plutons such as the Caesars Head, Dyartsville, Henderson, and Toccoa Granites (Davis, 1993; Mapes et al., 2002). Key differences in zircon populations suggest the Brindle Creek can also be further described as a terrane boundary in the Inner Piedmont. Zircon populations in the Cat Square terrane contain both 2.7, 1.8, 1.4, 1.1 Ga, and key Gondwanan 600 and 500 Ma components as well as 430 Ma zircons, with the <600 Ma zircons being sourced from the Carolina superterrane (Hatcher, 2002). Newton antiform paragneisses reveal peaks at 1.2, 1.15, 1.0 Ga (Grenvillian), and 1.4 Ga (Granite-Rhyolite province), which represent a Laurentian provenance (Merschhat et al., 2005b). A second orthogneiss sample from the Newton window yielded a U-Pb age of $1,050 \pm 18$ Ma age with metamorphic rims of ~350 Ma, possibly representing a fragment of Grenville crust, which further supports correlation with the Tugaloo terrane (Merschhat et al., 2005b, Fig. 1-2). Likewise, Byars (2010) identified a porphyroclastic biotite orthogneiss she called Potts Creek mylonitic gneiss, that proved to have an Ordovician zircon age.

Giorgis (1999) first identified the Brindle Creek fault in the South Mountains, northwestward from the study area; he recognized a clear truncation of foliation along a low-angle, southeast-dipping surface. Other workers have identified the Brindle Creek fault in the South Mountains (Bier, 2001), northward into the Brushy Mountains (Merschhat, 2002; Wilson, 2006; Gatewood, 2007) and to the east framing the Newton window (Byars, 2010; this study).

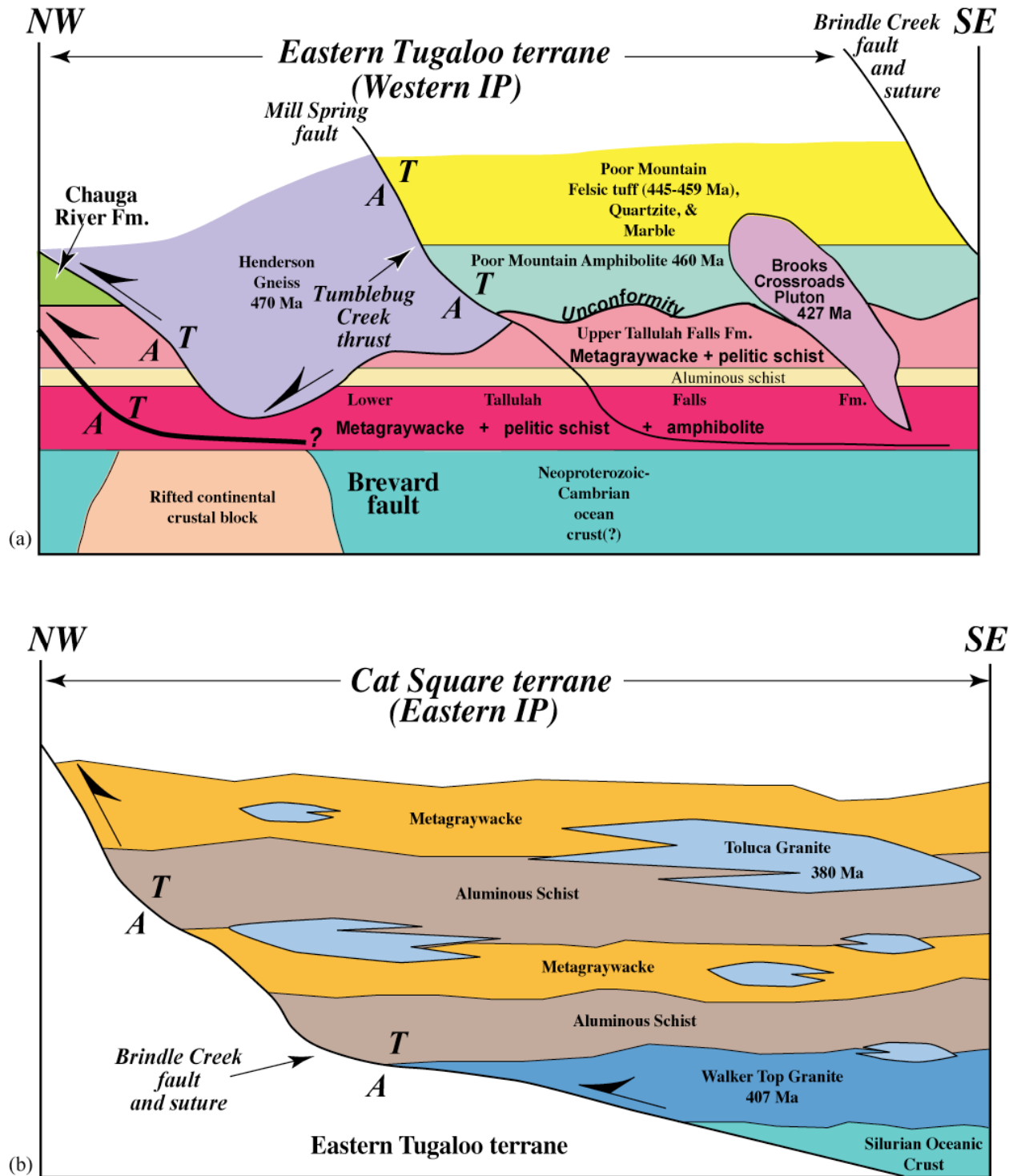


Figure 1-4. (a) Tectonostratigraphy of the western Inner Piedmont, eastern TugaloO terrane. (b) Tectonostratigraphy of the eastern Inner Piedmont Cat Square terrane. Figure from Hatcher (2005).

THE NEWTON WINDOW/ANTIFORM

Windows are a common element in mountain chains, occurring between either sedimentary or crystalline thrust sheets. The Newton antiform, as previously mapped by Goldsmith et al. (1988) (Fig. 1–3) in the Charlotte 1° x 2° sheet, is a broad NW-SE trending, doubly plunging, non-cylindrical, antiformal fold occurring between Statesville, Hickory, and Lincolnton North Carolina. This feature exposes a unique sequence in its core of biotite-hornblende gneiss, ultramafic rocks, and amphibolite that contrasts with surrounding Cat Square terrane lithologies, specifically abundant pelitic schist. The presence of this large isolated body of psammitic rocks in the eastern Inner Piedmont led to three possible tectonic scenarios: (1) mid-Paleozoic ophiolites associated with Devonian docking of the Carolina superterrane; (2) a window through the Brindle Creek thrust sheet; or (3) an unidentified terrane (Mersch et al., 2007). Geochronology samples collected by Mersch et al. (2005) from three localities within the core of the Newton Antiform reveal two SHRIMP U-Pb paragneiss detrital zircon assemblages with peaks at 1.2, 1.15, 1.0 Ga (Grenvillian), and 1.4 Ga (granite-rhyolite province?); additionally, a biotite-orthogneiss sampled near Reepsville, North Carolina (Reepsville Gneiss) provided a primary zircon U-Pb age of 1050 ± 18 Ma with a ~ 350 Ma metamorphic rim (Mersch et al., 2005) and is interpreted to represent a fragment of Grenville basement. The discovery of both a primary and detrital Laurentian zircon assemblage, along with the presence of a Grenville basement fragment, suggests the presence of a window with core rocks similar to the Neoproterozoic to Cambrian (?) lower Tallulah Falls Formation. The abundance of biotite-amphibolite gneiss, amphibolite pods, and ultramafic rock encountered in the core of the Newton Antiform is consistent with lithologies of the lower Tallulah Falls Formation found elsewhere in the western Inner Piedmont. Evidence gathered from detailed

geologic mapping revealed a moderately dipping Brindle Creek fault that truncates shallow to moderately dipping foliation of the lower Tallulah Falls Formation rocks against rocks of the Cat Square terrane, similar to the boundary that Goldsmith et al. (1988) mapped. Likewise, south of the study area the Brindle Creek fault displays sharp truncation of the mid-Paleozoic Walker Top Granite exhibiting mylonitic fabric (Byars, 2010). Geochronologic evidence, lithologies, map scale truncations, and the presence of mylonite permit the additional classification of the Newton antiform as a window.

REGIONAL STRUCTURAL FRAMEWORK

Griffin (1971) first described the Inner Piedmont as the eroded remains of a west-verging autochthonous nappe complex in his stockwork tectonic model; he concluded the Inner Piedmont represented a high-grade mobile infrastructure below a superstructure, represented by the greenschist facies Carolina superterrane. Griffin noticed regional ductile fabrics were crosscut by later brittle features and concluded a ductile event was followed by a brittle event. Alternatively, other interpretations favor an allochthonous origin for Inner Piedmont thrust sheets (Hatcher, 1974; Hatcher and Hooper, 1992). Hatcher and Hooper (1992) concluded the Inner Piedmont consists of Type-F thrusts characterized by plastic, lobate, fold-derived thrusts with penetrative mesofabrics that formed below the brittle-ductile transition. Griffin's recognition of a ductile, followed by brittle episode was correct, although he did not recognize multiple episodes of deformation in each regime (see Hatcher, 1974). Hatcher (1972) indicated the Inner Piedmont was not formed in one plastic deformational episode and further added to the number of deformational events recognized within the ductile regime. Later episodes of brittle deformation have been recognized throughout the Inner Piedmont (e.g., Hopson and Hatcher, 1988), first as

broad open folds associated with the Alleghanian orogeny, then as normal faults and joints related to Mesozoic extension (Merschhat and Kalbas, 2002).

The Inner Piedmont contains a gently dipping stack of ductile SW-directed crystalline type F thrust sheets (Hatcher and Hooper, 1992; Fig. 1-3), which record multiple episodes of complex folding and faulting. Type F thrusts transform to type C thrusts during exhumation, and cooling allows thrust sheets to attain a large size and transport distance (Hatcher and Hooper, 1992). Kinematic indicators in the Inner Piedmont include sheath folds, asymmetric tight folds, open folds, S-C fabric, rotated porphyroclasts, and mineral stretching lineations. The dominant foliation (S_2) and mineral stretching lineations (L_2) formed during peak metamorphism, and produced a curved mineral stretching lineation pattern interpreted to represent crustal flow in an ancient orogenic channel (Merschhat et al., 2005b; Hatcher and Merschhat, 2006).

The deformational history of the eastern Inner Piedmont is not isolated to one deformational episode. Six deformational events have been recognized in the southern Appalachian Inner Piedmont. The D_1 event occurred prior to recrystallization and due to later transposition became a rare feature only to be preserved in boudins and xenoliths in Tugaloo terrane rocks. The D_2 deformation event is the most pervasive and formed the dominant foliation (S_2), Type F thrust faults, and mineral stretching lineations (Davis, 1993). This event is also synchronous with peak metamorphism. The D_3 deformation event occurred post-peak metamorphism resulting in open folding of D_2 features. The D_4 deformation event produced N-S trending upright regional open folds, corresponding to Alleghanian brittle deformation (Merschhat and Kalbas, 2002). The D_5 deformational event produced broad open folds and joints during the late Alleghanian (Merschhat and Kalbas, 2002). The D_6 deformational event is associated with

Mesozoic extension through a series of joints, diabase dikes, and silicified brecciated normal faults (Merschhat and Kalbas, 2002).

METAMORPHISM

U-Pb dating of monazite and zircon metamorphic rims suggests peak metamorphism occurred from 365–330 Ma and reached upper amphibolite and granulite facies (Dennis and Wright, 1997; Mirante and Patino-Douce, 2000; Bier, 2001; Merschhat and Kalbas, 2002; Byars, 2010). Younger age clusters are also recognized at 325–320 Ma, and represent a younger Alleghanian overprint (Dennis and Wright, 1997; Mirante and Patino-Douce, 2000; Bier, 2001; Carrigan et al., 2001; Bream, 2003). Eastward from the Brevard fault zone, metamorphic grade increases from kyanite-staurolite grade to sillimanite I and higher across the core of the Inner Piedmont, and decreases to kyanite grade along the central Piedmont suture. Zoning profiles across cores and rims of Inner Piedmont garnets reveal metamorphism occurred as a single protracted event (Bier, 2001; Merschhat and Kalbas, 2002). Intense migmatization occurs as much as 7 km west of the Brindle Creek fault, and throughout the Brindle Creek thrust sheet, this led Merschhat and Kalbas (2002) to suggest the Brindle Creek thrust was emplaced while hot.

OBJECTIVES

1. Create a detailed 7.5-minute geologic quadrangle of the western Newton window.
2. Map the Brindle Creek fault in detail.
3. Collect regional structural data.
4. Determine metamorphic conditions of the Tugaloo and Cat Square terranes

METHODOLOGY

This study contains both field and laboratory components. The first field season of detailed geologic field mapping began February 2007 and ended in June 2007, and the second field season began in January of 2008 and continued into June of 2008. Mapping was done at

1:24,000 scale using the Mountain View, Banoak, Hickory, and Reepsville U.S.G.S. 7.5-minute topographic quadrangles as base maps. Structural elements including foliations, lineations, fold axes, crenulations, and joints were measured using a Brunton compass and compiled into a field notebook. Diagrams and maps were generated using Adobe Illustrator CS2. Field data were compiled into Microsoft Excel spreadsheets and appear in Appendix I. Stereoplots of fabrics observed in the study area were created using the program Stereonet created by Richard Allmendinger.

Rocks used for petrographic analysis and electron microprobe analysis were oriented in the field and labeled accordingly to preserve the original structural setting. Stations were given an individual number with rocks samples corresponding to station numbers. Rocks were cut parallel and perpendicular to foliation, or parallel to mineral lineation, to evaluate the minerals and fabric present. Petrographic analysis was carried out using a Leica polarizing microscope. Modal analyses were conducted on the Cat Square terrane Walker Top Granite using 1 mm steps, and lower Tallulah Falls hornblende-plagioclase gneiss and biotite gneiss using 0.3 mm steps.

CHAPTER 2

LITHOLOGIC UNITS

INTRODUCTION

Following the discovery of the Cat Square terrane and preceding the discovery of the Newton window, the eastern Inner Piedmont was thought to only contain metasedimentary rocks, anatectic melt, and plutons of the Brindle Creek thrust sheet. Reconnaissance mapping by Goldsmith et al. (1988) identified a large expanse of psammitic, amphibolite, and ultramafic rocks coring the Newton antiform, contrasting with the surrounding sillimanite-rich bedrock. These key lithologic differences proved to be significant in evaluating the regional tectonic history. Merschat et al. (2005a) sampled psammitic rocks exposed in the broad core of the Newton antiform, south of Hickory, North Carolina, for geochronologic analysis. Laurentian provenance zircons provided evidence that these rocks are part of the western Inner Piedmont Tugaloo terrane, and that the Newton antiform is also a window.

The Brindle Creek fault was first recognized on the west end of the Brindle Creek thrust sheet by Giorgis (1999). Then Bream (2003) demonstrated the Brindle Creek thrust sheet is a separate terrane. Goldsmith et al. (1988) delineated key lithologic features and contact patterns of the Newton window, but did not map the contact as a fault. In this study, three lithologic units are mapped in the Brindle Creek thrust sheet: biotite gneiss, sillimanite schist, and Walker Top Granite (Fig. 2–1; Table 2–1). Lithologic units mapped in the Newton window include the lower Tallulah Falls Formation biotite gneiss, amphibolite, and ultramafic rocks (Fig. 2–1; Table 2–1).

The occurrence of rock outcrops and topography is largely influenced by bedrock lithology. Topographic features of the study area vary from the higher elevation ridges of Baker Mountain to rolling lowlands and floodplains near the Jacob Fork River (Fig. 2–2). The

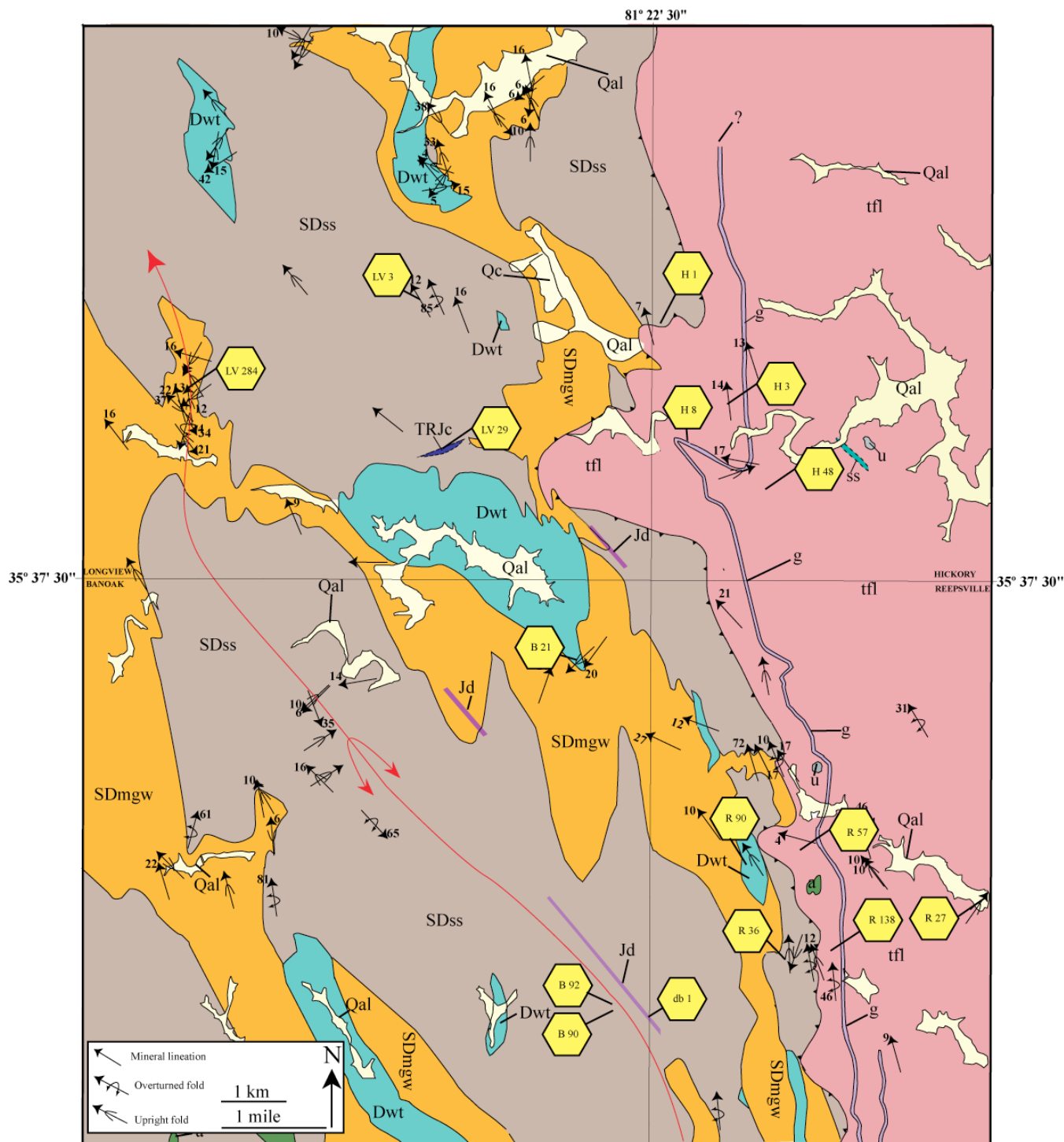


Figure 2–1. Simplified geologic map showing locations of thin sections and photographs that appear in this chapter. Yellow diamonds indicate station numbers corresponding to photos in the text. Cat Square terrane rocks: SDss=Siluro-Devonian sillimanite schist, SDmgw=Siluro-Devonian metagraywacke, Dwt=Devonian Walker Top Granite. Tugaloo terrane: tfl=lower Tallulah Falls metagraywacke/hornblende gneiss, ss=lower Tallulah Falls sillimanite/mica schist, a=amphibolite, u=soapstone/altered ultramafic rock, g=gondite, TRJc=Triassic- Jurassic cataclasite, Jd=Jurassic diabase dike, Qc=Quaternary colluvium, Qal =Quaternary alluvial material. Red line represents antiformal sheath fold axis.

Table 2–1. Table of ages, terranes, and a brief description of rock units identified in this study.

AGE	TERRANE	ROCK UNIT	DESCRIPTION
Neoproterozoic (?) to Ordovician	Tugaloo-Lower Tallulah Falls Formation	biotite gneiss	medium- to coarse-grained biotite gneiss, typical minerals include biotite, quartz, alkali-feldspar, plagioclase (An ₃₀), apatite, and clinozoisite
		hornblende-plagioclase gneiss	medium- to coarse-grained hornblende-plagioclase gneiss, typical minerals include hornblende, plagioclase (An ₃₄₋₃₈), quartz, clinozoisite, and epidote
		amphibolite	interlayers and boudins of fine- to medium-grained hornblende, and fine- to coarse-grained plagioclase, quartz, clinozoisite, and epidote
		gondite	fine- to medium-grained garnet-rich quartzite, granular texture, poorly foliated, typical minerals include quartz, garnet, muscovite, and plagioclase
Silurian to Mississippian	Cat Square	sillimanite schist	fine- to medium-grained garnet-rich quartzite, granular texture, poorly foliated, typical minerals include quartz, garnet, muscovite, and plagioclase
		biotite gneiss	medium- to coarse-grained biotite gneiss, typical minerals include biotite, quartz, alkali-feldspar, plagioclase (An ₃₀), apatite, and clinozoisite
		Walker Top Granite	medium- to dark-gray megacrystic orthogneiss, large alkali feldspar megacrysts occur up to 10 cm and exhibit myrmekitic rims, matrix is fine- to medium-grained and contains alkali-feldspar, garnet, quartz, and plagioclase (An ₂₈₋₃₄)
Triassic Jurassic		diabase	fine-grained diabase, exhibiting ophitic texture composed of olivine, clino- and orthopyroxene, and plagioclase
		cataclasite	fine- to coarse-grained angular fragments of quartz bound by silica cement crosscutting Cat Square terrane sillimanite schist

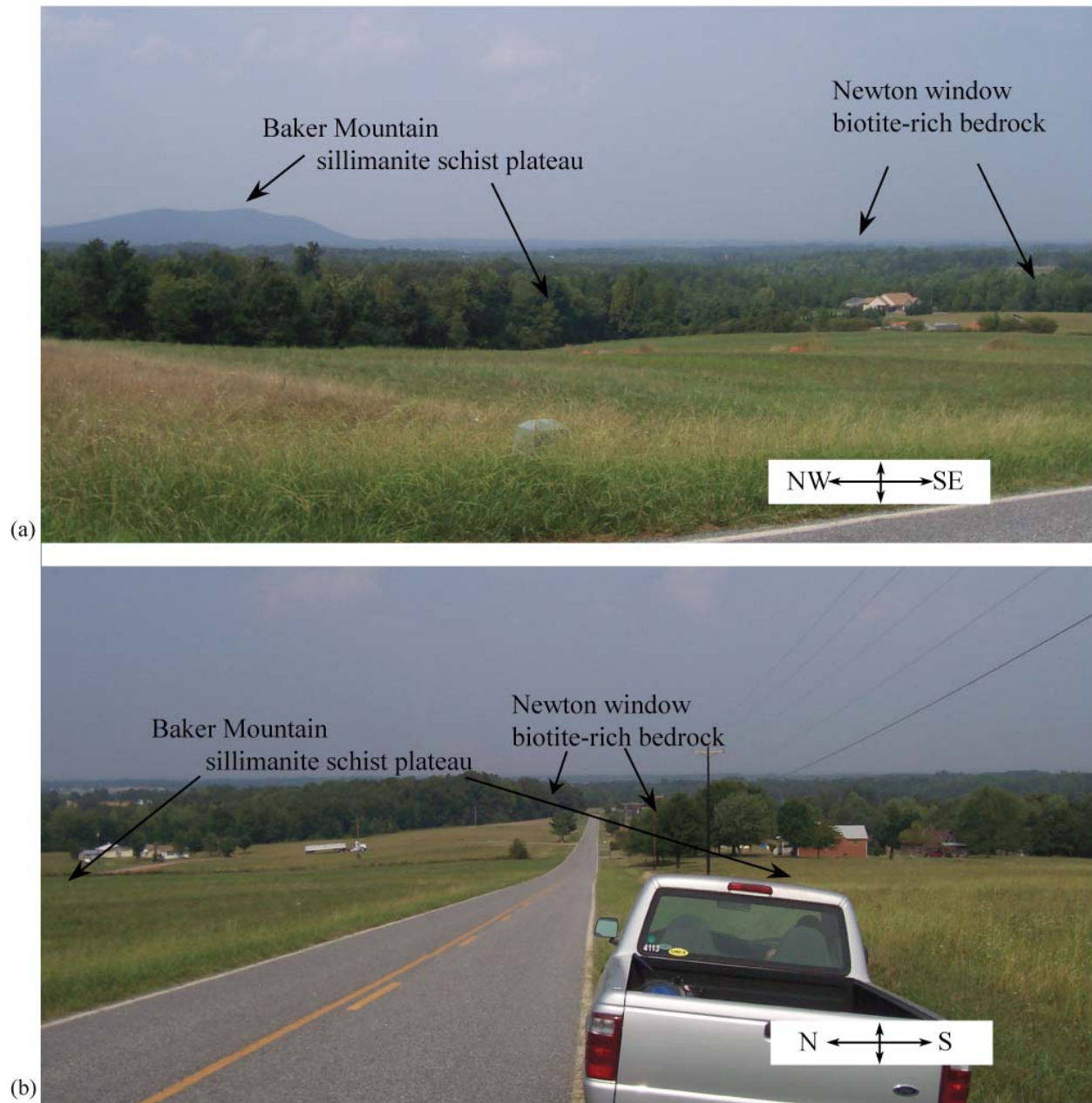


Figure 2–2. (a) Variations in topographic expression between sillimanite-rich bedrock to the northwest and biotite bedrock to the southeast. Baker Mountain is composed almost entirely of Cat Square terrane sillimanite schist and is the highest topographic feature in the study area. (b) Looking due east from a standpoint above sillimanite-rich bedrock; eastward topography becomes more subtle as the amount of biotite gneiss increases. Both photos shot from the southwest corner of the study area on West Plateau Road.

variations in topographic relief are largely influenced by bedrock composition, specifically the presence of pelitic schist that holds up steep ridges and forms soils that are relatively thin. However, Baker Mountain is an inselberg (monadnock) of the South Mountains further west (Fig. 2–2a). Alternatively, biotite-rich psammitic rocks and orthogneiss form low topographical areas and floodplains that erode relatively quickly, forming large packages of saprolite and well-developed soils.

Detailed field and petrographic observations from both Cat Square and Tugaloo terrane rocks are the focus of this chapter. Sample locations used for petrographic analysis are located in the detailed geologic map in Figure 2–1.

EASTERN INNER PIEDMONT ASHE–TALLULAH FALLS

Like Gaul, the Tallulah Falls Formation is divided into a tectonostratigraphy of three parts. A lower biotite gneiss member with abundant amphibolite boudins is separated from an upper biotite gneiss member by pelitic schist. The presence of common to abundant amphibolite distinguishes the lower from the upper Tallulah Falls. The ubiquitous amphibolite boudins delimits the lower Tallulah Falls as the only unit recognized in the Newton window in the study area. Trace element geochemistry indicates a MORB or island-arc tholeiite origin for amphibolites (Mersch, 2007; Byars, 2010). Pods of amphibolite and weathered ultramafic rock (soapstone) occur in the lower unit. Discontinuous interlayers of sillimanite-muscovite schist are present but isolated to the outcrop scale, and do not constitute regionally mappable layers, as would be the case if the garnet-aluminum schist member were present.

The lower Tallulah Falls metagraywacke is a medium- to coarse-grained biotite gneiss and hornblende-plagioclase (An₃₄₋₃₈) gneiss that locally contains interlayers and discontinuous

boudins of amphibolite (Fig. 2–3a, Table 2–2). Amphibolite boudins vary in length from 25 cm to 2 m (Fig. 2–3b) long and frequently preserve an earlier S_1 foliation. Amphibolite composition ranges from granular coarse-grained hornblende to fine- to medium-grained hornblende, plagioclase, and quartz \pm garnet \pm biotite \pm sillimanite with minor amounts of epidote, clinozoisite, myrmekite, opaques, and rutile. Lower Tallulah Falls biotite gneiss (Fig. 2–4a) wraps amphibolite boudins and typically contains large quartz \pm plagioclase \pm garnet leucosomes (Fig. 2–4b). Sheared plagioclase and quartz porphyroclasts are common in the lower Tallulah Falls metagraywacke. Remnants of ultramafic rocks are represented by discontinuous pods of soapstone, many too small to represent on the 1:24,000-scale geologic map. Amphibolite saprolite is orange-ochre when heavily weathered and produces a reddish-orange soil. Biotite gneiss weathers to an orange-ochre, while leucocratic layers produce a white soil (Fig. 2–5).

Thin section textures and fabrics indicate a high-temperature history of lower Tallulah Falls rocks. Anthophyllite occurs in small pods up to 4 cm long (Fig. 2–6a and Fig. 2–6b). Symplectic intergrowths of epidote and clinozoisite (Fig. 2–6c and 2–6d) occur between plagioclase (An_{34-38}) and hornblende grains, indicative of retrograde metamorphism (Fig. 2–6d). Leucocratic layers (Fig. 2–7a) in hornblende-plagioclase gneiss also show symplectic intergrowths (Fig. 2–7b) with dull brown to beige hornblende displaying 60° and 120° cleavage (Fig. 2–7c).

Interlayered with the lower Tallulah Falls hornblende-biotite gneiss are several gondite layers (Fig. 2–8a). This garnet-rich quartzite forms prominent exposures and weathers into blocky fragments coated with iron-manganese oxide. Gondite is fine- to medium-grained with a granular texture, and the foliation is not well developed due to the absence of biotite and other



(a)



(b)

Figure 2–3. Lower Tallulah Falls hornblende-biotite gneiss with amphibolite boudins at station H48 at the confluence of small tributary and Jacob Fork River, due north of Mountain View Church Road. (a) The typical appearance of a pavement outcrop located at a stream confluence. Notice the northwest-trending leucosomes within the foliated hornblende-biotite gneiss. Note backpack for scale. (b) Amphibolite boudins showing a rounded appearance within the lower Tallulah Falls Formation. Rock hammer for scale. Sheen on rock, in both photos, is from rain.

Table 2–2. Modal analyses of lower Tallulah Falls hornblende-plagioclase gneiss from station R 130 and R 50, and biotite gneiss at station H 3.

STATION	R 130a	R 50	H 3
COUNTS	1951	1616	1032
Plagioclase	44.2(An ₃₄)	40.9(An ₃₈)	28.3 (An ₃₀)
Hornblende	28.7	29.2	0
Biotite	11.0	12.8	34.6
Quartz	8.8	13.3	25.9
Alkali-feldspar	0.0	0.0	9.8
Zircon	0.5	0.9	0.5
Symplectite	1.1	1.1	0
Anthophyllite	3.6	0.0	0.0
Clinozoisite	0.7	0.5	0.2
Opaques	1.1	0.9	0.8
Apatite	0.2	0.4	0.4
Sphene	0.0	0.0	0.0
TOTAL	100.0	100.0	99.9

Plagioclase compositions were estimated using the Michel-Levy method (Nesse, 1991) in sample B 130a and R 50. An content of sample H 3 was determined using an electron microprobe.



Figure 2–4. (a) West-dipping lower Tallulah Falls Formation biotite gneiss near small waterfall at station R57 in tributary of Cow Branch Creek southeast of Plateau, North Carolina. Photo is facing south, parallel to strike, dip is to the west (right). (b) Large garnets in leucosome in amphibolite from same outcrop as Figure 2–4a.

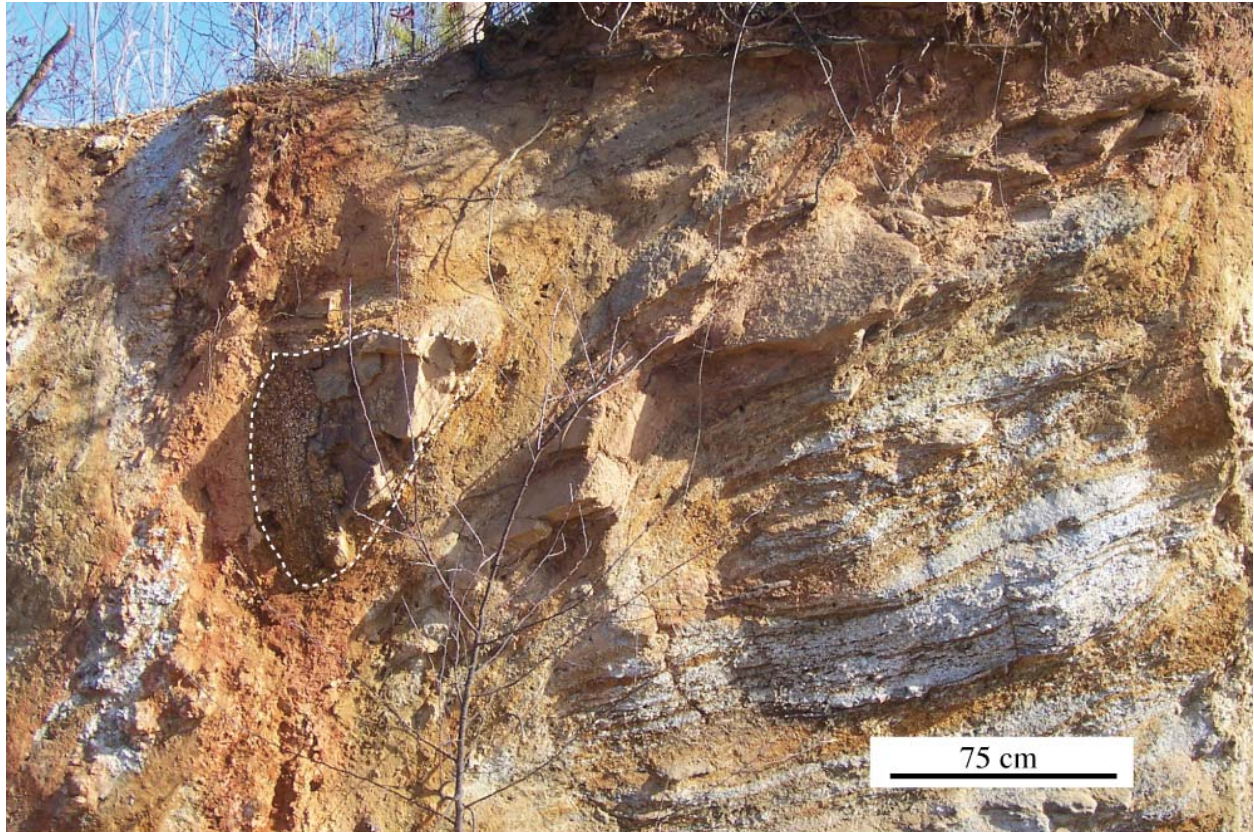


Figure 2–5. Saprolite exposure of lower Tallulah Falls biotite gneiss with amphibolite boudin at station R27 in borrow pit along State Route 2004, south of Cow Branch Creek bridge. Boudin outlined by the white dashed line. The orange-ochre and white mix of decomposed minerals encasing the amphibolite boudin is typical of amphibolite in soils underlain by the lower Tallulah Falls. Partially decomposed leucosomes create lighter colored saprolite. The orange-ochre colored saprolite, separating leucosomes, is derived from weathered biotite gneiss interlayers.

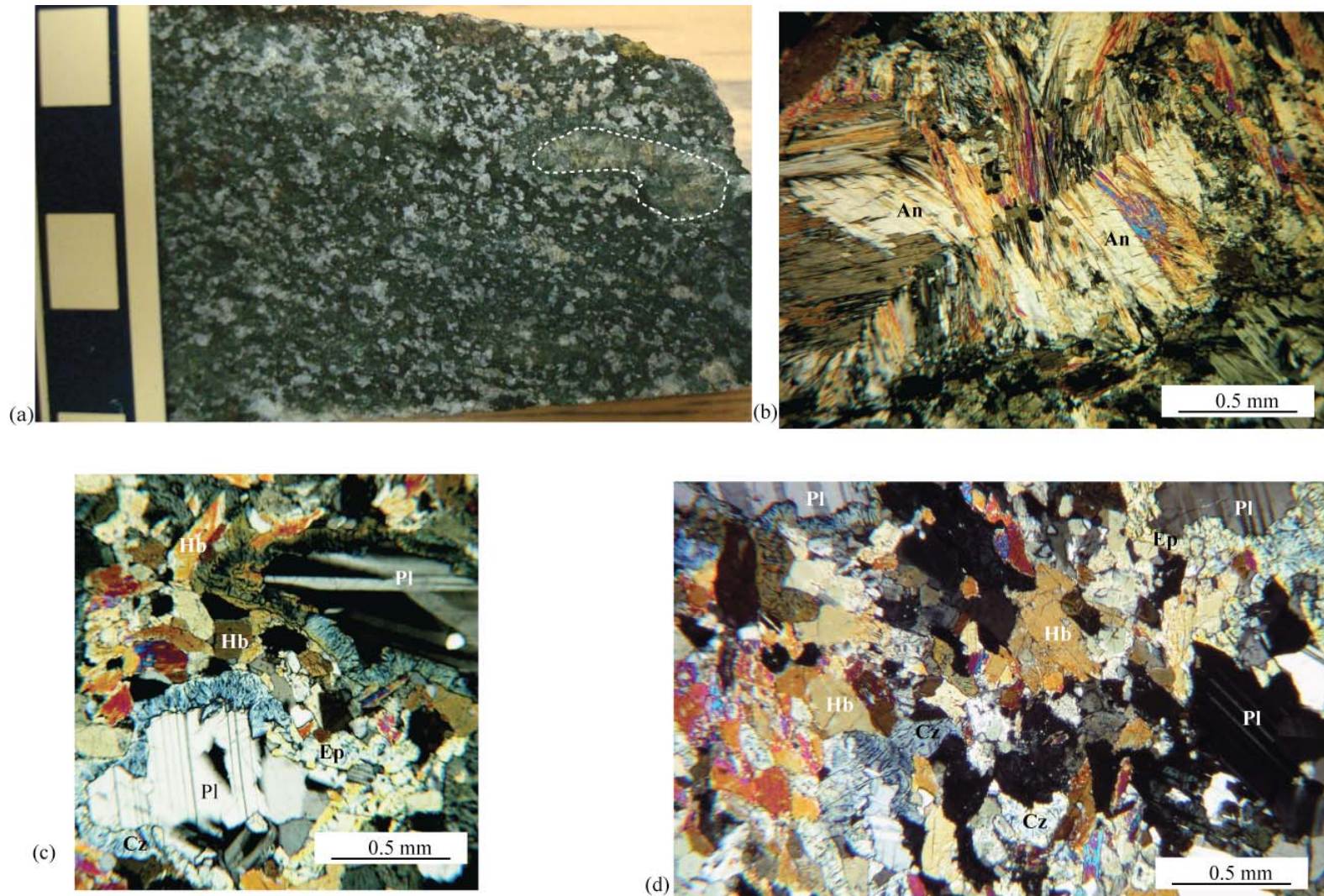


Figure 2-6. (a) Hand specimen of lower Tallulah Falls hornblende-biotite gneiss from station R 130 located in small tributary of Cow Branch Creek south of Plateau, North Carolina. This dark black, fine-to coarse-grained rock contains plagioclase porphyroclasts and small tabular pods of anthophyllite. Pod of anthophyllite is outlined by white dashes. (b) Anthophyllite pod in lower Tallulah Falls hornblende-biotite gneiss. (c) Symplectic intergrowths of clinozoisite and epidote crowning large plagioclase grains. (d) Clinozoisite and epidote symplectite occurring in fine-grained hornblende plagioclase matrix. Mineral abbreviations: Pl = plagioclase, Hb = hornblende, Cz = clinozoisite, Ep = epidote, An = anthophyllite.

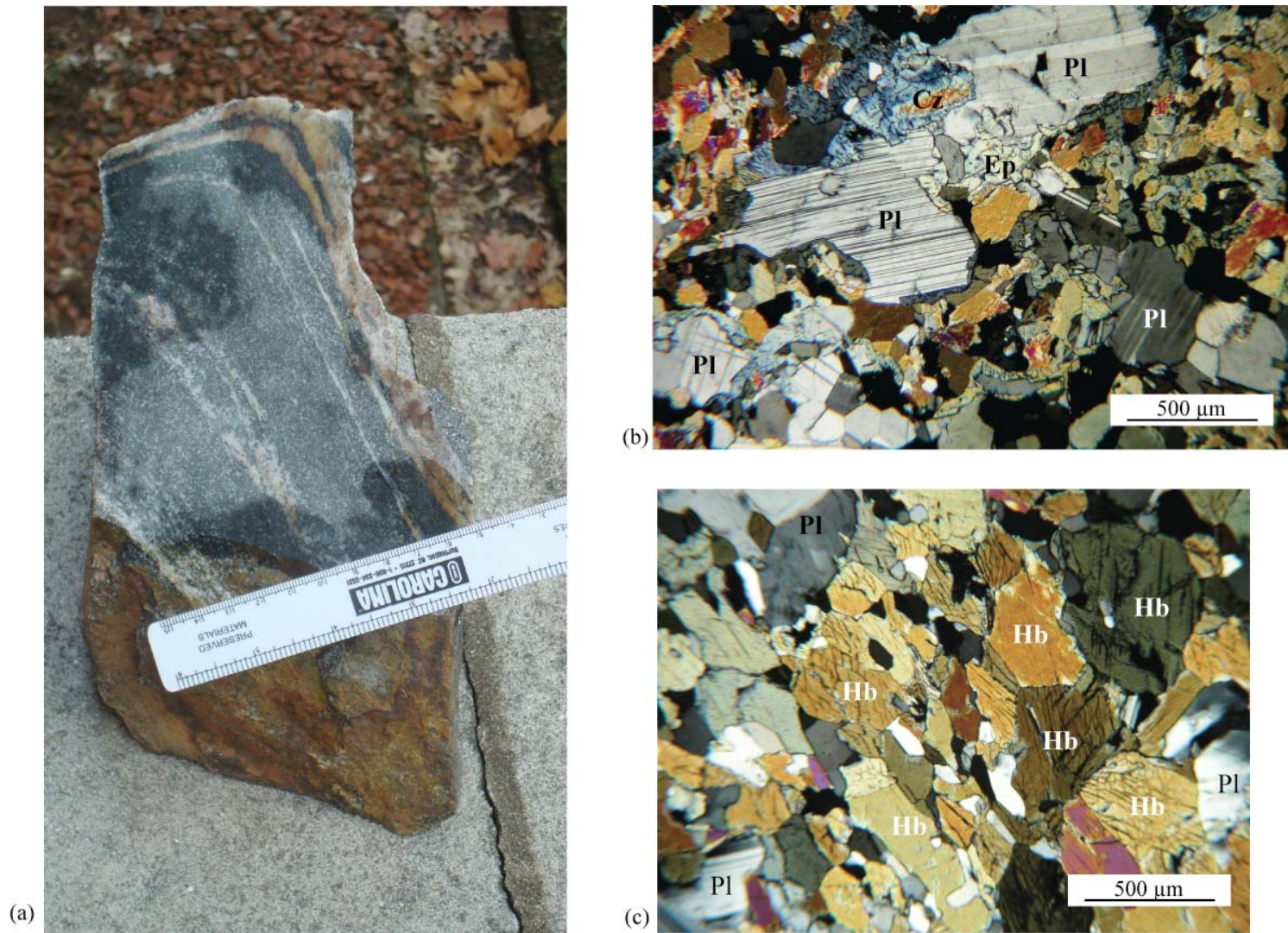
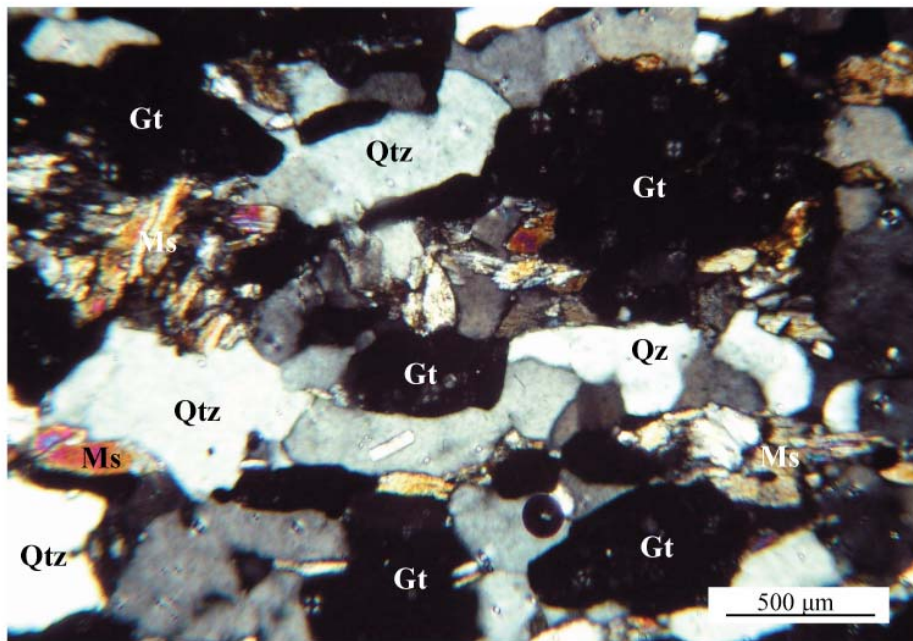


Figure 2-7. (a) Hand specimen of fine-grained lower Tallulah Falls Formation hornblende-plagioclase gneiss showing open folding of felsic layering. Hand specimen from station R 50, in small tributary near Cow Branch Creek southeast of Plateau, North Carolina. (b) Photomicrograph of large plagioclase grains in fine-grained hornblende plagioclase matrix. Symplectic intergrowths of clinozoisite and epidote occur between hornblende and plagioclase grains, indicative of retrograde metamorphism. (c) Photomicrograph of hornblende grains showing 60° and 120° cleavage. Mineral abbreviations: Pl = plagioclase, Hb = hornblende, Cz = clinozoisite, Ep = epidote.



(a)



(b)

Figure 2–8. (a) Top of gondite interlayer in lower Tallulah Falls Formation biotite gneiss at station H8 near Jacob Fork River, showing blocky resistant weathering and dark gray to black outer rind. Gondite erodes to produce dark resistant clasts in clayey soils derived from biotite gneiss. (b) Photomicrograph in XPL showing subhedral garnets between polygonal quartz, fine-grained biotite, and muscovite. Mineral abbreviations: Qtz = quartz, Gt = garnet, Ms = muscovite.

platy minerals (Fig. 2–8b). In thin section garnets are subhedral and evenly distributed throughout the quartz-dominated matrix. Minor amounts of biotite, muscovite, and plagioclase are distributed throughout the thin section. This unit was originally mapped as one layer (Goldsmith et al., 1988), but several layers were mapped in this area and to the south (Byars, 2010). Thickness varies from 10 to 25 cm so its thickness is exaggerated to be able to depict it on the geologic map (Plate 1).

EASTERN INNER PIEDMONT-CAT SQUARE TERRANE

Prior to the study by Bream (2003) the Cat Square terrane was previously unknown and the Brindle Creek thrust sheet was mapped as a repeated section of the Tallulah Falls Formation (e.g. Giorgis, 1999). Discovery of a mixed Laurentian and Gondwanan detrital zircon assemblage in the Brindle Creek thrust sheet metasediments indicated the presence of a genetically different sequence of rocks. Further age dating of Brindle Creek thrust sheet Walker Top, Toluca, and Cherryville Granites revealed crystallization ages ranging from 407 Ma to 325 Ma, significantly younger than Tugalo terrane plutons. Merschat and Hatcher (2007) postulated the Cat Square terrane represents the deformed equivalent of a remnant ocean basin receiving sediments from both Laurentian and peri-Gondwanan source terranes. Pelitic schists and psammitic rocks are interpreted to represent flysch sequences formed during the closing of the Cat Square basin. The presence of 430 Ma detrital zircons delimits the maximum age for sedimentation (Bream, 2003).

Cat Square Sillimanite Schist

The Cat Square terrane sillimanite schist is the most abundant lithologic unit in the map area; its presence is typically associated with topographically higher areas than biotite gneiss/metagraywacke (Fig. 2–1, Fig. 2–2a, Fig. 2–2b, Fig. 2–9a and Fig. 2–9b). Sillimanite



(a)



(b)

Figure 2-9. (a) Foliated Cat Square terrane garnet-sillimanite schist at station R 36 in field near John Grace Church Road, 100 m west of the Brindle Creek fault. Outcrop and soils appear reddish-purple due to the presence of bluish sillimanite and almandine garnet. Leaching of iron from garnet oxidizes to produce the reddish hue present in mature soils. Photo is looking north-northwest along trend of foliation. (b) Large outcrop of sillimanite schist at station LV 3, on top of Baker Mountain in Baker Mountain Park near Probsts Crossroads, North Carolina. Large exposures of blue-grey sillimanite form resistant outcrops holding up higher ridges.

schist is a silver-blue to medium-gray, fine- to coarse-grained, porphyroblastic garnet-sillimanite schist (Fig. 2–9a). Typical minerals include garnet, sillimanite, quartz, alkali-feldspar, plagioclase (An_{26}), opaques, \pm muscovite \pm zircon and ilmenite (Fig. 2–10a and 2–10b). Sillimanite occurs as fibrous and prismatic crystal clusters up to 10 cm long, tracing the dominant S_2 regional foliation. Garnet sizes range from 1 mm up to 5 cm and are commonly euhedral to subhedral and are rotated or fractured due to progressive deformation (Fig. 2–10a). Interlayers of quartzo-feldspathic gneiss (metasandstone), 3 cm to 1 m thick, occur in the sillimanite schist and contain sheared asymmetric garnets. Quartz-muscovite pegmatites typically occur in the sillimanite schist, crosscutting the regional foliation. Typically euhedral books of muscovite, up to 10 cm, and large quartz fragments were observed in float.

Sillimanite schist weathers to a coarse-grained saprolite composed of sillimanite, muscovite, garnet, and quartz giving soils an unique weathering characteristics. Immature soils are typically reddish-purple and contain coarse fragments of garnet and sillimanite with outcrops exhibiting a crumbly weathering profile (Fig. 2–9a). Mature soils occurring in well-tilled agricultural areas are dark reddish-purple and locally contain quartz fragments and sillimanite crystals.

Map-scale mafic complexes and amphibolite bodies are recognized in the sillimanite schist south of the study area where Byars (2010) identified layers of metadiorite, amphibolite, and metagabbro. These rocks were not observed in this study area.

Cat Square Biotite Gneiss

Cat Square terrane biotite gneiss is the least abundant lithology present in the study area, associated with lower topography, and typically outcrops in creeks (Fig. 2–11a and Fig. 2–11b).

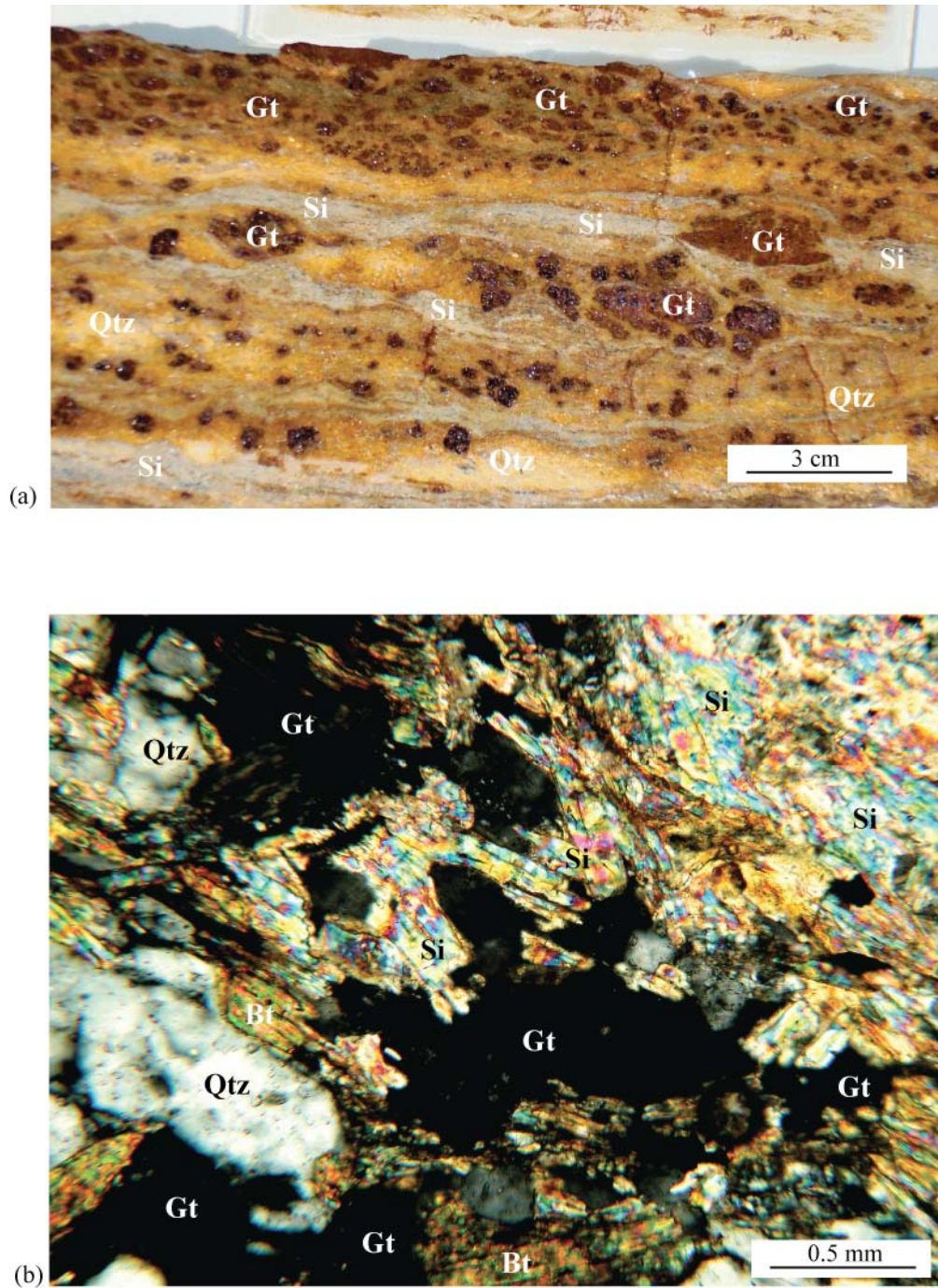
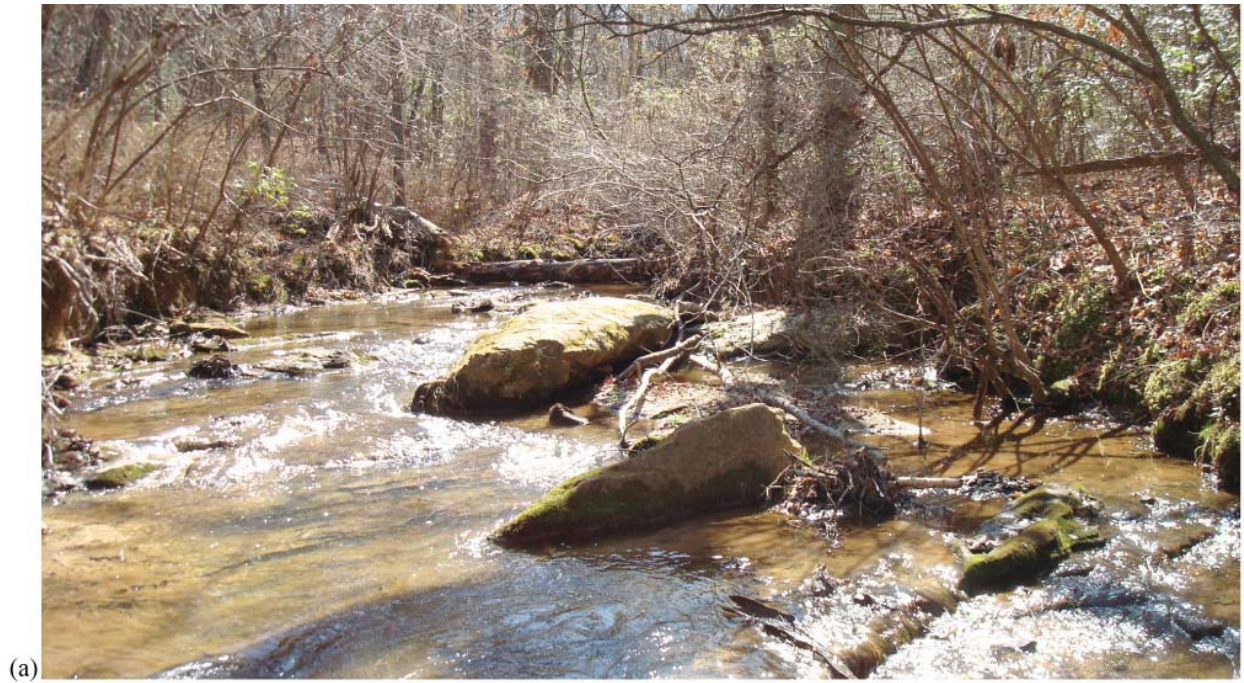


Figure 2–10. (a) Cat Square terrane sillimanite schist at station H1. Sample from roadside outcrop off NC state route 1132, northwest of Probsts Crossroads, North Carolina. Asymmetric garnets entrained in the S-C fabric vary in size and layered density. Bluish-gray sillimanite occurs between garnets and yellow-beige colored feldspar and quartz. (b) Photomicrograph of sample collected from the exposure in Figure 2–9a in XPL. Quartz and asymmetric garnets are dispersed between well-foliated, sillimanite, biotite, and muscovite. Mineral abbreviations: Si = sillimanite, Qtz = quartz, Gt = garnet, and Bt = biotite.



(a)



(b)

Figure 2–11. (a) Southwest-dipping outcrops of Cat Square terrane biotite gneiss at station B 90 in creek southeast of Lynn Mountain, off NC State Route 1002, near Banoak, North Carolina. (b) Saprolite exposure of southeast-dipping Cat Square terrane biotite gneiss at station B 92, downstream from station B 90. White, felsic layers contrast with grayish-black biotite rich interlayers, and are truncated by brownish-red alluvium.

Distinct lithologic differences occur between the lower Tallulah Falls and the Cat Square terrane biotite gneiss/metagraywacke, specifically the lack of amphibolite, amphibolite boudins, and ultramafic rocks. The Cat Square terrane metagraywacke exhibits alternating felsic and biotite-rich layers (Fig 2–12a) that range in thickness from 1 cm to 20 cm with feldspar and garnet porphyroblasts. Typical minerals present include biotite, quartz, plagioclase (An₃₂), alkali-feldspar, and muscovite with minor amounts of garnet, sillimanite, apatite, zircon, opaques, and ilmenite (Fig 2–12b and Fig. 2–12c). Discordant and concordant migmatitic layers occurring in this unit are composed of quartz \pm feldspar \pm muscovite, and range in thickness from 25 cm to 1 m.

Walker Top Granite

Giorgis (1999) named the Walker Top Granite for rocks occurring on Walker Top Mountain in Burke County, North Carolina, which lies northeast of the map area. Goldsmith et al. (1988) previously mapped the Walker Top as a less deformed equivalent of the Ordovician Henderson gneiss, although recent geochronology proved the Walker Top to have a Devonian to Mississippian age. A SHRIMP age gathered from an outcrop located south of the study area in Vale, North Carolina, indicated a crystallization age of 355 Ma (Byars, 2010).

Walker Top plutons vary in size and shape in this study area (Plate 1, Fig. 2–1). Three large linear plutons occur; two nearest the Brindle Creek fault and one in the interior of the Brindle Creek thrust sheet. A large asymmetric pod occurs in the interior of the study area, its contacts are folded within the regional country rock. Smaller isolated linear bodies were also observed during this study. All plutons display a north-northwest trend.

The Walker Top is a medium-to dark-gray, garnet-bearing, megacrystic quartz-biotite-plagioclase-alkali feldspar gneiss (Fig 2–13a). Local enclaves of migmatitic metagraywacke and

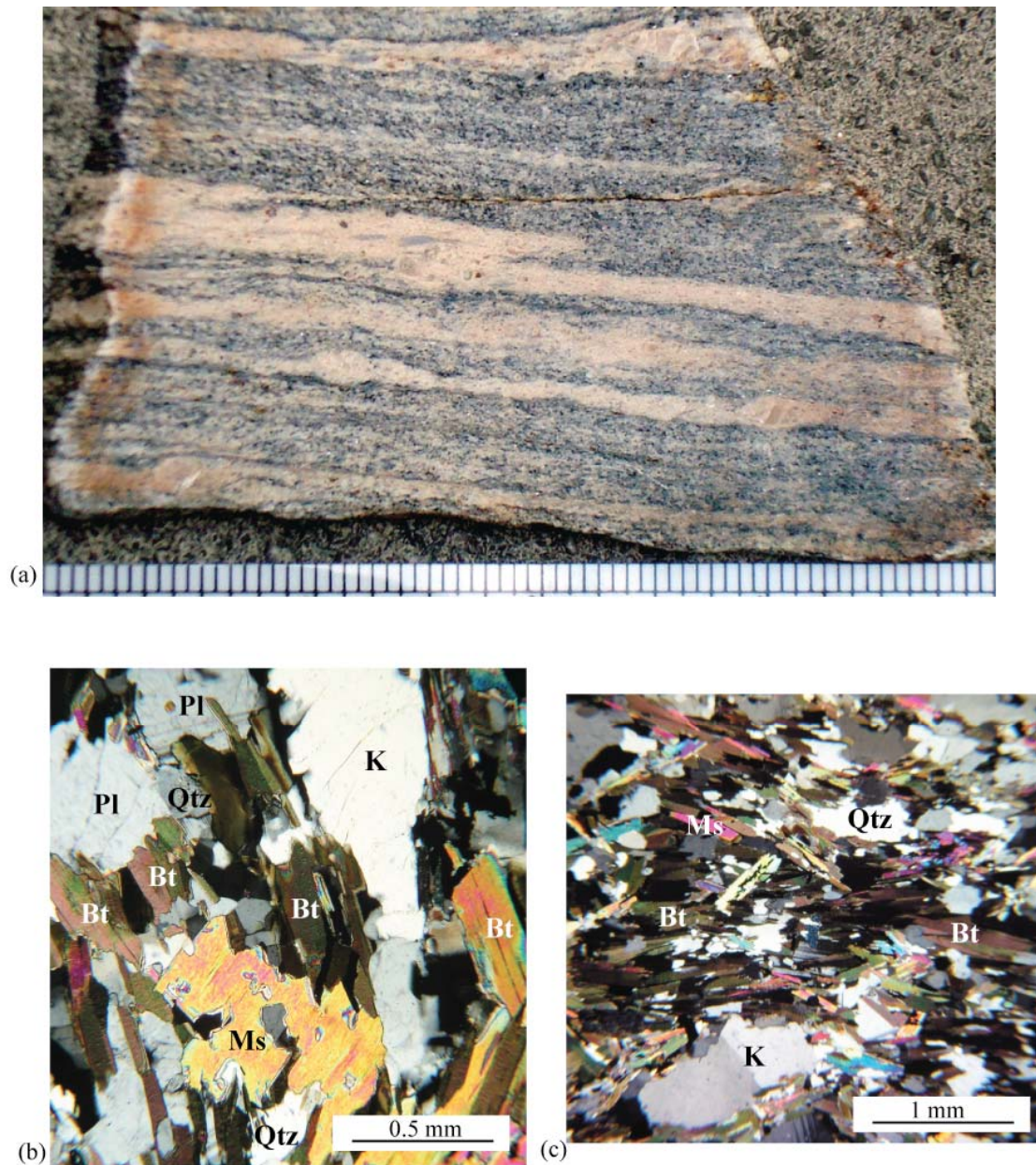


Figure 2-12. (a) Cat Square terrane biotite gneiss from station LV 284 in creek west of Faith Olive Church, southwest of Advent Crossroads, North Carolina. Felsic bands of quartz, alkali-feldspar and plagioclase (An_{32}) preserve asymmetric folding and rotated porphyroclasts. (b) Photomicrograph of thin section of sample in (a) in XPL, cut parallel to lineation. Anhedral quartz and plagioclase grains are dispersed within biotite and muscovite matrix. (c) Biotite and muscovite-rich matrix with interspersed quartz grains from station LV 284. Mineral abbreviations: Qtz = quartz, Pl = plagioclase, K = alkali feldspar, Bt = biotite, and Ms = muscovite.

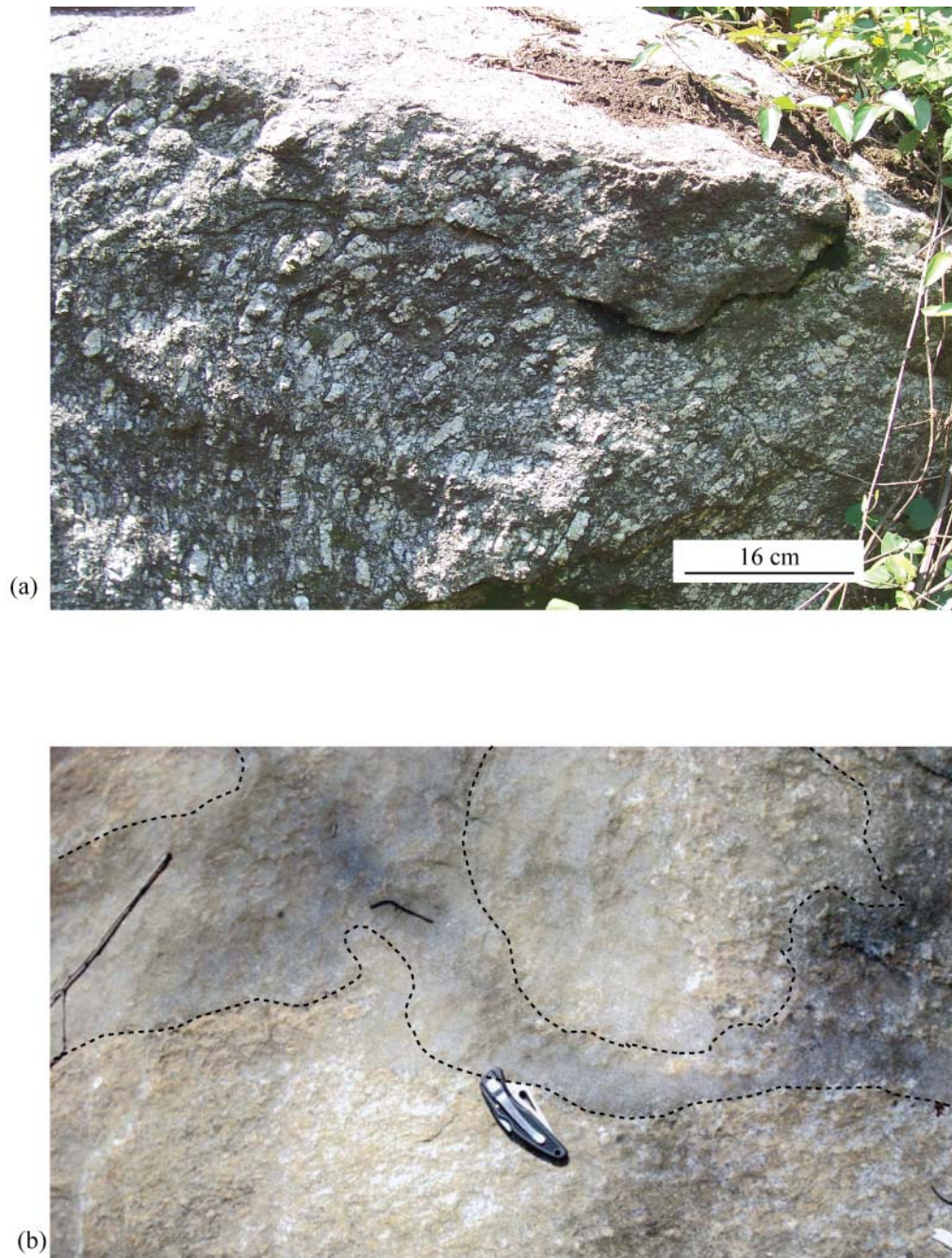


Figure. 2–13. (a) Walker Top Granite at station R 90 in small linear outcrop near Brindle Creek fault off NC State Route 2036, south of Plateau, North Carolina. Large megacrysts are aligned subparallel to foliation and folded by an open F_3 fold. (b) Fine-grained biotite schist xenolith in Walker Top Granite at station B 21, behind Sardis Church off NC Highway 10, east of Probsts Crossroads, North Carolina.

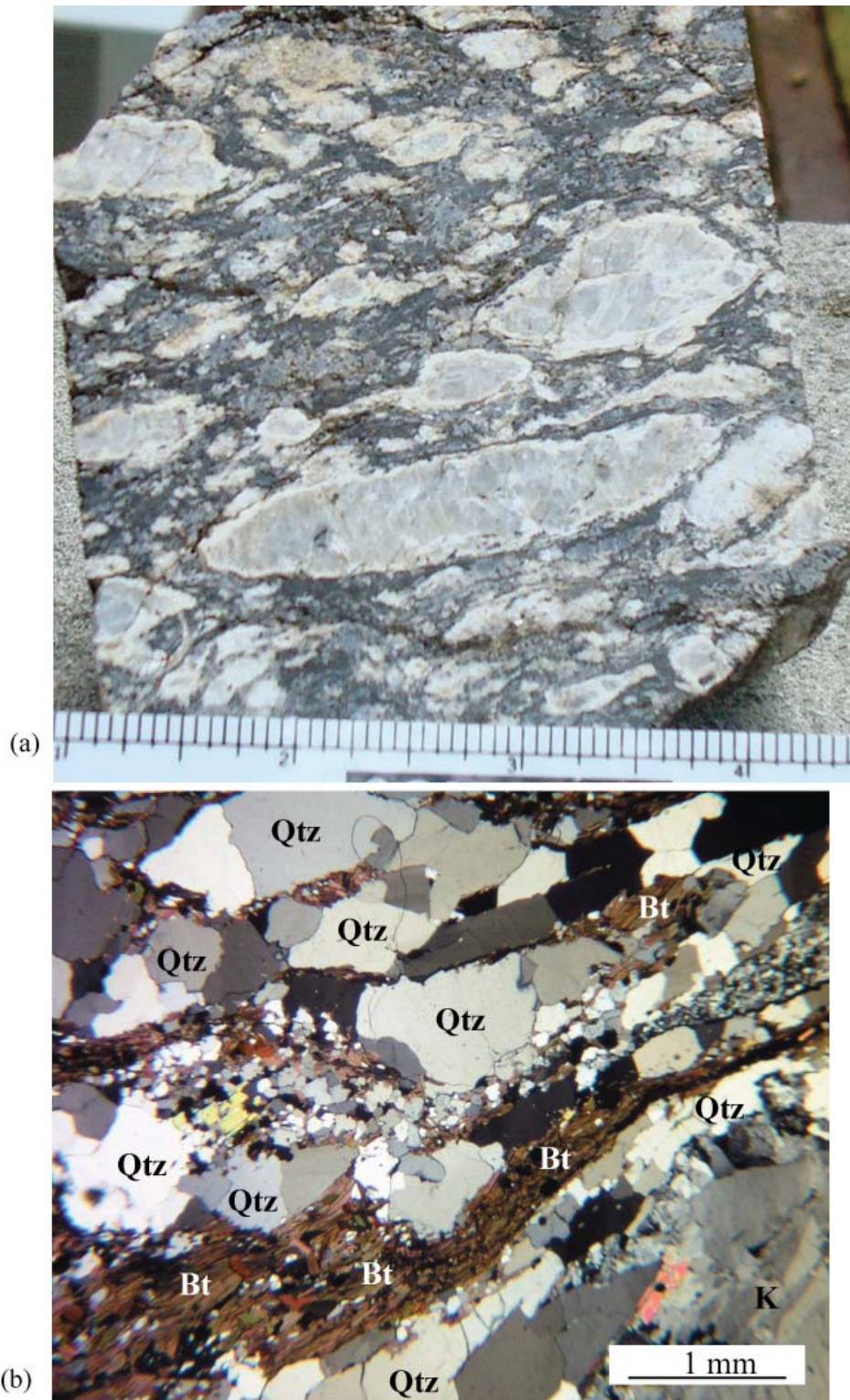


Figure 2–14. (a) Sawed hand specimen of Walker Top Granite from station LV 29 in large pluton in center of study area. Large alkali-feldspar megacrysts, up to 6 cm, are rimmed by myrmekite and are parallel to the S₂ foliation. (b) Photomicrograph of Walker Top Granite matrix displaying alternating layers of medium- to coarse-grained polygonal quartz, biotite, and alkali-feldspar. Mineral abbreviations: Qtz = quartz, Bt = biotite, and K = alkali feldspar.

aluminous schist occur within these plutons (Fig. 2–13b). Rotated porphyroclasts of alkali feldspar are round to tabular (2–14a), commonly exhibit myrmekitic rims, and are aligned subparallel to S_2 foliation (Fig. 2–14a). Walker Top matrix is fine- to medium-grained and contains alkali-feldspar, biotite, plagioclase (An_{28-34}), and quartz (Fig. 2–14b). Petrographic analysis shows myrmekitic rims surrounding alkali-feldspar (Fig. 2–14a) consist of fine- to medium-grained polygonal quartz crystals. Modal analysis of two samples from this study, LV 11 and B 185, plot in the granite field on the IUGS classification chart (Figure 2–15; Table 2–3; Streckeisen, 1976).

MESOZOIC FEATURES

Diabase dikes

Diabase dikes intruded ~199 Ma (Hames et al., 1999) and are an integral component of the Appalachian Inner Piedmont and Carolina Superterrane. They are consistently orientated ~N45°W and are near vertical (Ragland et al., 1983) in the southern Appalachians, with a crossing N-S set tracing major crustal tension fractures resulting from the breakup of Pangea. Diabase dikes form linear outcrop patterns that reach a width of 3 meters so their outcrop extent is exaggerated in the geologic map to be able to show them (Fig. 2–16a; Plate 1). Dike margins or evidence of a chilled margin were not observed in the field. The lack of a chilled margin has been attributed to rapid injection associated with decompression melting and magma fractionation (Hatcher, 2006). Exposures occur as boulders and isolated outcrops of dark black, fine-grained diabase (Fig. 2–16a and Fig. 2–16b). Olivine-dominated thin sections reveal an aphanitic, ophitic texture between olivine, clino- and orthopyroxene, and plagioclase laths (An_{42}) (Fig. 2–16c).

Table 2–3. (a) Modal analyses of two Cat Square terrane Walker Top Granite, samples B 185 and LV 11.

STATION COUNTS	B 185 2399	LV 11 2096
Plagioclase	16.5 (An ₂₈)	17.5 (An ₃₄)
Quartz	33.6	32.4
Biotite	18.3	14.2
K-feldspar	12.8	16.9
Muscovite	7.0	7.1
Hornblende	1.3	1.0
Garnet	2.0	2.7
Myrmekite	6.3	4.7
Epidote	0.5	1.0
Opx	0	0
Cpx	0	0
Opakes	1.3	2.0
Apatite	0	0.2
Zircon	0	0.3
Pyrite	0	0
Sphene	0	0
PERCENT	99.60	100.0

Plagioclase compositions were estimated using the Michel-Levy method (Nesse, 1991).

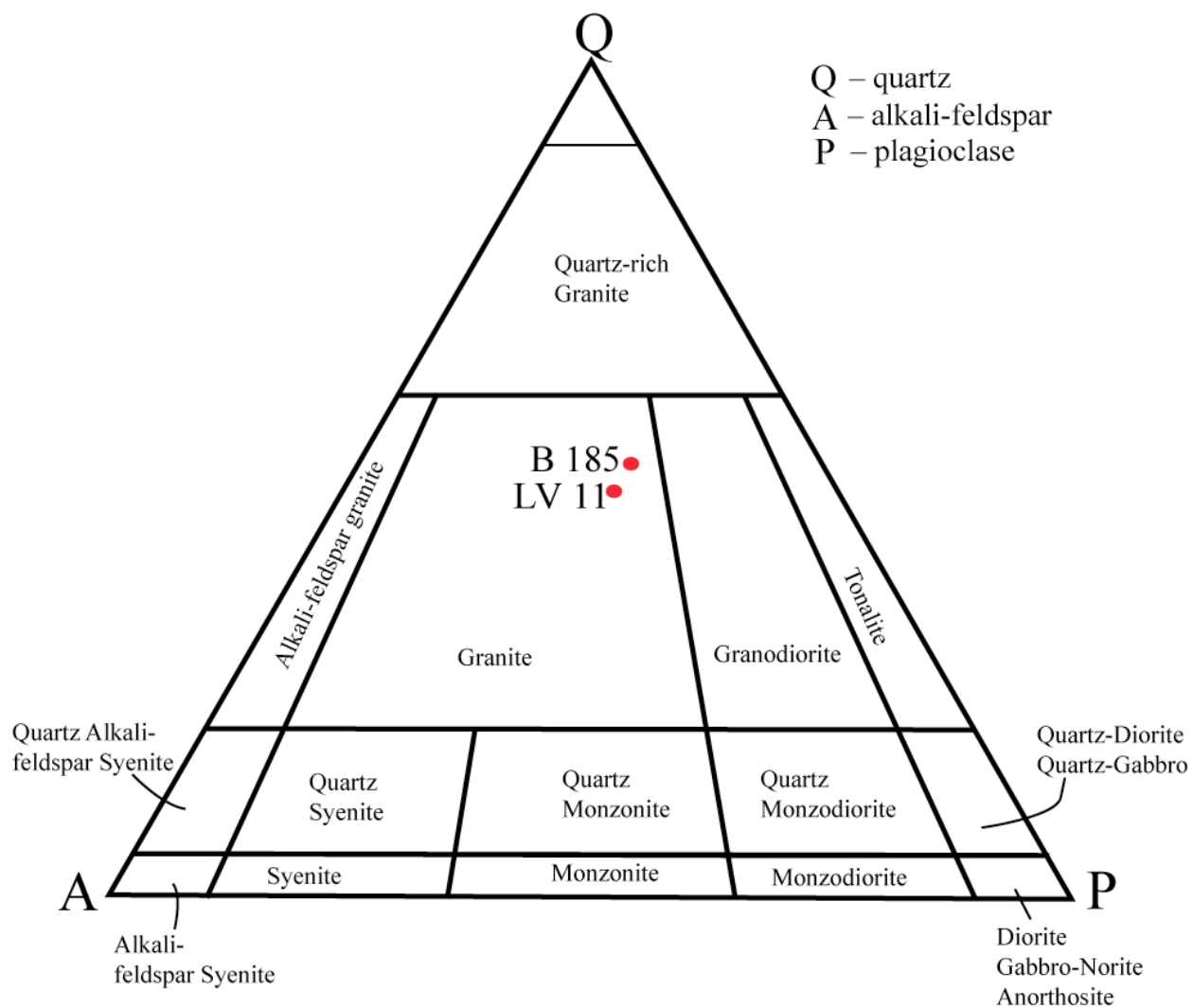


Figure 2–15. IUGS classification of the Cat Square terrane Walker Top Granite from station B 185 and LV 11.

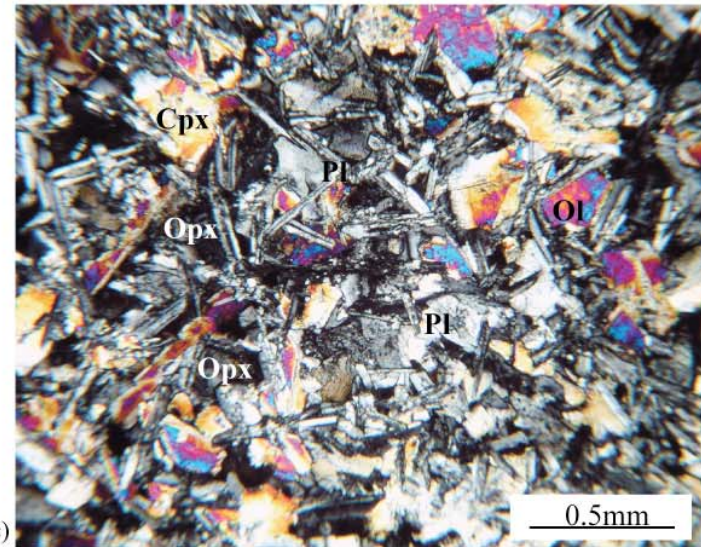


Figure. 2-16. (a) Jurassic diabase dike outcrop off of NC State Route 2035, southwest of Plateau, North Carolina. (b) Fine-grained diabase boulder showing orange-brown weathering rind and concoidal fracturing from same location as Figure 2-15a. (c) Photomicrograph of ophitic texture of plagioclase laths in a matrix of olivine, ortho-, and clinopyroxene. Mineral abbreviations : Pl = plagioclase, Cpx = clinopyroxene, Opx = orthopyroxene, and Ol = olivine.

Cataclasite

The Mesozoic silicified cataclasite first identified by Goldsmith et al. (1988) in this map area trends N65°E, dips steeply to the southeast, and cuts Cat Square terrane sillimanite schist (Fig. 2–1). Cataclasite formed coeval with Mesozoic diabase dike intrusion, 199 Ma (Garihan, 1993; Hames et al., 2000). Silicified cataclasite formed in a multiply reactivated brittle fault zone as a result of increased fluid flow. The outcrop trend of this unit is easily traceable by the prominent and often large gravel to boulder size fragments (Fig. 2–17a). Silica cement, precipitated from fault fluids, binds the fragments within the cataclasite. Angular fragments range from fine- to coarse (Fig. 2–17b, Fig. 2–17c, and Fig. 2–17d). Evidence of brittle deformation and pressure solution are present (Fig. 2–17b, Fig. 2–17c, and Fig. 2–17d).

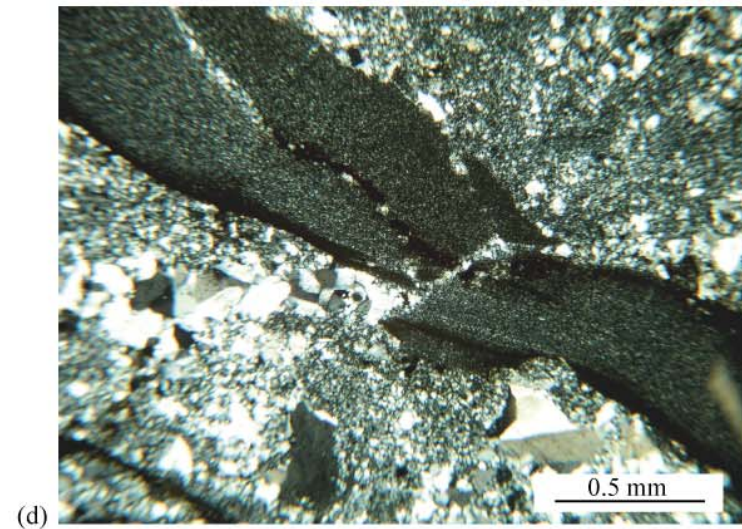
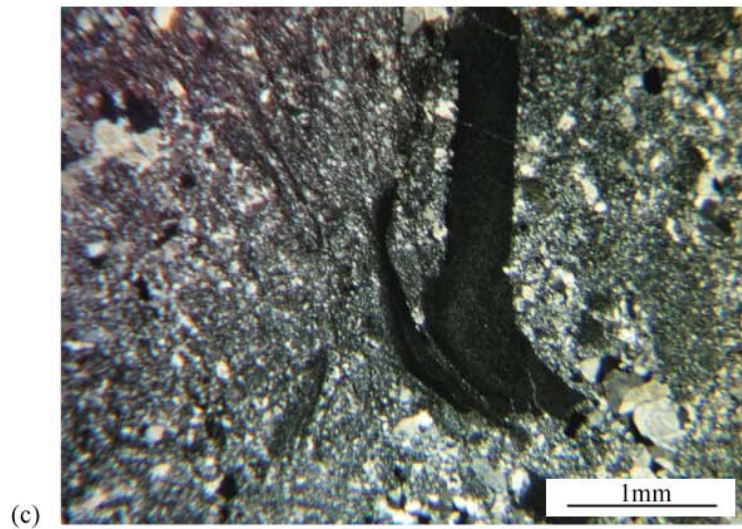


Figure 2–17. (a) Blocky weathering of silicified cataclasite at station LV 29 along Greedy Highway, northwest of Probsts Crossroads, North Carolina. Sledgehammer for scale. (b) Sawed hand specimen showing angular clasts fractured clasts and veins. Rocks cut perpendicular to strike of the fracture surface. (c) Photomicrograph showing angular quartz fragments of varying size and fine-to-medium crystalline quartz cement. (d) Fractured quartz vein filled by recrystallized fine-grained quartz.

CHAPTER 3

P-T ESTIMATES NEAR THE WESTERN NEWTON WINDOW

INTRODUCTION

Rocks of the Appalachian Inner Piedmont and eastern Blue Ridge comprise the Neoacadian metamorphic core of the southern Appalachians (Fig. 3–1). The three principal southern Appalachian orogenic events, the Taconic, Neoacadian, and Alleghanian, are recorded in Tugalo terrane rocks of the Newton window. The younger Cat Square terrane contains evidence of the Neoacadian and Alleghanian orogenies and associated metamorphism. Although the two terranes differ in age and tectonic histories, they are unified by progressive deformation and high-grade metamorphism during the Neoacadian orogeny (360–345 Ma) (Fig. 3–1) (Davis, 1993; Bier, 2001; Merschat and Kalbas, 2002; Merschat et al., 2005; Byars, 2010) and sillimanite I during the Alleghanian orogeny (325–300 Ma) (Dennis and Wright, 1997a).

Metamorphic grade increases across the Inner Piedmont. Near the Brevard fault zone, metamorphic grade increases from garnet and staurolite–kyanite to the northwest, to sillimanite and localized granulite facies across the broad core of the IP, decreasing to sillimanite I and lower grade to the east towards the Kings Mountain shear zone and Carolina Superterrane (Reed and Bryant, 1964; Bryant and Reed, 1970; Goldsmith et al., 1981; Butler, 1991; Bier et al., 2002; Byars, 2010) (Fig. 3–2). Alleghanian brittle reactivation along the Brevard fault zone resulted in retrograde metamorphism (Hatcher, 1993). Likewise, conditions decrease along the Central Piedmont suture, locally decreasing to staurolite and garnet grade (Goldsmith et al., 1988; Butler, 1991) (Fig. 3–2 and Fig. 3–3). Inner Piedmont metamorphic isograds parallel regional structures and faults, suggesting regional metamorphism occurred prior to or contemporaneously

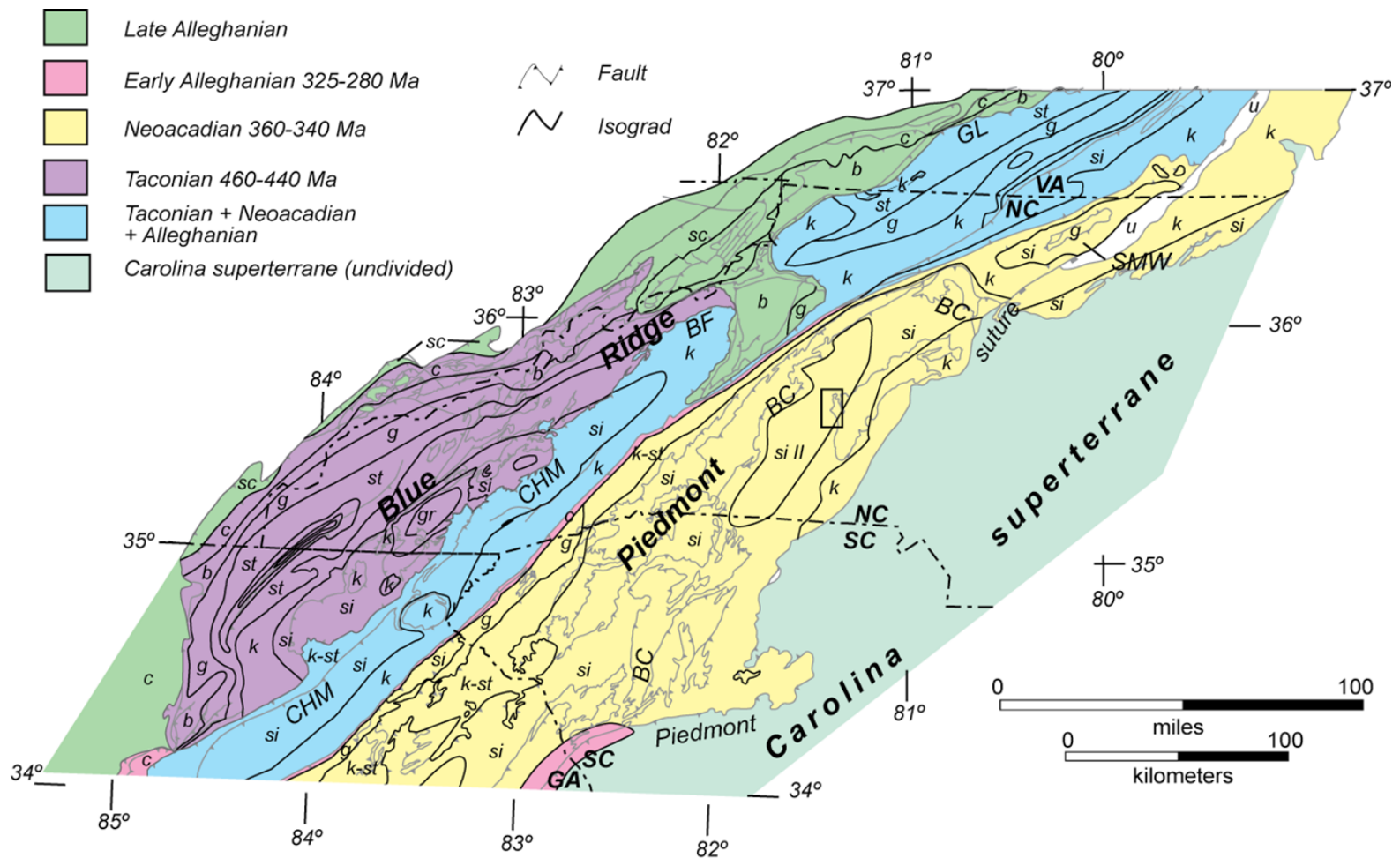


Figure 3-1. Metamorphic domains depicting zones components of the southern Appalachian Blue Ridge and Inner Piedmont with shared tectonothermal events (modified from Merschat, 2009). Extent of the domains was defined from areas with similar zircon rim ages, continuation of metamorphic isograds, and structural features. The Alleghanian event is more extensive than depicted in this diagram, but has been recorded throughout the Inner Piedmont (see Fig. 3-3). Black box outlines study area. Index mineral abbreviations: u-unmetamorphosed. sc-sub-chlorite. c-chlorite. b-biotite. g-garnet. st-staurolite. k-st-kyanite+staurilite. k-kyanite. si-sillimanite. si II-sillimanite II. gr-granulite. BC-Brindle Creek fault. BFZ-Brevard fault zone. BF-Burnsville fault. CHM-Chattahoochee-Holland Mountain fault. GL-Gossan Lead fault. SMW-Sauratown Mountain window.

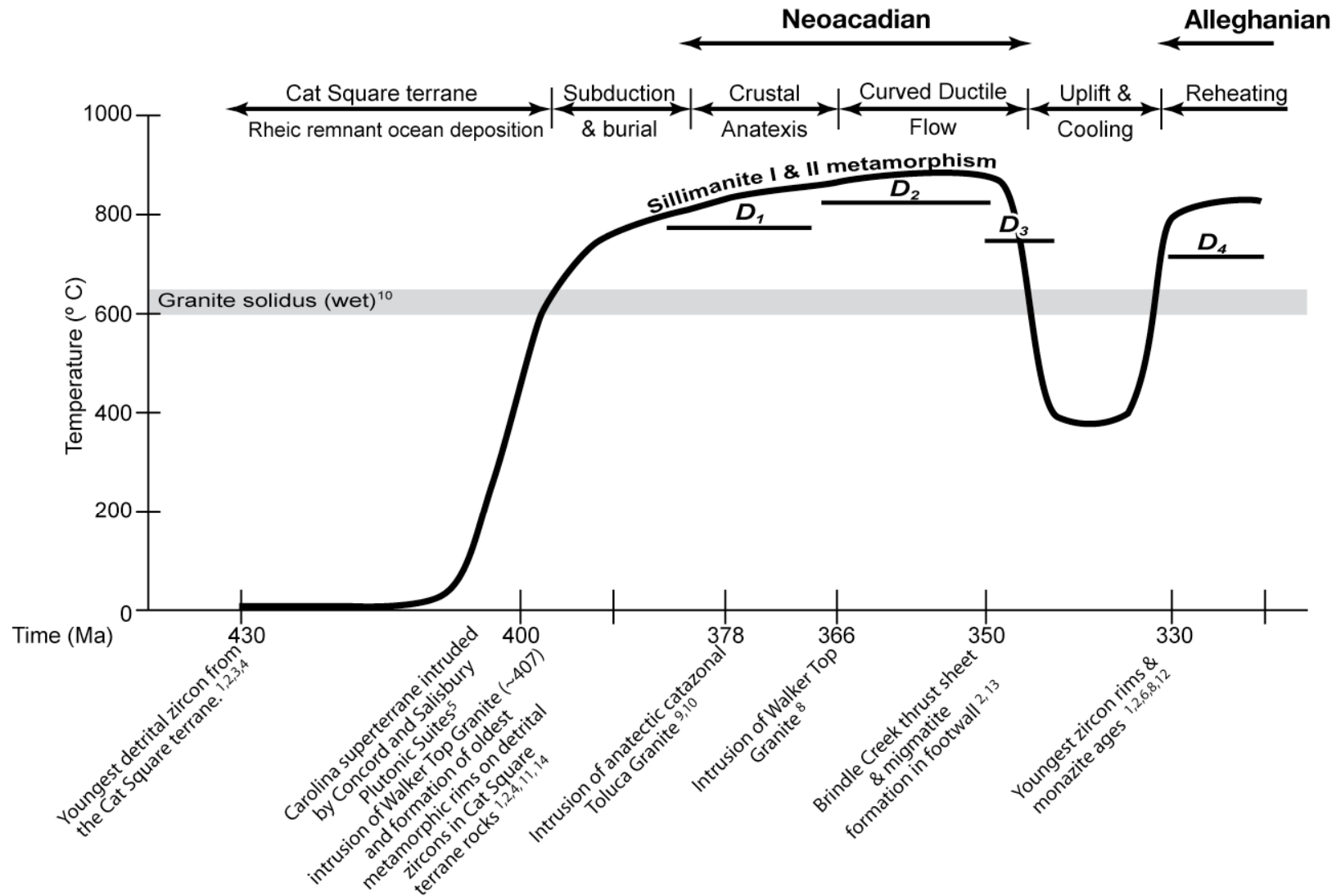


Figure 3–2. Tectonothermal time line for the Inner Piedmont. Data sources: 1–Bream (2002). 2–Bream (2003). 3–Bream et al. (2001). 4–Bream et al. (2004). 5–McSweeney et al. (1984, 1991). 6–Carrigan et al. (2001). 7–Davis (1993). 8–Dennis & Wright (1997a, 1997b). 9–Giorgis et al. (2002). 10–Luth et al. (1964). 11–Mapes (2002). 12–Mapes et al. (2002). 13–Mirante & Patino-Douce (2000). 14–Gatewood (2007). Figure modified from Hatcher and Mersch (2006) and Gatewood (2007).

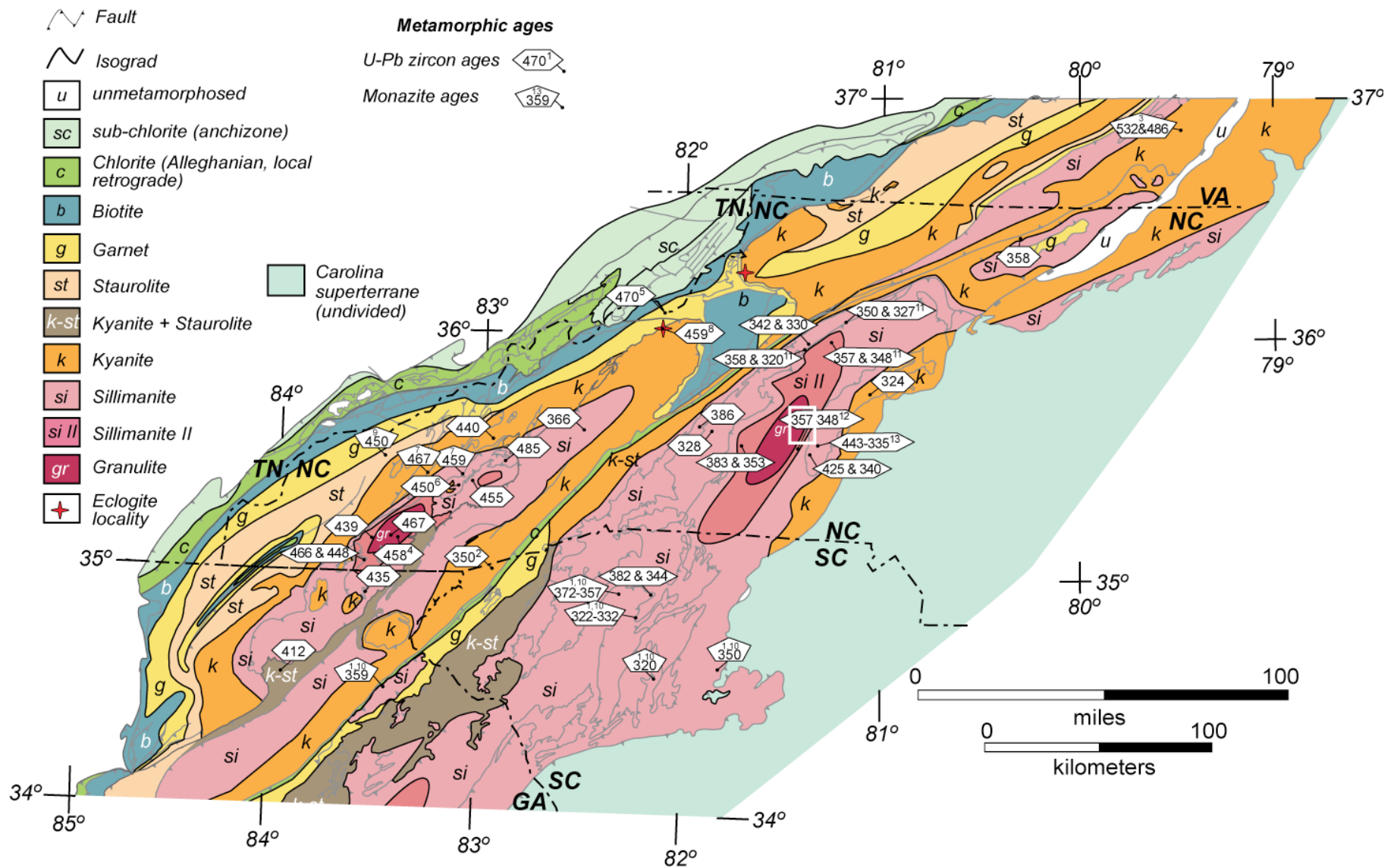


Figure 3-3. Metamorphic isograd map of the southern Appalachian Blue Ridge and Inner Piedmont compiled by Mersch et al. (2009) (Hadley and Goldsmith, 1963; Carpenter, 1970; Hadley and Nelson, 1971; Rankin et al., 1972; Espenshade et al., 1975; Goldsmith et al., 1988; Mersch et al., 1988; Eckert et al., 1989; Hopson et al., 1989; Butler, 1991; Hatcher and Goldberg, 1991; Quinn, 1991; Nelson et al., 1998; Settles, 2002; Higgins et al., 2003; Mersch et al., 2003; Tull and Holm, 2005; Hatcher and Mersch et al., 2006; Hatcher et al., 2007; Tull, 2007). Sources of zircon rim and monazite data are 1–Dennis and Wright (1997a,b); 2–Carrigan et al. (2003); 3–Hibbard et al. (2003); 4–Moecher et al., (2004); 5–Ownby et al. (2004); 6–Berquist et al. (2005); 7–Moecher et al. (2005); 8–Miller et al., (2006); 9–Corrie and Kohn (2007); 10–Dennis (2007); 11–Gatewood (2007); 12–Byars et al. (2008a); 13–Mersch et al. (in prep.). Unlabeled ages are data presented in Mersch et al. (2009). Ar/Ar, Sm/Nd, and Rb/Sr mineral ages are from Dallmeyer et al. (1986); Dallmeyer (1988); Connelly and Dallmeyer (1993); Goldberg and Dallmeyer (1997). White box outlines study area. Figure modified from Mersch et al. (2009).

with emplacement. Rocks in this study area occur in the high temperature core of the IP, represented by the widespread presence of the index mineral sillimanite. The ubiquitous presence of sillimanite puts these rocks well into the sillimanite zone or upper amphibolite facies conditions. Likewise, IP rocks are pervasively migmatitic. Garnet zoning profiles from both the eastern and western Inner Piedmont indicate the IP was metamorphosed during a single prograde metamorphic event (Davis, 1993; Bier et al., 2002; Merschat and Kalbas, 2002). Previous peak P-T estimates range from 500° – 800° C and 3–7 kbar (Davis, 1993; Mirante and Patino-Douce, 2000; Bier et al., 2002; Merschat, 2003), indicative of a Barrovian P–T path which is typical of a path encountered during crustal thickening during collision at convergent boundaries, followed by erosion and thermal relaxation (Spear, 1993).

The purpose of this chapter is to report new P–T estimates for psammitic rocks occurring in the vicinity of the western Newton window, both in the Cat Square and Tugaloo terrane, and relate these data to those collected by others. This chapter will describe relationships of P–T conditions across the Brindle Creek fault, and re-evaluate the P–T–t path of the eastern Inner Piedmont in light of new Inner Piedmont geochronologic and P–T data.

TIMING OF METAMORPHISM

Eastern Blue Ridge, western Inner Piedmont, and rocks exposed within the Newton window consist of Tugaloo terrane rocks, and contain a Laurentian zircon assemblage (Bream et al., 2001). Three metamorphic peaks are recognized in the Inner Piedmont 360, 345, and 330 Ma (Fig. 3–2 and Fig. 3–3). In the South Carolina Inner Piedmont Dennis and Wright (1997a, 1997b) reported monazite ages of ~360 Ma and ~325 Ma, using conventional (TIMS) U–Pb methods reflecting Neocadian and early Alleghanian orogenesis. Mirante and Patino-Douce (2000) reported an electron microprobe U–Pb monazite age of ~330 Ma for IP granulite facies

metamorphism near Athens, Georgia. Carrigan et al. (2001) reported a summed probability age of ~352 Ma for ion microprobe zircon rims from the western IP and eastern Blue Ridge. A 342 Ma U-Pb ion microprobe age records growth of metamorphic zircon rims and coeval migmatite generation in intermediate and mafic metagneous rocks in the Brindle Creek fault footwall near Lenoir, North Carolina (Kalbas et al., 2002; Bream, 2003). Similarly, Gatewood (2007) reported SHRIMP U/Pb zircon rim ages of ~364 and 345 Ma from the Hibriten mylonite in the Brushy Mountains in the IP in northwestern North Carolina. Alleghanian ages of 330-325 Ma record the earliest thermal events connecting the Tugaloo, Cat Square, and Carolina terranes (Dennis and Wright, 1997a, 1997b).

FIELD AND PETROGRAPHIC OBSERVATIONS

Peak metamorphism occurred contemporaneously with peak deformation based on the equilibrium metamorphic assemblages mapped in the study area, each contributed significantly to the assemblage of geologic structures and minerals present in the study area (Fig. 3–4). Cat Square and Tugaloo terrane mineral assemblages indicate a high-temperature origin. Sillimanite schist is the most abundant rock type in the eastern Inner Piedmont and in this study area (Figs. 3–5 a, b). The presence of sillimanite and alkali-feldspar in Brindle Creek thrust sheet pelitic schist puts these rocks well into upper amphibolite facies conditions. A small untraceable layer of muscovite-sillimanite schist occurs in lower Tallulah Falls rocks in the Newton window. Commonly observed metamorphic accessory minerals include garnet, biotite, hornblende, and muscovite. The presence of similar metamorphic minerals across the Brindle Creek fault in the Cat Square and Tugaloo terranes suggests metamorphism occurred syn- to post-emplacement of faults. The presence of the second sillimanite isograd is based on the coexistence of sillimanite and alkali-feldspar (Chatterjee and Johannes, 1974). Byars (2010) recognized evidence of second

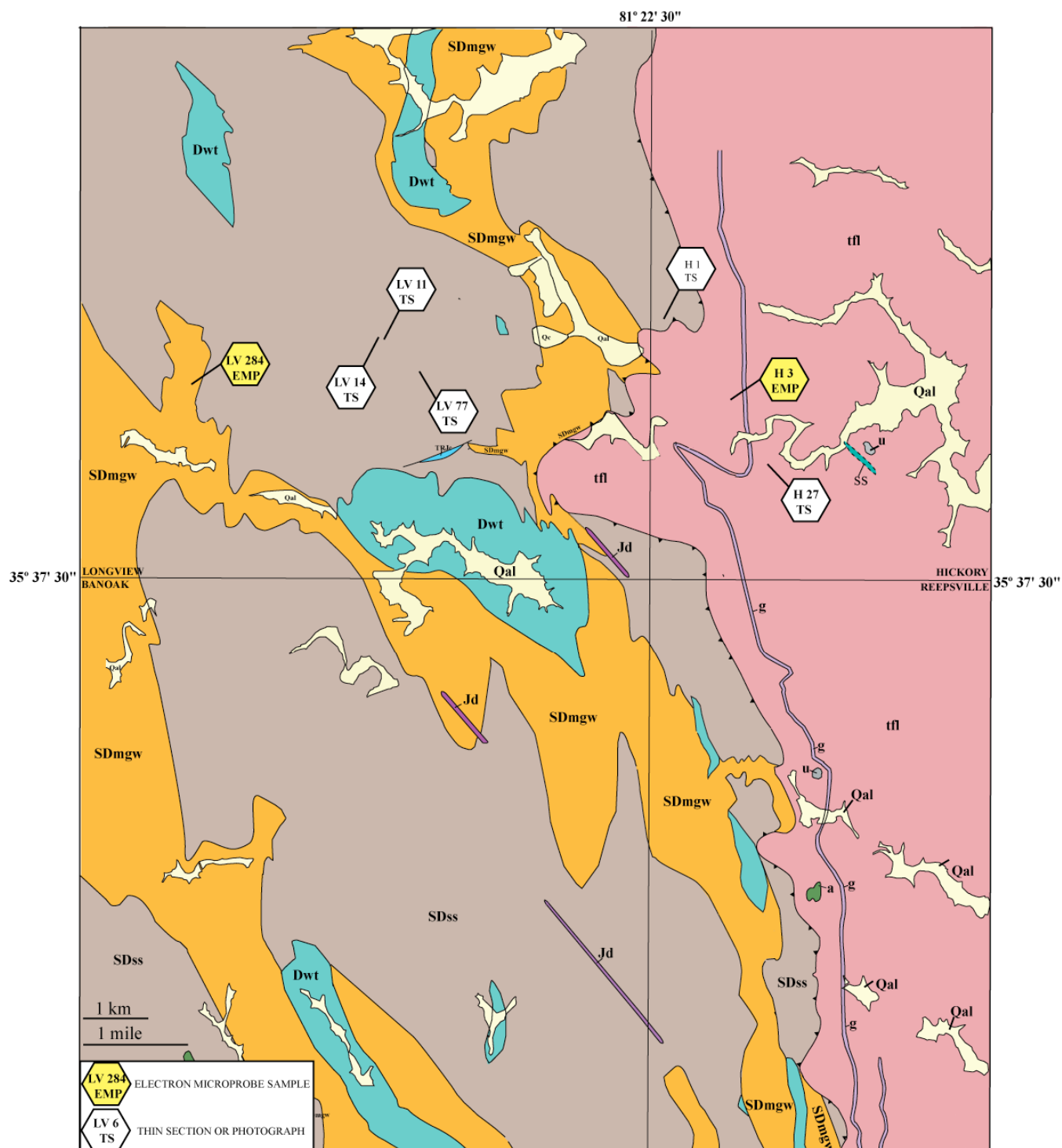


Figure 3–4. Simplified geologic map and location map of thin sections, photographs, and samples used for calibration of metamorphic conditions in this chapter. Cat Square terrane: SDss=Siluro-Devonian sillimanite schist, SDmgw=Siluro-Devonian metagraywacke, Dwt=Devonian Walker Top Granite. Tugaloo terrane: tfl=lower Tallulah Falls metagraywacke/hornblende gneiss, ss=lower Tallulah Falls sillimanite/mica schist, a=amphibolite, u=soapstone/altered ultramafic rock, g=gondite, TRJc=Triassic- Jurassic cataclasite, Jd=Jurassic diabase dike, Qc=Quaternary colluvium, Qal=Quaternary alluvial material.



Figure 3–5. (a) Large resistant outcrop of Cat Square terrane sillimanite-garnet schist on top of Baker Mountain at station LV 14, looking south. (b) Sawed hand-specimen of sillimanite schist near the Brindle Creek fault.

sillimanite, as well as granulite facies conditions in thin sections of rocks occurring south of the study area. Sillimanite occurs as fine- to coarse (<10 mm) fibrolitic to bladed crystals throughout the study area. Alkali-feldspar is present in sillimanite schist in the Cat Square terrane. Sillimanite- rich interlayers in lower Tallulah Falls Formation biotite gneiss contain muscovite and likely occur below the second sillimanite isograd. Likewise, the abundance of metamorphic hornblende in the lower Tallulah Falls rocks suggests amphibolite facies equilibration (Fig. 3–5b). Pyroxenes associated with mafic complexes south of the study area have been interpreted to be the product of granulite facies metamorphism (Byars, 2010).

MIGMATITE

All rocks across the Inner Piedmont contain migmatite (Giorgis, 1999; Merschat and Kalbas, 2002). Likewise, rocks in the vicinity of the Newton window display intense migmatization (Fig. 3–6). Griffin (1969) observed migmatite beneath the Six Mile thrust sheet in northwestern South Carolina. Hatcher (2002) and Merschat and Kalbas (2002) speculated the Brindle Creek thrust sheet was emplaced hot and the additional heat and crustal thickening produced a zone of intense footwall migmatization. In the Brushy Mountains, Kalbas (2003) indicated migmatites have a P-T range of 600-700° C and 3.0-7.7 kbar. Zircon rims in migmatite record metamorphic peaks at 342 and 330 Ma, indicating the timing of localized melting (Kalbas, 2003). In the study area migmatite occurs as concordant and discordant layers interfingering Cat Square and Tugaloo terrane rocks. Typical assemblages include fine- to coarse-grained quartz, feldspar, and muscovite. In some outcrops, late-stage melting crosscuts regional fabrics. The widespread presence of migmatite across the Inner Piedmont suggests conditions were above melting temperatures for quartz.

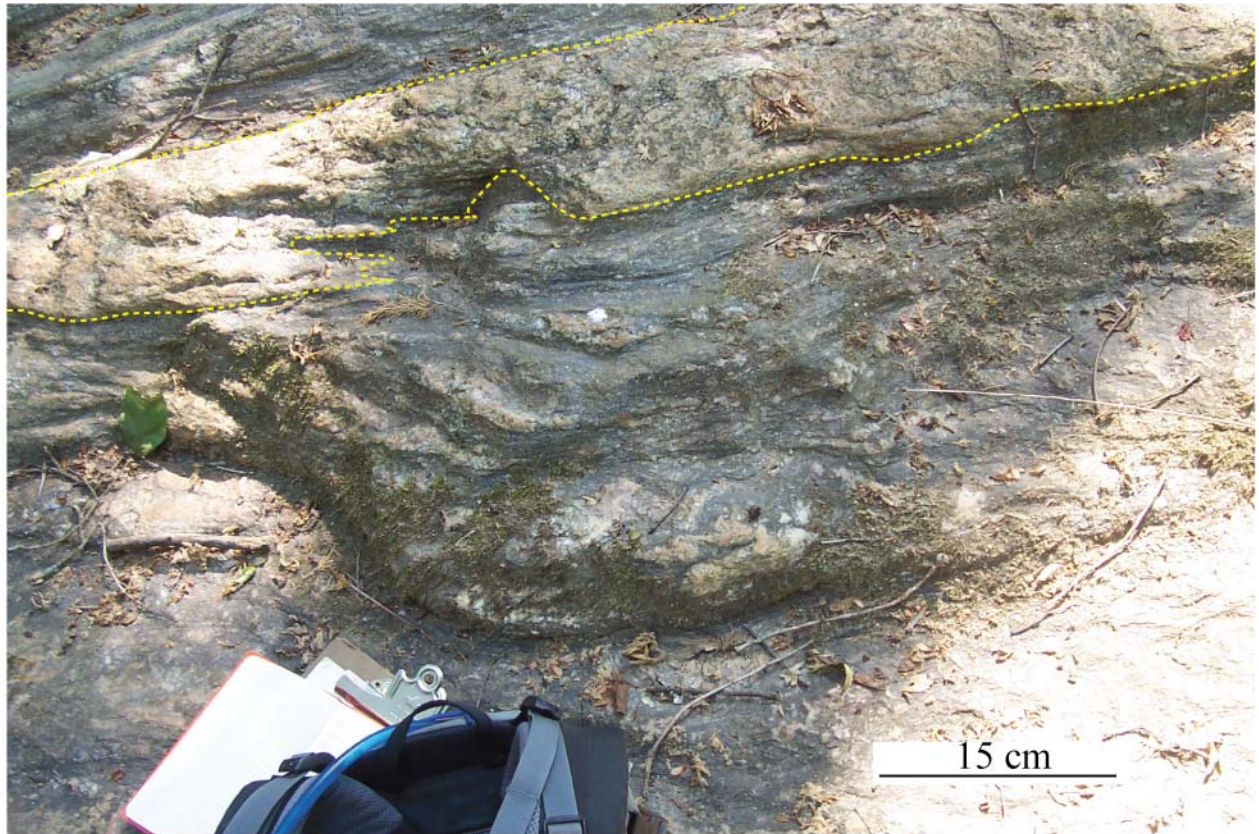


Figure 3–6. (a) Migmatite in lower Tallulah Falls Formation biotite gneiss at station H27 in the Jacob Fork River, east of the Catawba County line near Probst Crossroads, North Carolina. Here migmatite consists primarily of quartz and feldspar that crosscut regional foliation.

PEGMATITE

Pegmatites are commonplace in the high temperature Inner Piedmont and intruded contemporaneously with peak deformation and metamorphism. While some contacts between pegmatite and country rock occur parallel to structural and high-temperature fabrics, most crosscut metamorphic country rock. Pegmatitic intrusions are not extensive and rarely form bodies large enough to map at 1:24,000 scale. Typical are coarse-grained, muscovite \pm quartz \pm plagioclase dominated intrusions that contain minor amounts of tourmaline on the hand specimen scale (Fig. 3–7).

PRESSURE AND TEMPERATURE CONDITIONS

Temperature and pressure conditions are critical for understanding the thermotectonic setting of rocks deformed under high-grade, regional metamorphic conditions. Two samples, a Cat Square terrane biotite gneiss/metagraywacke and lower Tallulah Falls biotite gneiss/metagraywacke, were chosen for electron microprobe analysis. This section of the chapter will describe the results of electron microprobe analysis in the context of the tectonothermal history of the rocks analyzed.

ANALYTICAL METHODS

The samples were collected while mapping the Brindle Creek fault, which frames the Newton window in the eastern Inner Piedmont of North Carolina. The first sampled unit is the lower Tallulah Falls biotite gneiss/metagraywacke. The sample collection site is located in the footwall of the Newton window, and contains a similar texture and mineralogy (on the hand specimen scale) to other biotite gneiss in the Lower Tallulah Falls unit. The second unit sampled is the Cat Square terrane metagraywacke located in the interior of the Brindle Creek thrust sheet,



Figure 3–7. (a) Hand specimen of coarse quartz and plagioclase dominated pegmatite with minor tourmaline from LV 77. (b) Large muscovite-quartz pegmatite on top of Baker Mountain at station LV 77, due south of the large microwave antenna, Baker Mountain County Park near Mountain View, North Carolina.

in the western half of the study area. The structural orientations (i.e., strike, dip, mineral lineation) of these rocks were measured to preserve the relationship of the rock within the tectonic fabric of the host unit. Lab preparation began with identification of a slice perpendicular to foliation in effort to find a large garnet, since biotite and plagioclase are plentiful. Garnets were moderately distributed throughout the sample. Chips were selected based on the size and abundance of the garnet, the proximity to the edge of the rock, and fracturing in the garnet

Two samples were chosen and cut into a 1"x1" chip, epoxied, and mounted, analysis side down, to a round slide appropriate for the microprobe. Using the thin section saw, the excess chip was removed and ground to a desired thickness for polishing. Samples were polished with 600 micron grit to remove scour marks, and gradually stepped down from 6 micron, 3 micron and 1 micron, until pits were polished out.

Electron microprobe analysis was done using the Cameca SX50, with the aid of the ZAF (PAP) program, operated by the Department of Earth and Planetary Sciences at the University of Tennessee. Analyses were collected during automated sessions, using point and line collection methods. Acceleration voltage for analyses was 15 kV and a beam current of 20 na was used for all analyses. Beam size varied depending on the mineral phase analyzed: a 5 μm beam was used for biotite and plagioclase; and a 2 μm beam was used for garnet. A peak counting time of 20 seconds was used on all samples. The following standards were analyzed before and after automated sessions: wollastonite (Ca, Si), spinel (Mg), hematite (Fe), albite (Na), orthoclase (K), chromium (Cr), and rhodonite (Mn). The EMP was calibrated prior to use, and standards reanalyzed following data collection periods. X-ray maps of major garnet cations Fe, Mg, Ca, and Mn were gathered to identify chemical gradients, if any, and minerals to be analyzed. Analyses for pressure and temperature estimates were obtained from line traverses across grain

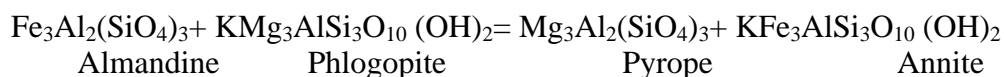
boundaries. Individual points were selected based on the distance from the grain boundary, cation totals, and weight percent totals. Analyses used for pressure and temperature calibrations were no more than 10 µm from the grain boundary and mineral pairs were no more than 20 µm apart. Pressure and temperature estimates were plotted using GTB software developed by Spear (1993).

SURVEY OF GEOTHERMOMETERS AND BAROMETERS

Geothermometers and barometers are based on specific calibrations of metamorphic equilibrium using the temperature and pressure dependence of the equilibrium constant obtained from experimental data (Spear, 1993). To determine the thermobarometric setting of rocks in the Inner Piedmont, analytical measurements of chemical compositions were obtained from coexisting phases using the electron microprobe. Using the chemical composition of coexisting phases, lines of equilibrium constant can be drawn on a P-T grid. The Berman (1990) modification of Fe-Mg exchange thermometer of Ferry and Spear (1978) was chosen to estimate temperatures on both samples due to the presence of Ca and Mn in garnet. The GASP barometer by Hodges and Spear (1982) was chosen for calibrations of garnet and plagioclase.

Garnet-biotite exchange thermometer

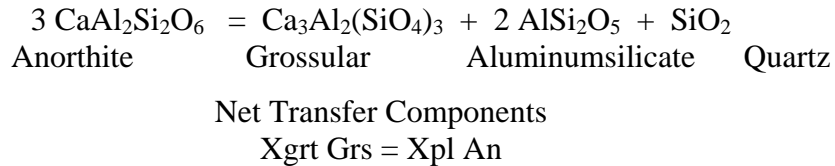
The garnet-biotite Fe-Mg thermometer is based on an exchange reaction that is temperature dependent and involves little, if any, change in volume. Partitioning of elements between phases decreases as temperature increases and cations seek to form pure solid solutions between existing phases (Spear, 1993). The primary exchange components of this reaction are the Fe and Mg contents of biotite and garnet at grain boundaries.



Exchange components
 $\text{FeMgGrt-1} = \text{FeMgBt}$

GASP (garnet-aluminosilicate-silica-plagioclase) barometer

The GASP (garnet-aluminosilicate-silica-plagioclase) geobarometer is based on the net transfer of cations during the production and consumption of phases as pressure increases. This barometer involves the consumption of the grossular component in garnet as pressures increases, enriching the anorthite content in plagioclase. Due to the lack of aluminosilicate, employment of this barometer establishes only estimates of the upper pressure limit.



H3 LOWER TALLULAH FALL BIOTITE GNEISS/METAGRAYWACKE

The host rock, located at station H3, is a migmatitic biotite gneiss/metagraywacke from the footwall lower Tallulah Falls Formation rocks occurring inside the Newton window (Fig. 3–3). This exposure was sampled due to the abundance of biotite gneiss and lack of matrix amphibolite. This sample is fine- to medium-grained biotite gneiss, with biotite defining a well-developed S_2 foliation (Fig. 3–8a). Subhedral garnet porphyroblasts are encased by biotite, and form tails off the garnet/biotite grain boundary. Major phases in this sample include: biotite, garnet, quartz, plagioclase, and muscovite. Garnets occur as subhedral porphyroblasts, are fractured, and contain inclusions of biotite, plagioclase, rutile, ilmenite, apatite, and zircon (Fig. 3–8b). Garnets are the largest phase by size in the sample (~6 mm), and comprise 10 percent of the slide area. Inclusions of biotite, ilmenite, and rutile define a relict growth foliation sub-parallel to the regional S_2 foliation in the core of the garnet. Rotation of the garnet axes during high-temperature deformation probably best explains the conjugate orientations of core and

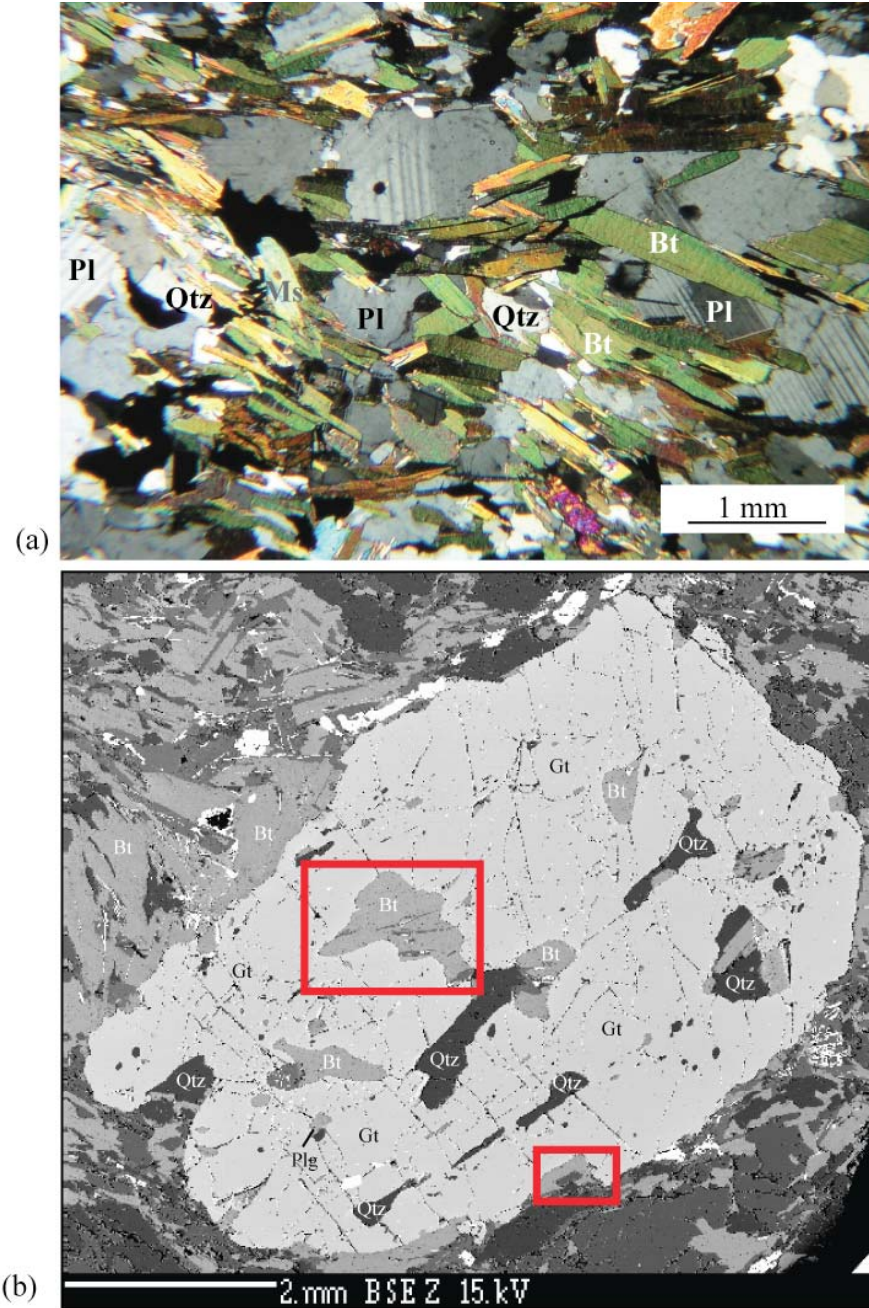


Figure 3–8. (a) Photomicrograph of lower Tallulah Falls biotite gneiss at station H 3. (b) Back scatter electron photomicrograph of large almandine garnet in sample H3 used for microprobe analysis. Two foliations are present, an earlier growth foliation defined by quartz and biotite inclusions in the garnet core, and the dominant S_2 foliation of which the garnet is a porphyroblast. Mineral abbreviations: Bt = biotite, Gt = garnet, Plg = plagioclase, Qtz = quartz. Areas outlined in red are used for temperature and pressure determinations indicated in Table 3–1.

matrix biotite. Biotite is the dominant matrix phase and, by visual estimates, makes up 30 percent of the slide area. Biotite exists as tabular or needle-like crystals with bird's-eye texture. Core biotite contains equal portions of phlogopite and annite (50 percent each), whereas garnet-rim/matrix biotite contains a slightly larger annite composition (54 percent) with lesser phlogopite (46 percent). Quartz comprises 20 percent of the slide area and occurs as anhedral crystals assimilating between void spaces, evenly partitioned within the foliation. Plagioclase occurs as anhedral crystals comprising 15 percent of the slide area. Plagioclase occurs as inclusions in the garnet core and has an average composition of An₃₄. Matrix plagioclase, occurring near the garnet rim, has an average composition of An₃₀ (Table 3–1). The variation of anorthite composition between matrix and inclusion plagioclase is likely due to Ca in garnet being redistributed between inclusions. Muscovite is euhedral, fine-to-medium grained, and occurs in the plane of the biotite foliation. Rutile and hematite comprise 5 percent of the sample and appear opaque in thin section under cross polars. Hornblende is present and constituted less than 5 percent of the sample.

X-ray maps were constructed for four major cations (Fe, Mg, Ca, and Mn) in order to understand the chemical distribution of these elements in garnet. X-ray maps and EMP analyses indicate the garnet is mostly almandine, with minor pyrope, spessartine, and grossular content. The Fe X-ray map indicates a slight increase in concentration from the bottom-left to top-right of the diagram, across the garnet interior (Fig. 3–9a). The higher Fe concentration portion of the garnet, in the northeast corner, is interpreted to represent the garnet rim. The lower concentration core occurs in the middle and bottom-left portions of the garnet, indicated by the darker color X-ray. Biotite inclusions show a marked decrease in Fe concentration with respect to the matrix. Mg is the second most abundant element in the garnet and is evenly distributed

Table 3–1. Selected analyses from lower Tallulah Falls biotite gneiss/metagraywacke from station H3. Garnet results indicate a primarily almandine garnet with minor pyrope, grossular, and spessartine components. Biotite inclusions in the garnet core contain equal portions of Mg and Fe. Matrix biotite exhibits higher Mg concentrations than core analyses. Plagioclase ranges in anorthite content from 34% in the core to 30% at the rim/matrix intersection.

GARNET			BIOTITE		PLAGIOCLASE			
	CORE	RIM	CORE	RIM	CORE	RIM		
WEIGHT PERCENT OXIDES								
Si	37.5	37.6	36	38.7	59.4	59.6		
Ti	0.04	0.02	1.82	1.59	0	0		
Al	20.9	21.0	18.2	21.6	25.4	25		
Mg	3.14	4.02	10.8	8.77	0.008	0.019		
Fe ²⁺	32.7	31.8	19.2	15.3	0.058	0.087		
Mn	4.32	3.95	0.174	0.114	0	0		
Ca	2.19	2.05	0.008	0.014	7.18	5.83		
K	0	0	9.69	9.66	0.031	0.075		
Na	0.04	0.029	0.172	0.349	7.53	8.7		
OH	0	0	3.96	3.913	0	0		
TOTAL	100.85	100.47	99.56	100.01	99.61	99.311		
CATIONS								
Si	2.97	3	5.44	5.66	2.68	2.68		
Ti	0.002	0.001	0.206	0.175	0	0		
Al	1.99	1.97	3.25	3.73	1.33	1.32		
Mg	0.374	0.401	2.43	2.11	0.001	0.001		
Fe ²⁺	2.19	2.12	2.43	2.47	0.002	0.003		
Mn	0.292	0.266	0.022	0.014	0	0		
Ca	0.187	0.175	0.001	0.002	0.344	0.3		
K	0	0	1.87	1.8	0.002	0.004		
Na	0.006	0.004	0.05	0.099	0.654	0.701		
OH	0	0	4	4	0	0		
TOTAL	8.0	7.9	19.70	20.06	5	5.078		
Fe/(Fe+Mg)	0.854	0.841	Fe/(Fe+Mg)	0.500	0.539	Ca/(Ca+Na)	0.345	0.30
Prp	0.123	0.135	Ann	0.500	0.539	An	0.344	0.3
Alm	0.720	0.716	Phg	0.500	0.461	Ab	0.647	0.697
Grs	0.061	0.059				Or	0.004	0.003
Sps	0.096	0.090						

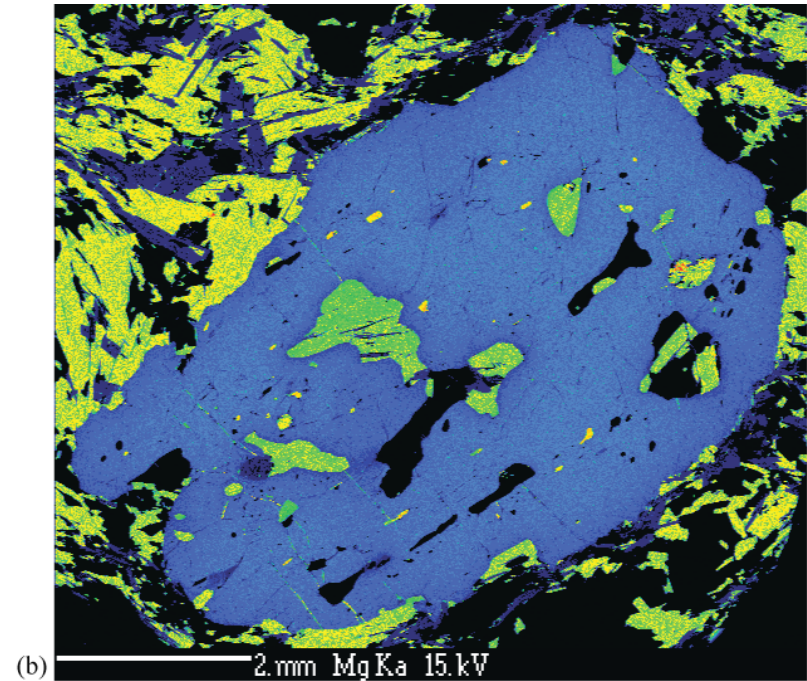
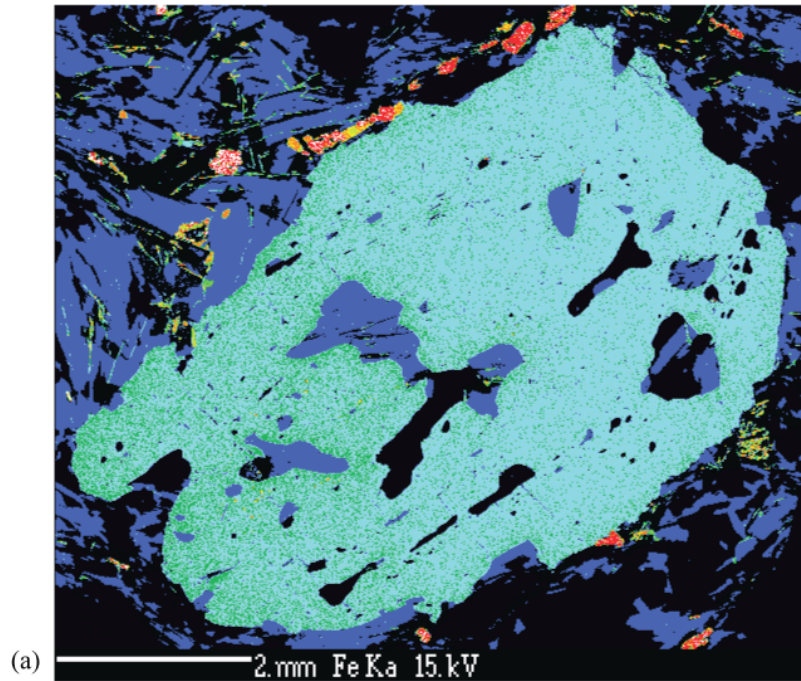


Figure 3–9. (a) X-ray map of Fe in sample H3, lower Tallulah Falls garnet-biotite gneiss. Red indicates areas of high cation concentration. Cation concentration decreases from red to green to blue then black. Black areas are nondetect. (b) X-ray map of Mg in sample H3, lower Tallulah Falls garnet-biotite gneiss. Lighter areas are higher in the amount of Mg, darker areas are lower. Areas of relatively deficient Mg concentrations occur around biotite inclusions and within 15 microns of the garnet rim. Biotite inclusions in the garnet core are higher in Mg than surrounding matrix biotite.

throughout (Fig. 3–9b). Decreases in garnet Mg concentration occur around the rim and biotite inclusions, although biotite matrix and inclusions are rich in Mg. Matrix biotite contains a higher concentration of Mg than inclusion biotite, probably due to the unlimited supply of Mg. Rimming the northwest portion of the garnet is a thin zone of higher Mn concentration. Ca remains concentrated along garnet margins, and deficient between inclusions in the largest part of the garnet interior. Ca X-ray patterns do not indicate diffusion (Fig. 3–10a). Mn maintains an equal composition throughout the garnet, although increases occur near some garnet/inclusion grain boundaries (Fig. 3–10b).

LV284 CAT SQUARE TERRANE BIOTITE GNEISS/METAGRAYWACKE

The host rock located at station LV 284 is a Cat Square terrane biotite gneiss/metagraywacke, in the western portion of the study area (Fig 3–3). The sampled unit displays a strong tectonic fabric and a distinct northwest-trending mineral stretching lineation defined by biotite, quartz, and feldspar. This sample is located within a large regional sheath fold (Fig. 3–3). P–T estimates from this sample will also define the thermal deformational setting for this structure. The host unit shares similar major mineral phases with the lower Tallulah Falls metagraywacke: biotite, garnet, plagioclase, quartz, and alkali-feldspar. Minor amounts of rutile, ilmenite, apatite, and zircon are present. The host rock displays gneissic banding with leucosomes and melanosomes varying in thickness from 1 to 4 cm. The host rock melanosomes display a fine-to medium-grained texture, composed predominantly of biotite, plagioclase, and quartz. Euhedral to subhedral almandine garnets are dispersed throughout the biotite matrix, making up 10 percent of the slide area, and are fractured with minimal weathering or alteration (Fig. 3–11). Garnets contain inclusion rich cores, and inclusion poor rims. Biotite is the dominant matrix phase and comprises 35 percent of the slide area. Biotite exists as tabular

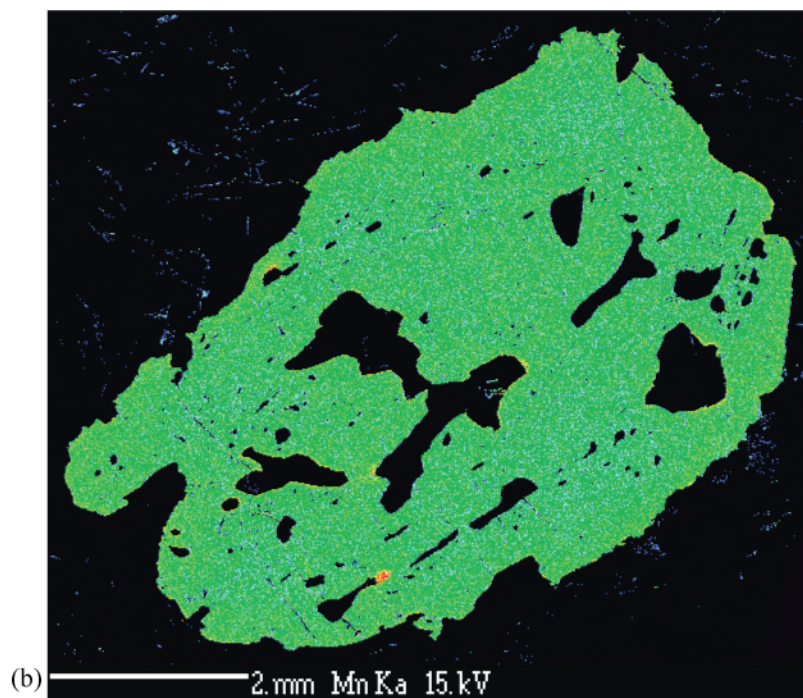
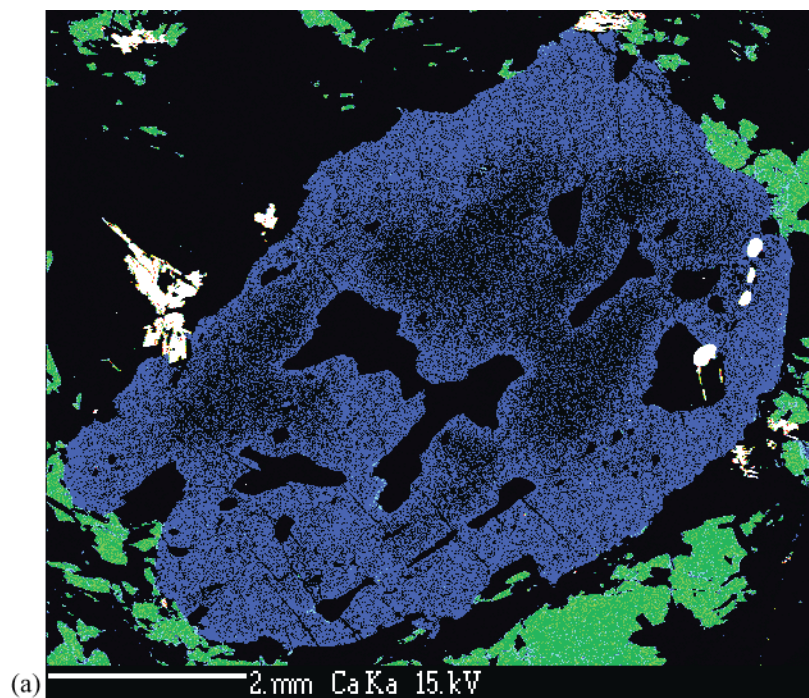


Figure 3–10. (a) X-ray map of Ca in sample H3, lower Tallulah Falls garnet-biotite gneiss. Lighter areas are higher in the amount of Ca, darker areas are lower. Ca is concentrated toward the garnet rim, and the interiors between biotite inclusions are deficient. (b) X-ray map of Mn in sample H3, lower Tallulah Falls garnet-biotite gneiss. Lighter areas are higher in the amount of Mn, darker areas are lower. Mn is equally dispersed among the garnet core and rim.

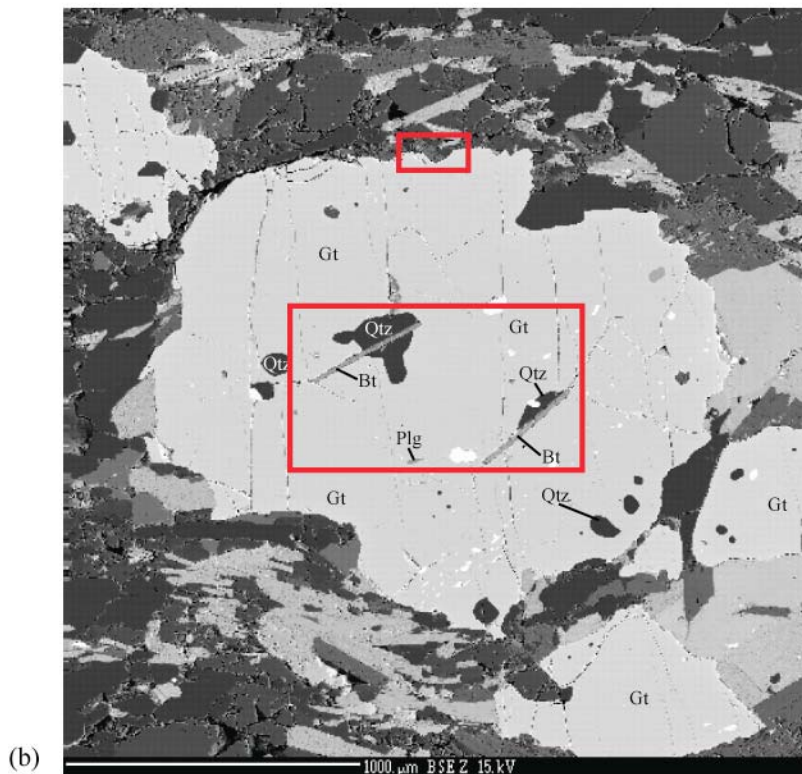
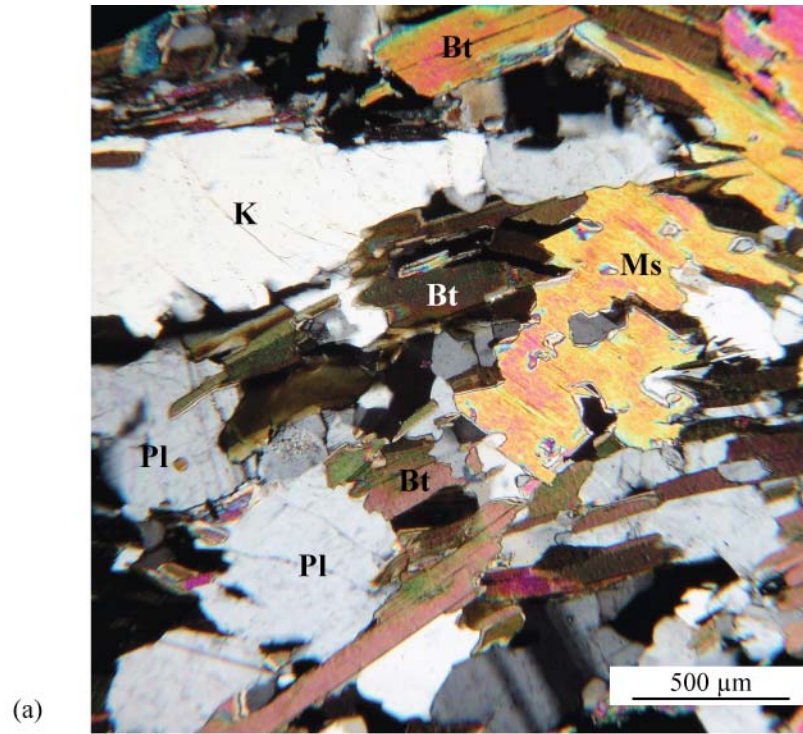


Figure 3–11. (a) Photomicrograph of thin section from LV 284. (b) Backscatter electron photomicrograph of large garnet in Cat Square terrane biotite gneiss from station LV 284. Biotite defines a previous foliation, formed during the growth of the garnet with progressive metamorphism. Biotite and muscovite define the enveloping foliation. Inclusion suites in the garnet include biotite, quartz, rutile, ilmenite, apatite, quartz, and zircon. Mineral abbreviations: Gt = Garnet, Bt = biotite, Qtz = quartz, and Plg = plagioclase. Areas outlined in red are used for temperature and pressure determinations indicated in Table 3–2.

or needle-like crystals with bird's eye texture. Acicular biotite in the garnet core traces a growth foliation and has been sheared. Quartz comprises 20 percent of the slide area and occurs as anhedral crystals evenly distributed within the foliation. Biotite wrapping the garnet suggests rotation contributed to volume loss through shearing of the preexisting garnet. Interspersed within the biotite matrix are plagioclase and quartz. Plagioclase comprises 15 percent of the sample in matrix and as inclusions in the garnet core. Anorthite content ranges from An₍₂₉₎ in matrix plagioclase to An₍₃₄₎ as inclusions in the garnet core, this variation is likely due to Ca being redistributed to the plagioclase inclusion. Alkali-feldspar comprises 15 percent of the section. Representative analyses indicate garnets are almandine rich and contain minor spessartine, grossular, and pyrope components (Table 3–2). Biotite varies in composition between annite and phlogopite end members. Biotite inclusions in the garnet interior contain equal portions of phlogopite (52 percent) and annite (48 percent), whereas garnet-rim/matrix-biotite contains a larger annite content (55.5 percent) with lesser phlogopite (44.5 percent).

The Fe X-ray map shows a transition in concentration between the lower and upper half of the garnet (Fig 3–12a). Higher order colors on the Fe X-ray map indicate this is an almandine garnet. The relatively lower Fe concentration portion of this garnet is interpreted to represent the garnet core, indicated by the yellow brown tone, and is inclusion rich. The garnet rim occurs in the upper half of the photo indicated by brighter yellow, higher Fe concentrations. The garnet rim is inclusion poor. Sheared garnet fragments occur to the above and below of the main garnet in Fe X-ray map. Similar concentration trends exist across the large garnet into the sheared garnet. The garnet fragment in the northwest of the Fe X-ray map displays a similar concentration of Fe as the upper half of the large garnet. Likewise the garnet fragments in the bottom left portion of the Fe X-ray map display the relatively lowest concentration of the garnet.

Table 3–2. Selected results from Cat Square terrane LV 284 microprobe analysis. Garnet results indicate the presence of an almandine garnet. Biotite inclusions in garnet contain nearly equal concentrations of Fe and Mg. Matrix biotite exhibits higher Mg concentrations than core analyses. Plagioclase ranges in anorthite content from 34% in the core to 29% at the rim/matrix intersection.

	GARNET		BIOTITE		PLAGIOCLASE			
	CORE	RIM	CORE	RIM	CORE	RIM		
WEIGHT PERCENT OXIDES								
Si	36.67	36.47	35.28	36.34	59.7	59.8		
Ti	0.012	0.021	2.528	2.54	0	0		
Al	21.09	21.07	18.25	17.94	25.2	24.9		
Mg	3.086	2.441	11.58	13.37	0.01	0.002		
Fe ²⁺	35.72	35.29	18.94	16.35	0.08	0.06		
Mn	2.686	4.172	0.096	0.549	0	0		
Ca	1.128	0.968	0.051	0.074	7.07	6.07		
K	0	0	8.53	9.048	0.051	0.048		
N	0	0	0.327	0.027	7.63	8.73		
OH	0	0	3.96	3.913	0	0		
TOTAL	100.4	100.43	99.56	100.14	99.74	99.61		
CATIONS								
Si	2.961	2.89	5.33	5.57	2.67	2.7		
Ti	0.001	0.001	0.287	0.293	0	0		
Al	2.007	2.17	3.25	3.241	1.33	1.24		
Mg	0.372	0.295	2.607	2.113	0.01	0.01		
Fe ²⁺	2.412	2.294	2.394	2.642	0.08	0.07		
Mn	0.184	0.287	0.012	0.071	0	0		
Ca	0.098	0.084	0.008	0.012	0.341	0.295		
K	0	0	1.643	1.769	0.004	0.003		
N	0	0	0.096	0.008	0.647	0.697		
OH	0	0	4	4	0	0		
TOTAL	8.0	8.0	19.63	19.40	5	5.02		
Fe/(Fe+Mg)	0.866	0.886	Fe/(Fe+Mg)	0.479	0.555	Ca/(Ca+Na)	0.345	0.297
Prp	0.121	0.100	Ann	0.479	0.555	An	0.341	0.295
Alm	0.787	0.775	Phg	0.521	0.445	Ab	0.647	0.697
Grs	0.032	0.028				Or	0.004	0.003
Sps	0.060	0.097						

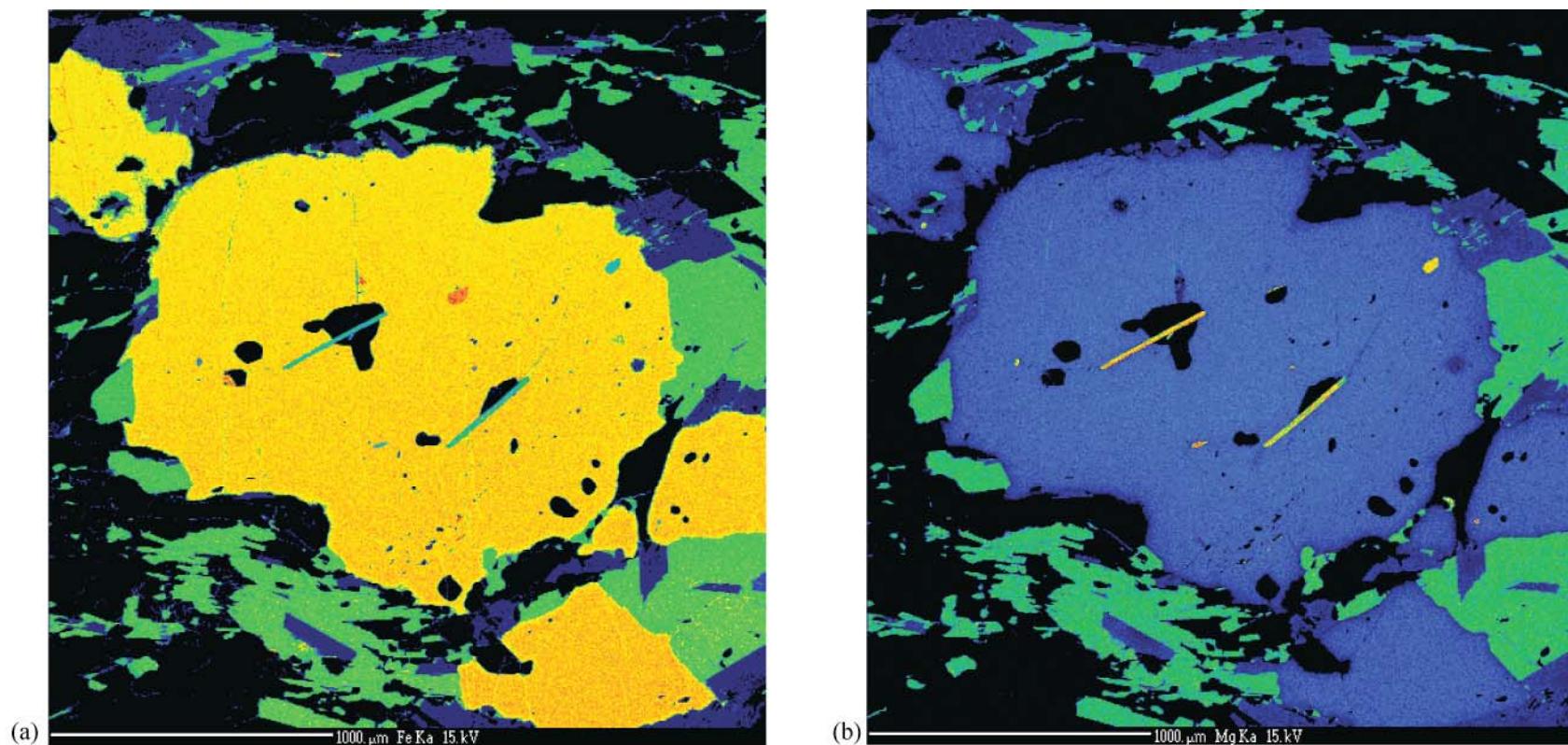


Figure 3–12. (a) X-ray map of Fe in microprobe section LV 284 from Cat Square terrane garnet-biotite gneiss. Lighter areas are higher in the amount of Fe, darker areas are lower. A slight chemical zonation occurs between the lighter yellow, higher Fe concentration, upper half of the garnet and the darker yellow-orange, lower concentration, lower garnet. The outer 5 micron rind of contrasting garnet Fe concentrations is related to diffusion along the grain boundary. (b) X-ray map of Mg in microprobe section LV 284 from Cat Square terrane garnet-biotite gneiss. Lighter areas are higher in the amount of Mg, darker areas are lower. Mg is largely unzoned throughout the garnet although a sharp diffusion-related decrease occurs within 15 microns of the garnet/inclusion-matrix grain boundaries. Biotite inclusions contain higher levels of Mg than the surrounding matrix biotite.

X-ray map patterns of Mg concentrations remain relatively constant throughout the garnet except around the outer 10 μm from the rim (Fig. 3–12b). The zone of decreasing Mg concentration surrounding the garnet rim is likely due to diffusion with matrix biotite. Ca remains consistent throughout the large garnet and surrounding fragments (Fig 3–13a). Interior zones between garnet inclusions are relatively Ca poor with increasing concentration occurring toward the garnet rim. Ca appears to not be influenced by diffusion. Mn shows the most pronounced evidence of diffusion. Mn is evenly dispersed throughout the garnet except around the rim and inclusions where concentrations increase drastically (Fig. 3–13b).

RESULTS AND DISCUSSION

The presence of a diffusion profile indicates these samples equilibrated at temperatures equal or lesser to peak metamorphism. Diffusion is thermally driven and largely dependent on three factors heat, chemical species, and minerals involved (Spear, 1993). Garnets diffuse slowly, resulting in the generation of a chemical gradient or diffusion profile between the core and rim, although under high-grade metamorphic conditions garnets tend to homogenize due to increasing diffusion rates (Spear, 1993). Alternatively biotite has a rapid diffusion rate and quickly equilibrates (Spear, 1993). Numerical models indicate crystal size and cooling rate are important factors controlling diffusion and preservation of peak conditions (Spear, 1993). Net transfer and exchange reactions produce chemical gradients in crystals resulting in distinct zoning patterns that are related to the presence and abundance of other phases in the rock (Spear, 1993). The presence of these patterns helps in determining the evolutionary context in which to describe electron microprobe analyses, and determining the P–T–time path. Special treatment should be given to temperature calibrations occurring within the zone of diffusion, as they are estimates of the closing temperature of the Fe–Mg exchange reaction (Spear, 1993). To minimize

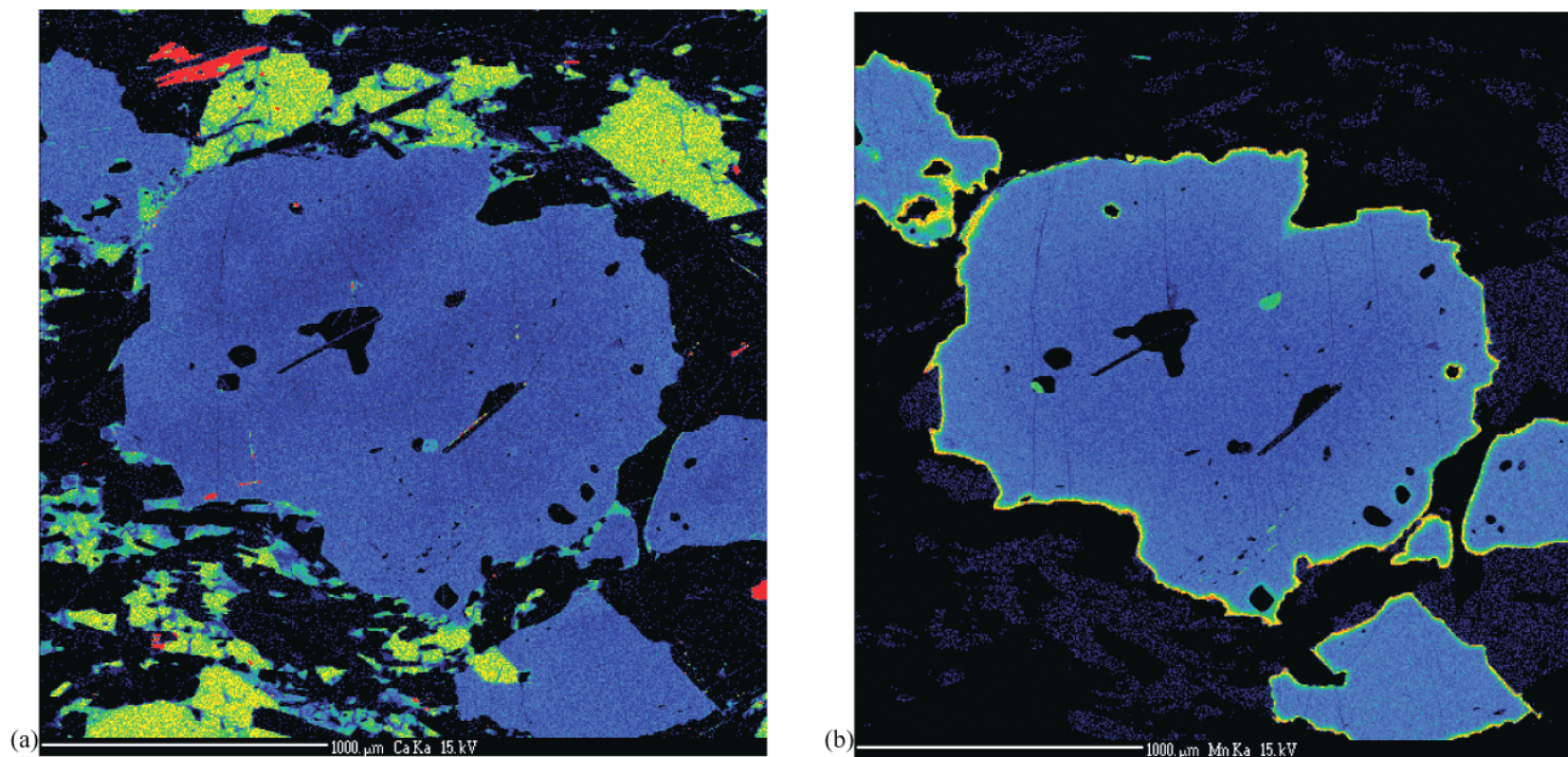


Figure 3–13. (a) X-ray map of Ca in microprobe section LV 284 from Cat Square terrane garnet-biotite gneiss. Lighter areas are higher in the amount of Ca, darker areas are lower. Ca is evenly distributed throughout the garnet. (b) X-ray map of Mn in microprobe section LV 284 from Cat Square terrane garnet-biotite gneiss. Lighter areas are higher in the amount of Mn, darker areas are lower. Mn remains relatively unzoned throughout the garnet except around the garnet rim grain boundary. Inclusions in the garnet remain relatively nonparticipatory with regard to Mn exchange.

the influence of diffusion on P–T estimates spot analyses were collected outside the zone of diffusion. Pressure calibrations using the GASP barometer can only be seen as upper estimates because aluminum silicate was not present in either sample (Spear, 1993).

Electron microprobe analyses agree with field observations of the western Newton window and place the sampled rocks into the sillimanite stability field (Holdaway, 1971) (Fig 3–14). Pressure estimates were generated using the GASP barometer of Hodges and Spear (1982), and temperature estimates were generated using the Berman modification of the garnet-biotite thermometer of Ferry and Spear (1978). Electron microprobe analyses of Cat Square terrane garnet-biotite and garnet-plagioclase pairs indicate a range in temperature and pressure of 620° C, 3.6 kbar and 710° C, 6.1 kbar, respectively (Fig. 3–14) (Table 3–1). Temperature and pressure estimates from the lower Tallulah Falls Formation analyses yield range in conditions from 570° C, 4.1 kbar and 690° C, 6.3 kbar, respectively (Fig. 3–14) (Table 3–2). P–T estimates from this survey correlate with other eastern Inner Piedmont conditions (Fig. 3–15), overlapping the estimates by Bier (2001) to west, in the South Mountains. Previous field observations and P–T estimates in the central Inner Piedmont indicate an increase in temperatures further away from the Brevard fault zone (Fig. 3–16). Considering the Inner Piedmont metamorphic peaks at 330, 345, and 365 Ma, a P–T–time path can be constructed. Metamorphism occurred over a 35 million-year period based on the span of recognized metamorphic peaks; in that time metamorphic conditions reached upper amphibolite and granulite facies, resulting in the production of peak metamorphic mineral assemblages. Using a geobarometric gradient of 3.3 km/kbar, the maximum burial depth for both Cat Square and Tugaloo terrane rocks is ~20 km and subduction and accretion occurred at a rate of 1 kilometer per 1.75 million years.

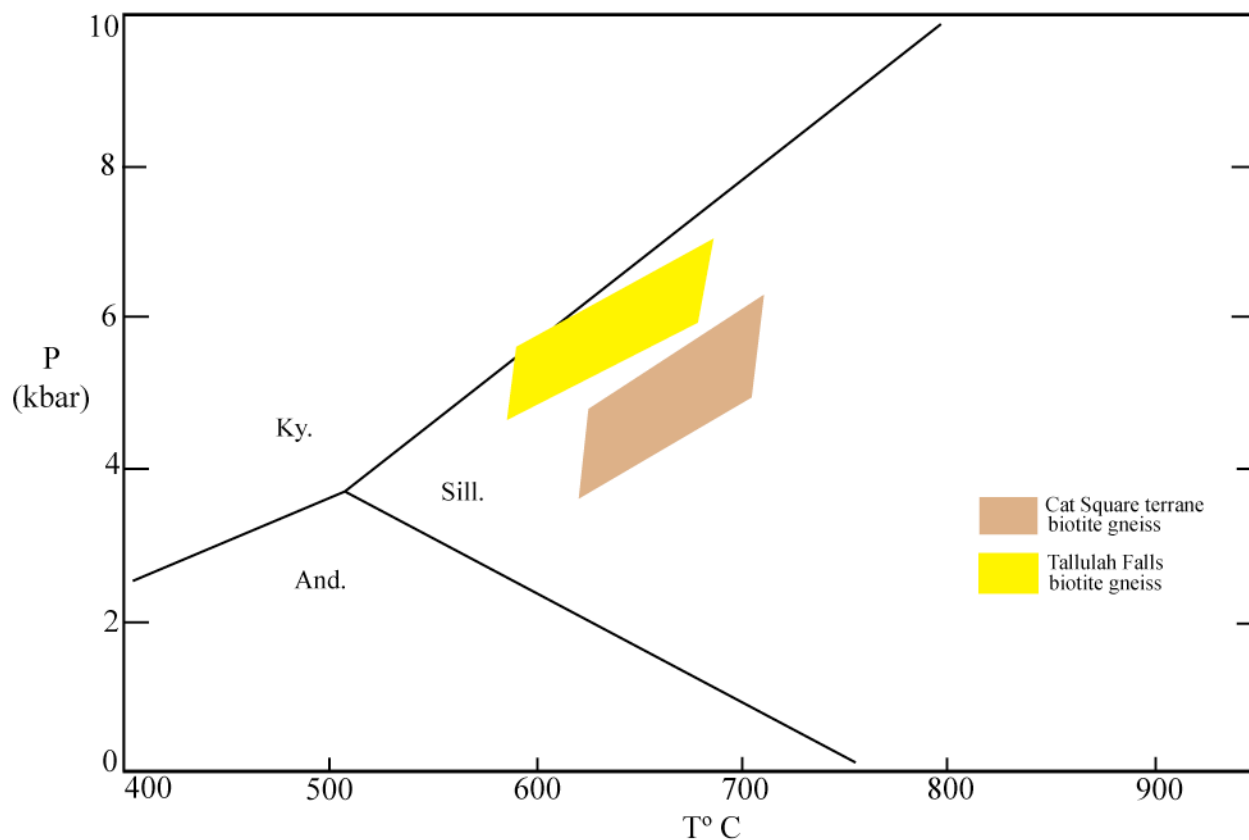


Figure 3–14. PT diagram of Tallulah Falls and Cat Square terrane biotite gneiss/metagraywacke conditions. Temperatures in the Cat Square terrane biotite gneiss/metagraywacke are slightly higher than calibrations of the lower Tallulah Falls. Garnet interior pressure estimates in the Tallulah Falls ($4.7 \text{ kbar} \pm 1 \text{ kbar}$) are higher than Cat Square terrane ($3.6 \text{ kbar} \pm 1 \text{ kbar}$) but fall within the range in error for this barometer. Rim pressure estimates, assumed to represent peak metamorphic conditions, indicate pressures were similar across the two terranes, 6.1 and 6.3 kbar, respectively. Calculated temperatures for the Cat Square terrane garnet interior and rim range from 620°C and 710°C , and lower Tallulah Falls estimates range from 570°C and 690°C .

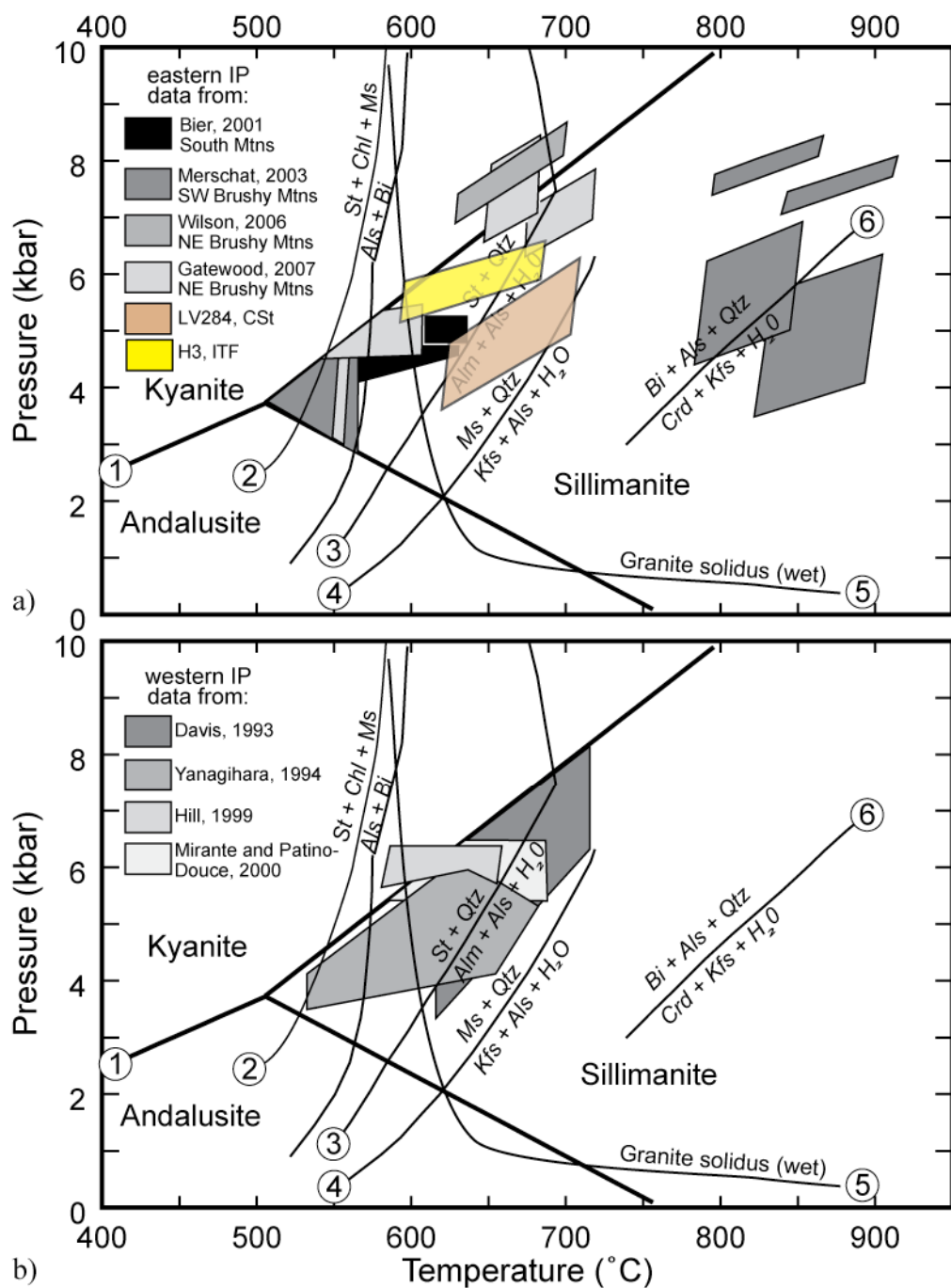


Figure 3–15. Metamorphic P-T estimates plotted for recent Inner Piedmont studies (modified from Gatewood, 2007). (a) P-T estimates for eastern Inner Piedmont. (b) P-T estimates for western Inner Piedmont. Univariant curves are from: (1) Holdaway (1971); (2) Albee (1965); (3) Pigage and Greenwood (1982); Chatterjee and Johannes (1974); (5) Luth et al. (1964); and (6) Holdaway and Lee (1977). Mineral abbreviations: St–staurolite, Chl–chlorite, Ms–muscovite, Als–aluminum silicate, Bi–biotite, Qtz–quartz, Alm–almandine, Kfs–potassium feldspar, Crd–cordierite. CST–Cat Square terrane, ITF–lower Tallulah Falls.

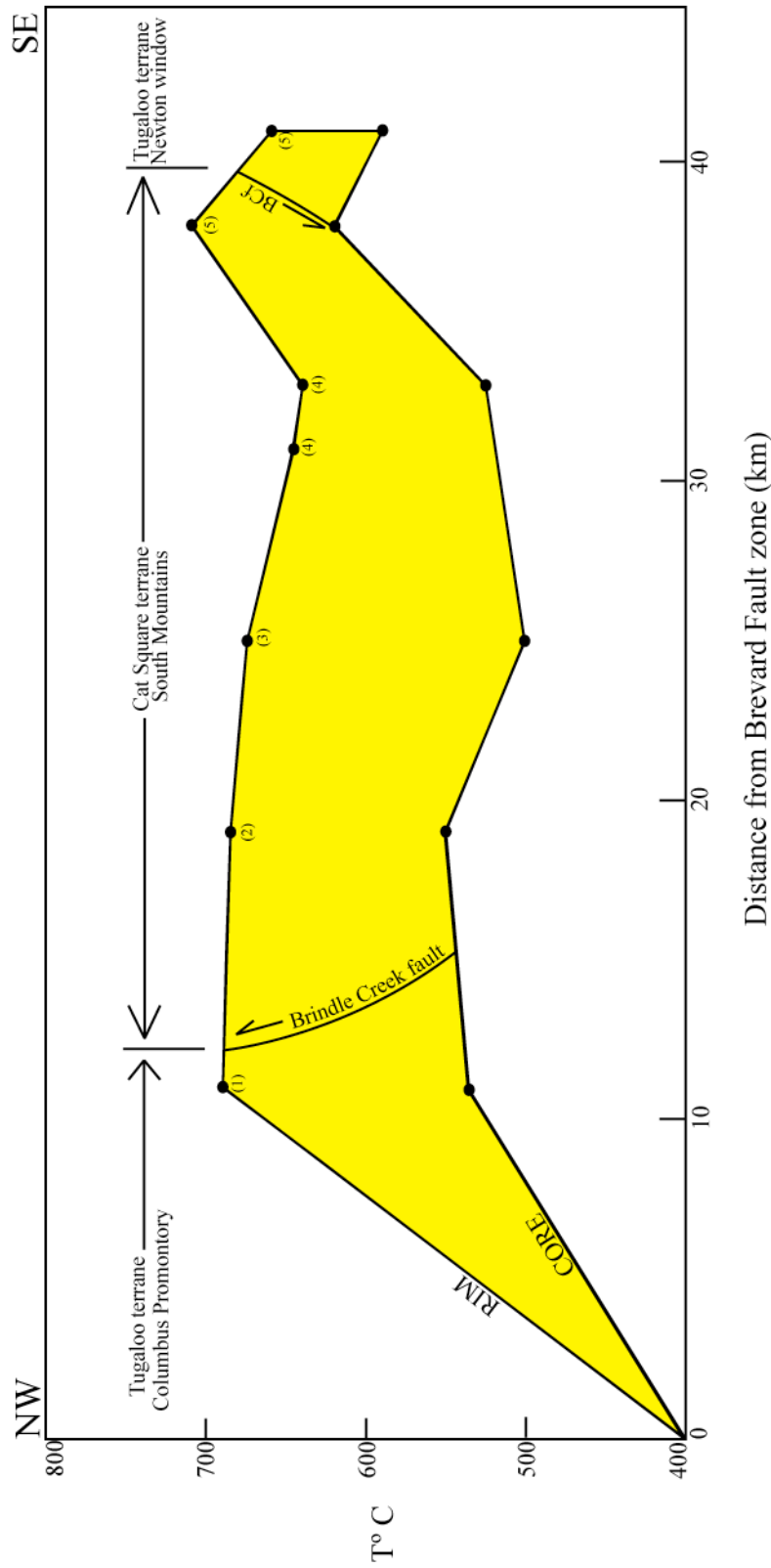


Figure 3–16. Graph of rim and core temperature estimates versus distance from the Brevard fault zone eastward across the Inner Piedmont core to the Newton window. A gradual temperature decrease in the eastern South Mountains is likely due to folding of isotherms across a regional synform. Data sources are 1–Davis (1993), 2–Hill (1999), 3–Giorgis (1999), 4–Bier (2001), and 5–this study. BCF = Brindle Creek fault.

CHAPTER 4
STRUCTURAL EVOLUTION OF THE WESTERN CENTRAL NEWTON WINDOW
BASED ON MAP PATTERNS AND GEOLOGIC STRUCTURES

INTRODUCTION

Geologic structures preserve the kinematic history of crustal deformation processes and, in the case of the southern Appalachian Mountains, the crustal evolution of the eastern Laurentian margin. The composite Inner Piedmont consists of a gently dipping stack of macroscopic, migmatitic, polydeformed, crystalline thrust sheets exposed from northern North Carolina to Alabama (Hatcher and Hooper, 1992; Hatcher, 2004) (Fig. 4–1). Thrust sheets composing the western Inner Piedmont include the Marion, Tumblebug Creek, Six Mile-Sugarloaf Mountain, and Walhalla nappe (Davis, 1993; Yanagihara, 1994). Eastern Inner Piedmont thrust sheets were restricted to the Brindle Creek preceding discovery of the unnamed thrust sheet exposed within the Newton window. Six deformational events (Table 4–1) have shaped the Newton window since the Early Devonian. These events reflect the crustal evolution from deposition of Cat Square terrane sediments and burial, through Neocadian and Alleghanian deformation and metamorphism, to Mesozoic and Cenozoic crustal extension, recording the subsequent transition in deformation style from ductile to brittle conditions. High temperature foliations and structural elements such as curved fold hinges, curved mineral stretching lineations, and map- scale sheath folds indicate a high-temperature (Neocadian) polyphase deformational regime. These features were superposed by early Alleghanian folding and high temperature resetting of zircon rims, and were subsequently overprinted by late Alleghanian long-wavelength regional open folds. This chapter discusses the kinematic indicators in the context of the deformational episodes recognized within the study area and the Inner Piedmont.

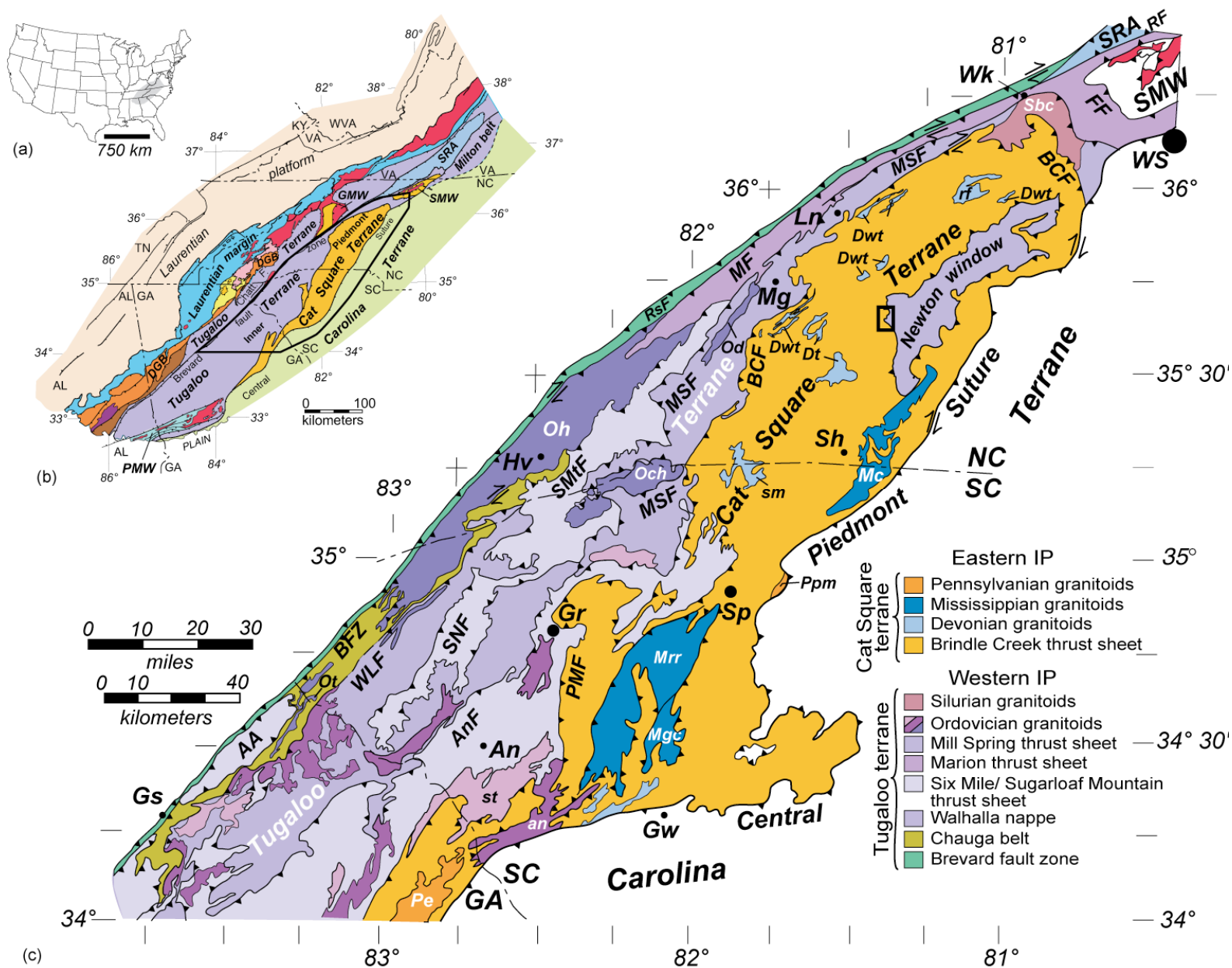


Figure 4–1. (a) Index map of the eastern U.S. showing the location of the study area. (b) Tectonic map of the southern Appalachians showing the location of the Inner Piedmont and major tectonostratigraphic terranes. DGB–Dahlonge gold belt. GMW–Grandfather Mountain window. PMW–Pine Mountain window. SMW–Sauratown Mountains window. SRA–Smith River allochthon. Chatt. F.–Chattahoochee fault. Dark purple–Elkahatchee pluton (Middle Ordovician). Yellow, pink, light orange, and brown–internal Blue Ridge terranes. Red–Grenville and pre-Grenville basement. (c) Tectonic map of the Inner Piedmont in the Carolinas and northern Georgia, compiled and modified from Rankin et al. (1972), Espenshade et al. (1975), Goldsmith et al. (1988), Hopson and Hatcher (1988), Hatcher and Hooper (1992), Nelson et al. (1998), and fig. 1 in Hatcher (2002, and sources cited therein). Black rectangle indicates location of study area. Faults and thrust sheets: AA–Alto allochthon. AnF–Anderson. BCF–Brindle Creek. BFZ–Brevard. FF–Forbush. MF–Marion. MSF–Mill Spring. PMF–Paris Mountain. RF–Ridgeway. RsF–Rosman fault. SMtF–Sugarloaf Mountain fault. SMW–Sauratown Mountains window. SNF–Six Mile–Seneca. SRA–Smith River allochthon. WLF–Walhalla. Named Ordovician (purple) and Ordovician(?) (lighter purple) granitoids: Och–Caesars Head. Od–Dysartsville. Oh–Henderson. Ot–Toccoa. Obc–Brooks Crossroads. an–Antreville. st–Starr. Undated plutons in the western Inner Piedmont (probably Ordovician) are colored lighter shades of purple. Silurian granitoid: Devonian and Devonian(?) plutons (light blue): rf–Rocky Face. Dt–Toluca. Dwt–Walker Top. sm–Sandy Mush. Darker blue–Mississippian plutons: Mc–Cherryville. Mgc–Gray Court. Mrr–Reedy River. Pennsylvanian plutons: Pe–Elberton. Ppm–Pacolet Mills (in Carolina terrane). Towns: An–Anderson. Gr–Greenville. Gs–Gainesville. Gw–Greenwood. Hk–Hickory. Hv–Hendersonville. Ln–Lenoir. Mg–Morganton. Sh–Shelby. Sp–Spartanburg. Wk–Wilkesboro. WS–Winston-Salem. Figure from Mersch et al., 2008.

Table 4–1. Summary and relative timing of deformational events in the Inner Piedmont, North Carolina. *

EVENTS	STRUCTURES			METAMORPHIC CONDITIONS	REGIONAL EVENTS	OROGENY & TIMING
	Fabrics	Folds	Faults			
D₁	S ₁ Taconic foliation preserved in amphibolite boudins; garnet grain tails in NW footwall rocks	F ₁ Intrafolial folds and isoclinal folds preserved in boudins	Initial development of the CPS	M ₁ Moderate to high pressure and temperature	Initial collision and subduction of IP beneath Carolina terrane	Pre- to early Acadian post ~410 Ma
D₂	S ₂ Penetrative foliation L ₂ Mineral lineation; curving pattern, trends NE-SW, E-W, & NW-SE	F ₂ reclined, tight to isoclinal passive folds; recumbent folds; meso- to macro scale passive flow SW vergent sheath folds	emplacement of ductile Inner Piedmont thrust sheets; BCFZ, TCFZ, MSFZ; early deflection along Neocadian BFZ	M ₂ Peak metamorphism, upper amphibolite facies, sillimanite I & II grade	Continued subduction, emplacement of crystalline thrust sheets, and SW deflection along Neocadian BFZ, channel flow	Neocadian 360 – 345 Ma
D₃	S ₃ Rare secondary foliation	F ₃ Inclined to upright, open to tight, NW verging folds; folding of BCFZ	movement along ductile fault zones, further SW deflection of IP thrust sheets	Decreasing P-T conditions, high to moderate pressure and temperature	continued emplacement of eastern IP and Carolina superterrane; uplift, unroofing, and cooling of the IP	Late Neocadian
D₄	S-C and related fabrics in BFZ, & CPS Mineral lineations in BFZ	F ₄ Upright, open folds, trend NW-SE, & NE;	Ductile reactivation of BFZ & CPS; formation of NA	Upper amphibolite to low pressure and temperature – greenschist facies (retrogressive)	Initial emplacement of the composite Blue Ridge-IP thrust sheet and exhumation	Alleghanian 325-300 Ma
D₅	Joints	Regional broad, open folds, most trend NE & NW	Brittle movements associated with the Rosman fault of the BFZ	low temperature	Continued emplacement and exhumation of the composite Blue Ridge-IP thrust sheet	Late Alleghanian ~260 Ma
D₆	Joints	Regional broad, open folds, trend NE	Meso- and macroscale normal faults	zeolite	Continued rifting and uplift	Mesozoic extension Cenozoic uplift

* Modified from Davis, 1993; Yanagihara, 1994; Bream, 1999; Giorgis, 1999; Hill, 1999; Williams, 2000; Bier, 2001; Kalbas, 2003; Mersch, 2003; Gatewood, 2007; and Byars, 2010. BCFZ = Brindle Creek fault zone; BFZ = Brevard fault zone; CPS = central Piedmont suture; MSFZ = Mill Spring fault zone; TCFZ = Tumblebug Creek fault zone; NA = Newton antiform. NW = Newton window.

DEFORMATIONAL EVENTS

D₁ Deformation

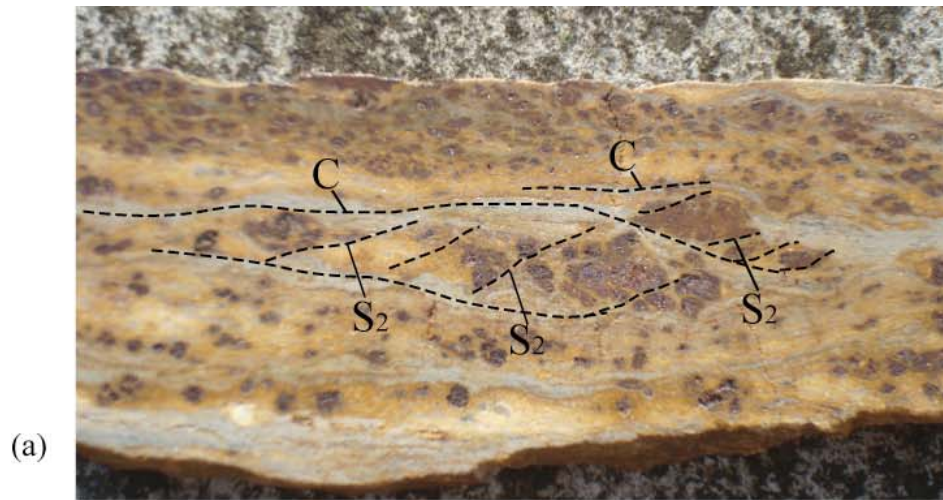
D₁ deformational features, originating from Taconic orogenesis (480-450 Ma), occur in the Blue Ridge and western Inner Piedmont terranes (Mersch et al., 2005). Evidence of D₁ is limited in metasedimentary units due to later transposition of earlier fabrics by peak metamorphism and deformation associated with the Neoacadian orogeny (360-340 Ma). Evidence for D₁ preserving the S₁ foliation is preserved within boudins and inclusion trails within garnets of the Ashe-Tallulah Falls Formation rocks. South of the study area, Byars (2010) recognized Ordovician ~466 Ma overgrowths on zircons from the Potts Creek mylonite, a feature occurring within lower Tallulah Falls Formation rocks, indicating the participation of these rocks in Taconian orogenesis.

D₂ Deformation

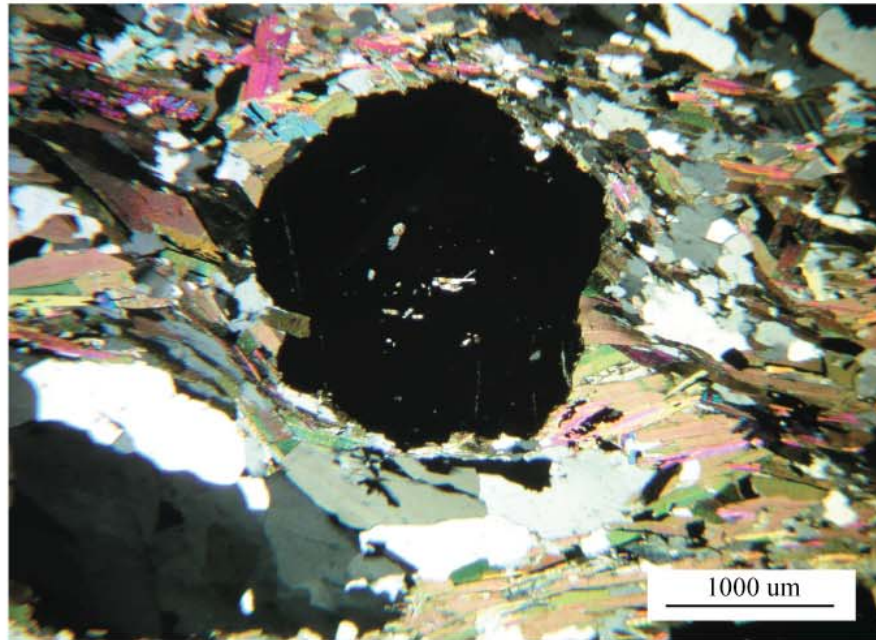
The D₂ event encompasses structures produced by peak Neoacadian orogenesis, reflecting the initial collision and subduction of the Inner Piedmont beneath the overriding, suprastructural, Carolina superterrane. Dominant penetrative structural elements such as S₂ foliations, L₂ mineral lineations, and F₂ folding formed contemporaneously during this event.

Foliations

S₂ foliations in the map area are defined by the parallel alignment of phyllosilicates, amphiboles, and other nonequant minerals (Fig. 4–2a, 4–2b, 4–2c). Measurement of 927 foliations in portions of the Banoak, Longview, Hickory, and Reepsville 7.5-minute quadrangles revealed variation from north-south to northwest strike, with moderate to gentle dip (Fig. 4–3a and 4–3b). Similar S₂ foliation attitude exists across the Brindle Creek fault; suggesting



(a)



(b)



(c)

Figure 4–2. (a) S-C fabric in garnet-sillimanite schist from station H1 from outcrop on north side of NC State Route 1132 near intersection of NC State Route 1132 and 1131, southwest of Hickory North Carolina. C– type shear bands transect dominant S₂ foliation in Cat Square terrane sillimanite schist. Asymmetric garnets indicate sinistral shear sense. (b) Naked almandine garnet porphyroclast with quartz-muscovite-biotite pressure shadow concordantly aligned with coarse quartz and feldspar to form the dominant S₂ foliation. Sample from station H3, located southwest of Hickory North Carolina near the Jacobs Fork River from footwall lower Tallulah Falls Formation metagraywacke. (c) Weathered outcrop exposure of Cat Square terrane sillimanite schist at station R204 in borrow pit near headwaters of north fork of Rhodes Mill Creek showing a moderate westward dip of S₂ foliation.

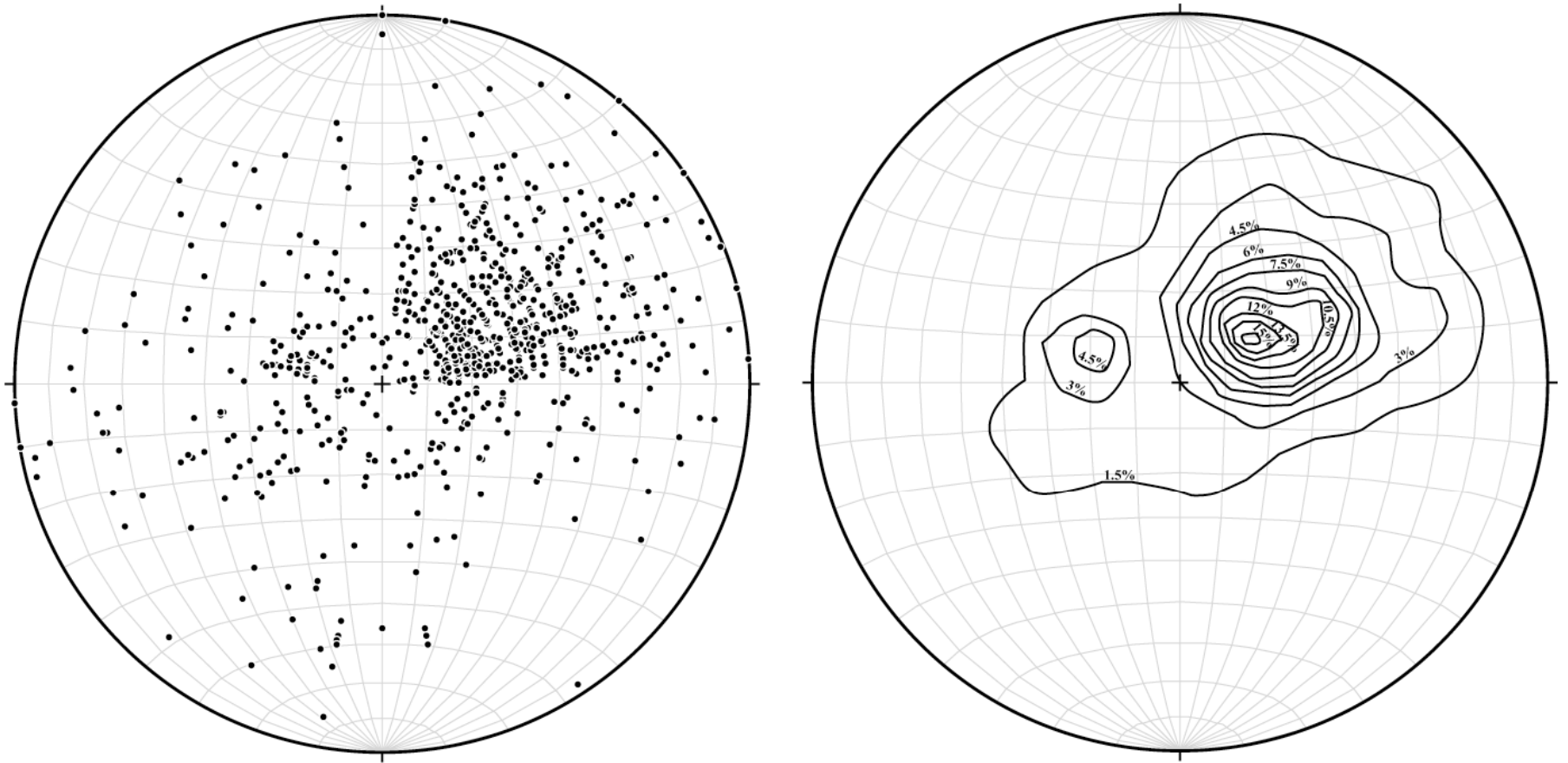


Figure 4–3. (a) Equal-area stereo scatter plot of 927 poles to S_2 foliation. (b) Contoured equal-area plot of 927 poles to S_2 foliation shown in Figure 4–3a. Contours 1.5, 3.0, 4.5, 6.0, 7.5, 9.0, 10.5, 12, 13.5, and 15 percent per 1% area.

emplacement occurred syn- to post-foliation formation (Plate I). Likewise, similar S_2 foliations exist across folded contacts between foliated Devonian Walker Top plutons, pegmatite, and granitic melts, suggesting plutonism occurred coeval with S_2 foliation formation.

Form lines constructed from S_2 foliations in the study area indicate the presence of six structural domains. Domains are numbered according to previously recognized domains across the broad core of the Inner Piedmont (Davis, 1993; Bier, 2001; Bier, 2002; Mersch et al., 2005) (Fig. 4-4). Two large domains, IX and X, occur in the study area and contain a majority of fabric data (Fig. 4-5, 4-6, and 4-7). Domain IX occurs west of the Brindle Creek fault and comprises a northwest-trending set of structures strongly aligned with the fault. Domain X displays a larger component of north-northwest trending structures compared to domain IX, although both display a similar alignment with the Brindle Creek fault. Domains VI and XII are probably part of larger unmapped domains to the east and the west of the study area. Domain VI trends north-northwesterly, similar to domain X. Conversely domain XII trends northeast, oblique to all other features in the study area. Domains XI and XIII serve as transitional domains representing intermediate areas between larger homogeneous domains IX and X.

Lineations

Quartz rods, bladed and fibrolitic sillimanite, feldspars, quartz, and platy muscovite/biotite define the dominant mineral lineation (L_2) (Figs. 4-8a, 4-8b, 4-8c, and 4-8d). The L_2 mineral lineation formed during peak metamorphic conditions (Bream, 2003), 360-340 Ma, and is interpreted as a mineral stretching lineation based on the parallel alignment with other Inner Piedmont shear-sense indicators (Fig. 4-8d) (Davis, 1993; Giorgis, 1999; Mersch et al., 2005; Hatcher and Mersch, 2006). Scatter plots of 31 mineral lineations indicate the presence of three discrete populations: northwest, southwest, and southeast sets (Fig. 4-9a).

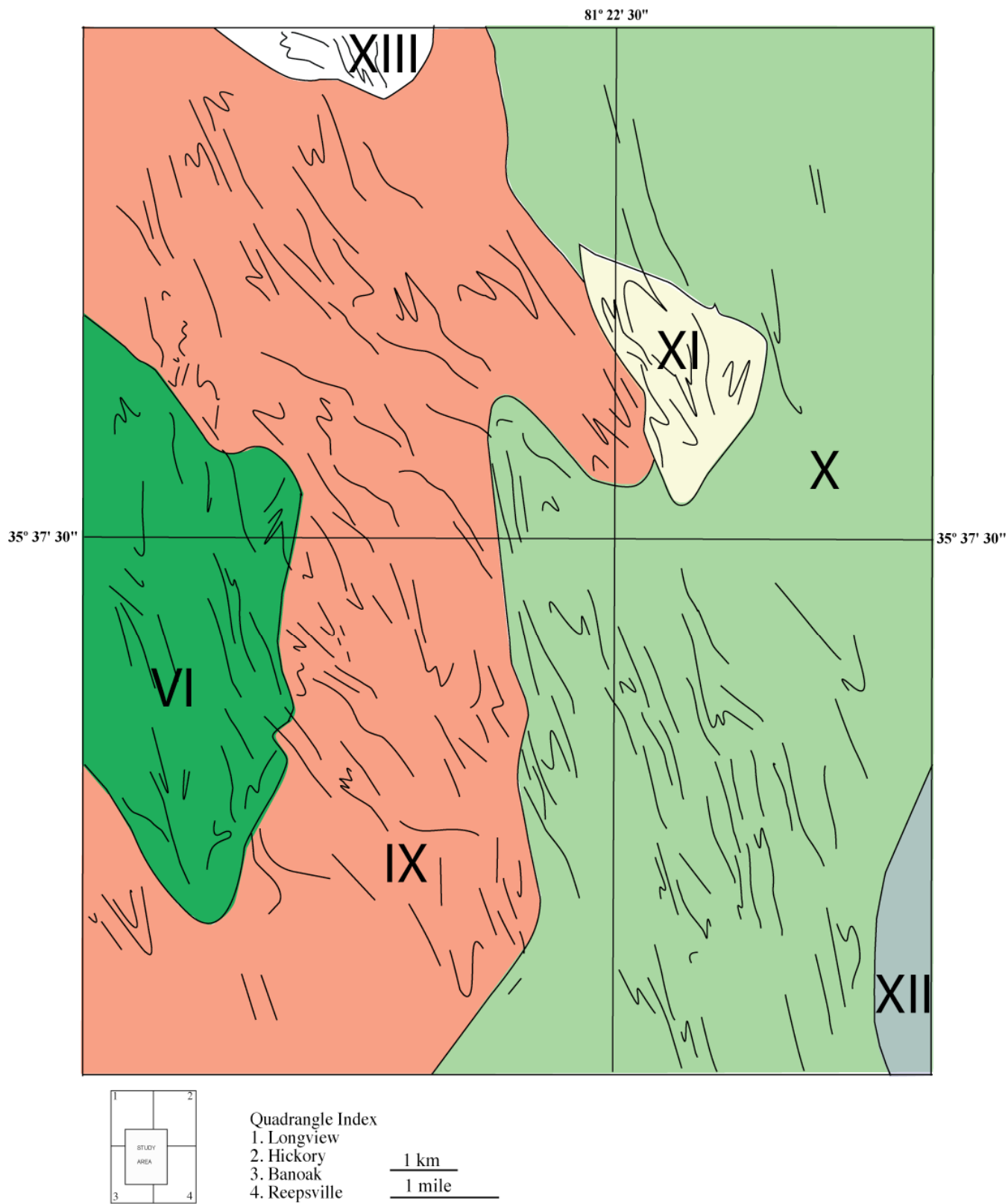


Figure 4-5. S_2 foliation form-line and domain map constructed from the trend of S_2 foliation in portions of the Longview, Hickory, Reepsville, and Banoak 7.5 minute quadrangles.

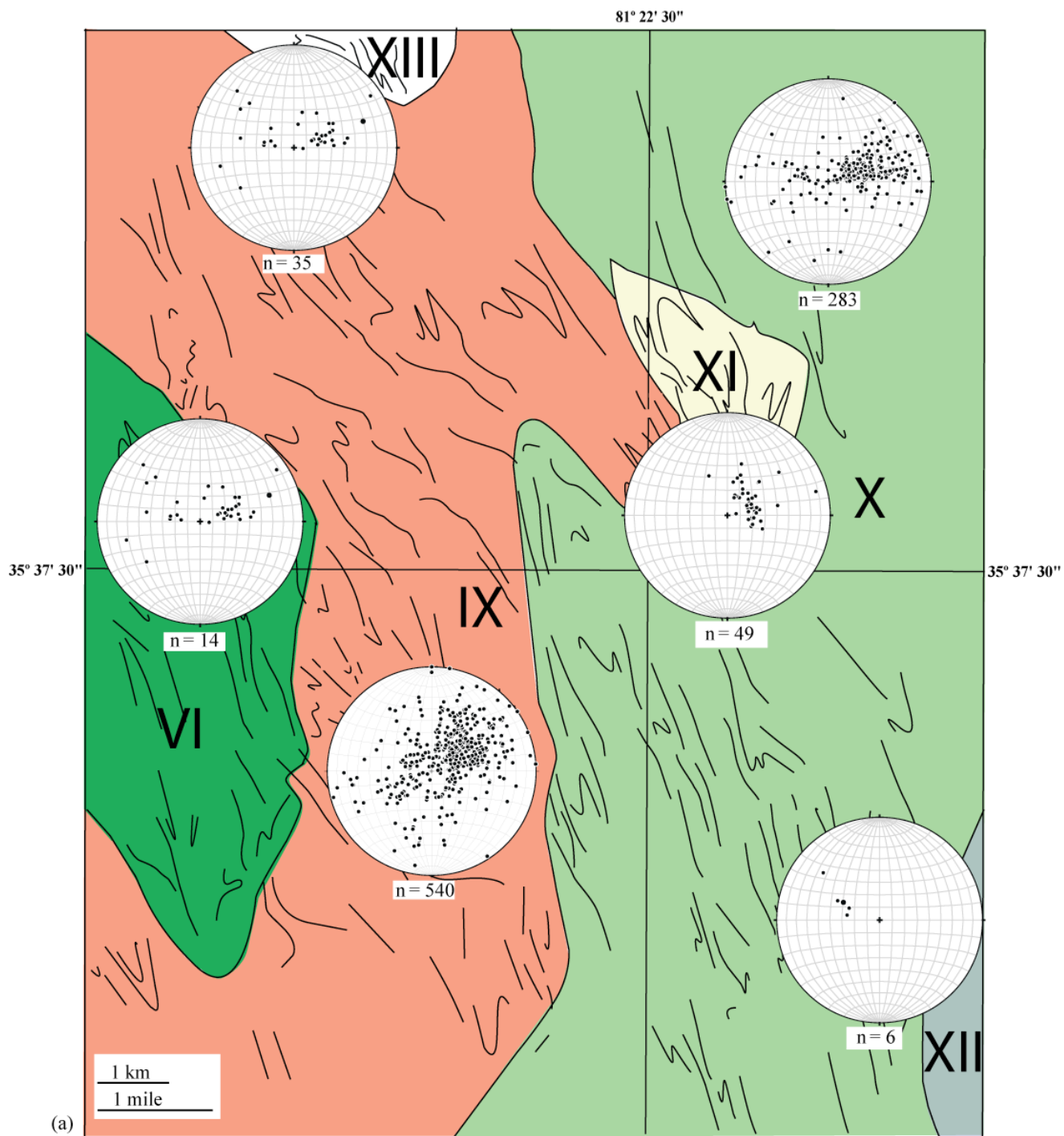


Figure 4–6. (a) S_2 foliation form-line and domain map with equal-area stereoplots of poles to foliations of individual domains. (b) Equal-area stereoplots of poles to S_2 foliations in domains in Figure 4–6a. (next page)

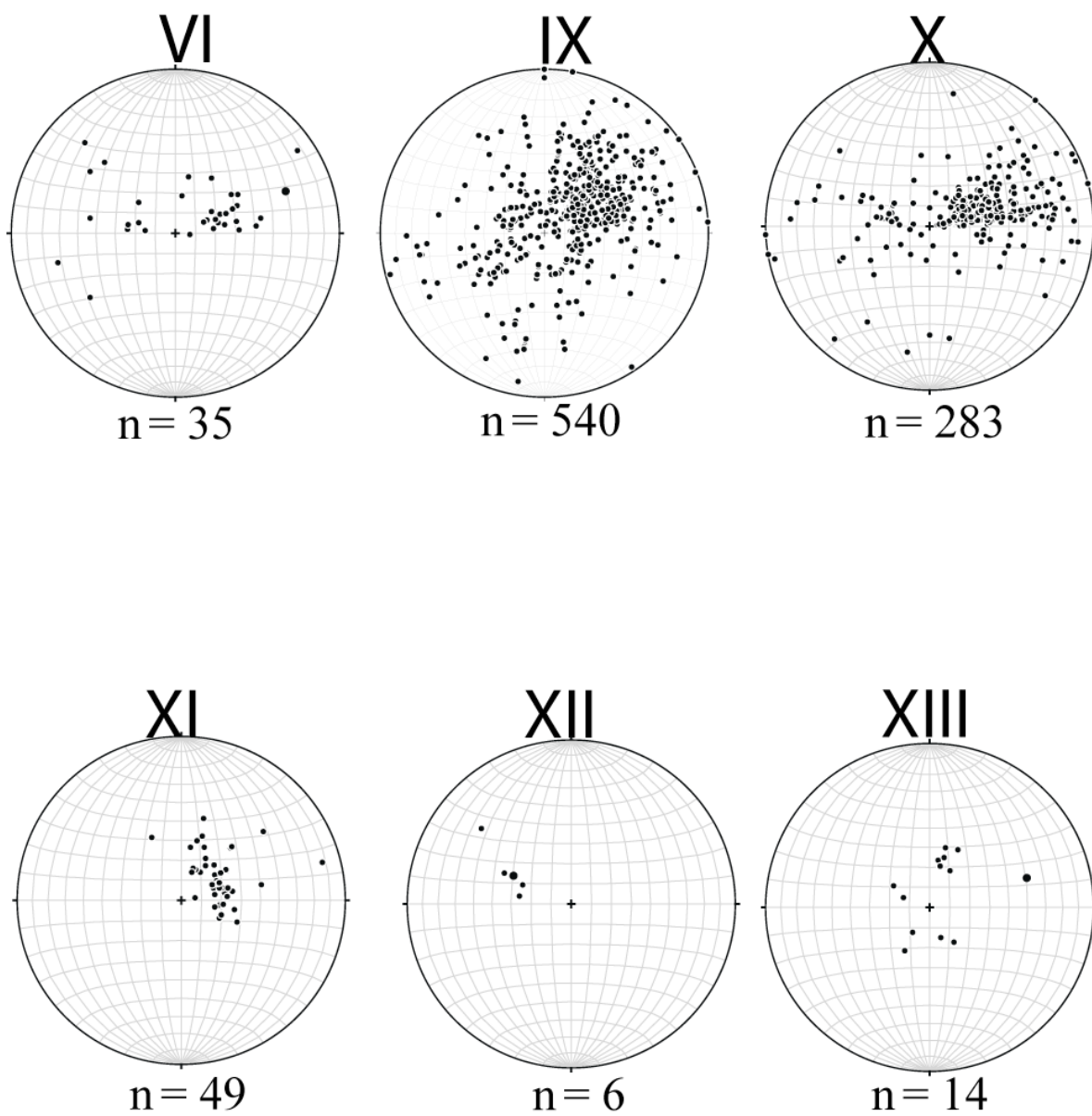


Figure 4–6b. Caption on previous page.

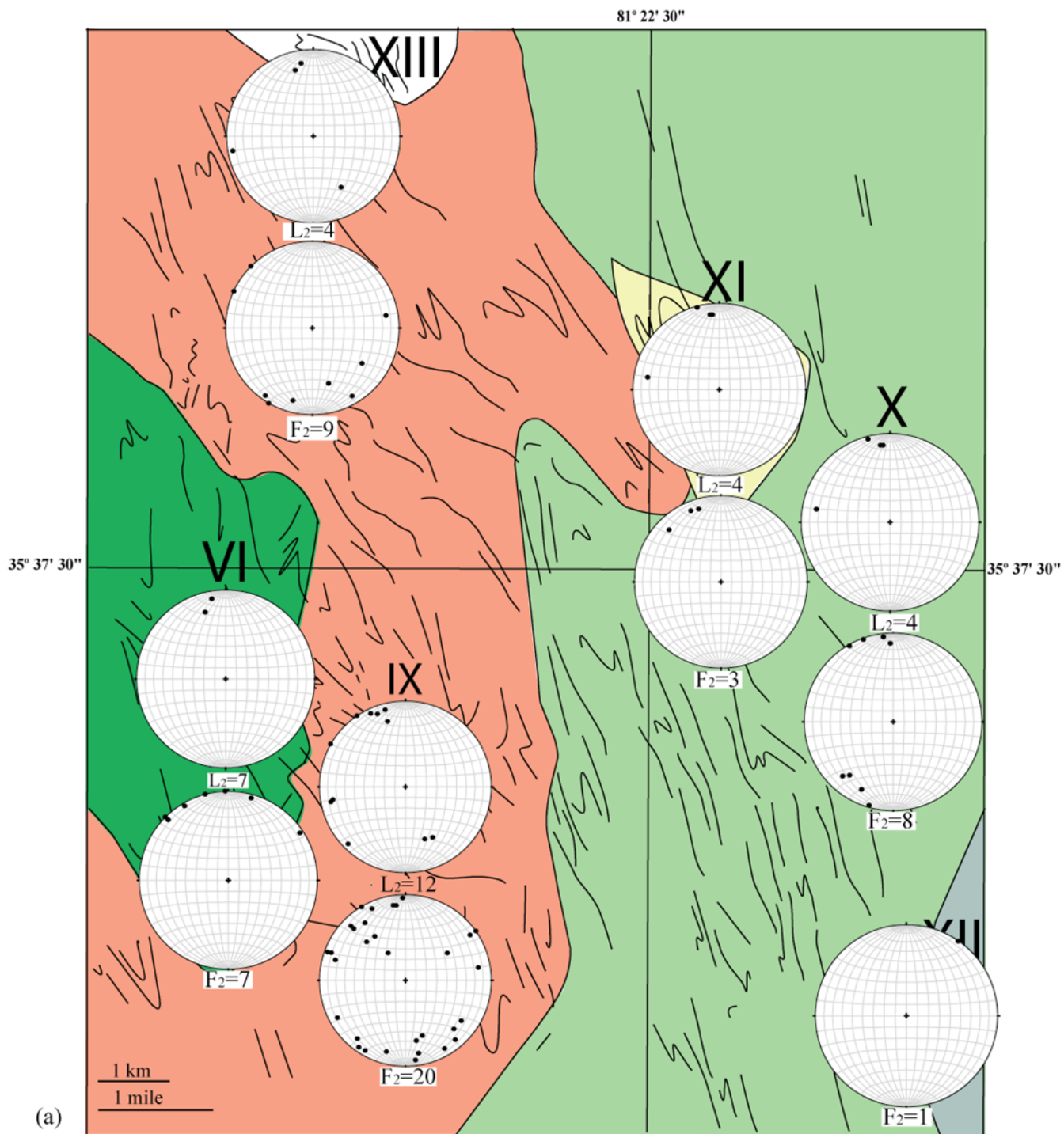


Figure 4-7. (a) S₂ foliation form-line and domain map with equal-area stereoplots of L₂ mineral lineations and F₂ fold axes. (b) Equal-area stereoplots of L₂ mineral lineations and F₂ fold axes of individual domains. (next page)

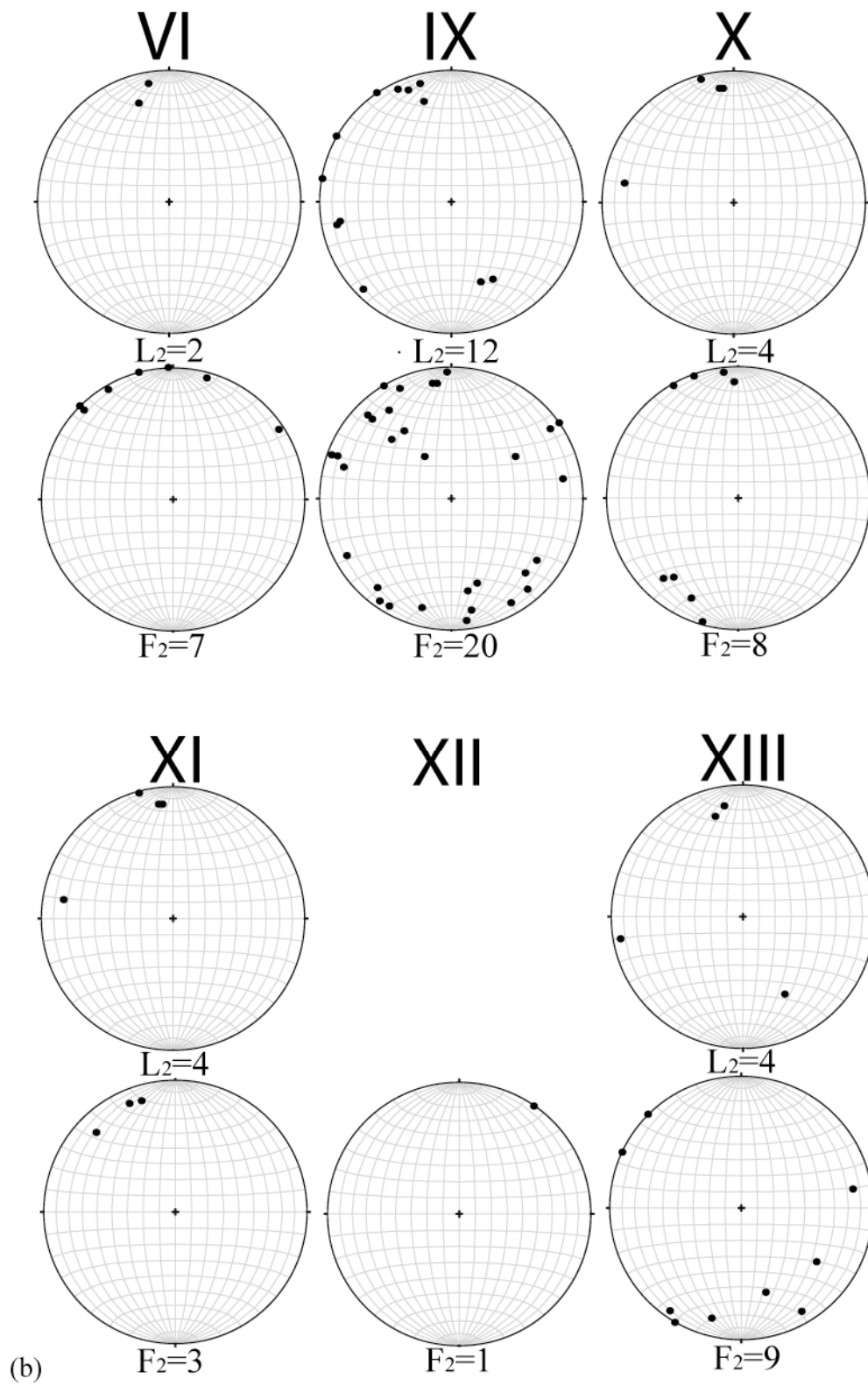


Figure 4-7b. Equal-area stereoplots of L_2 mineral lineations and F_2 fold axes corresponding to domains in Figure 4-7a.

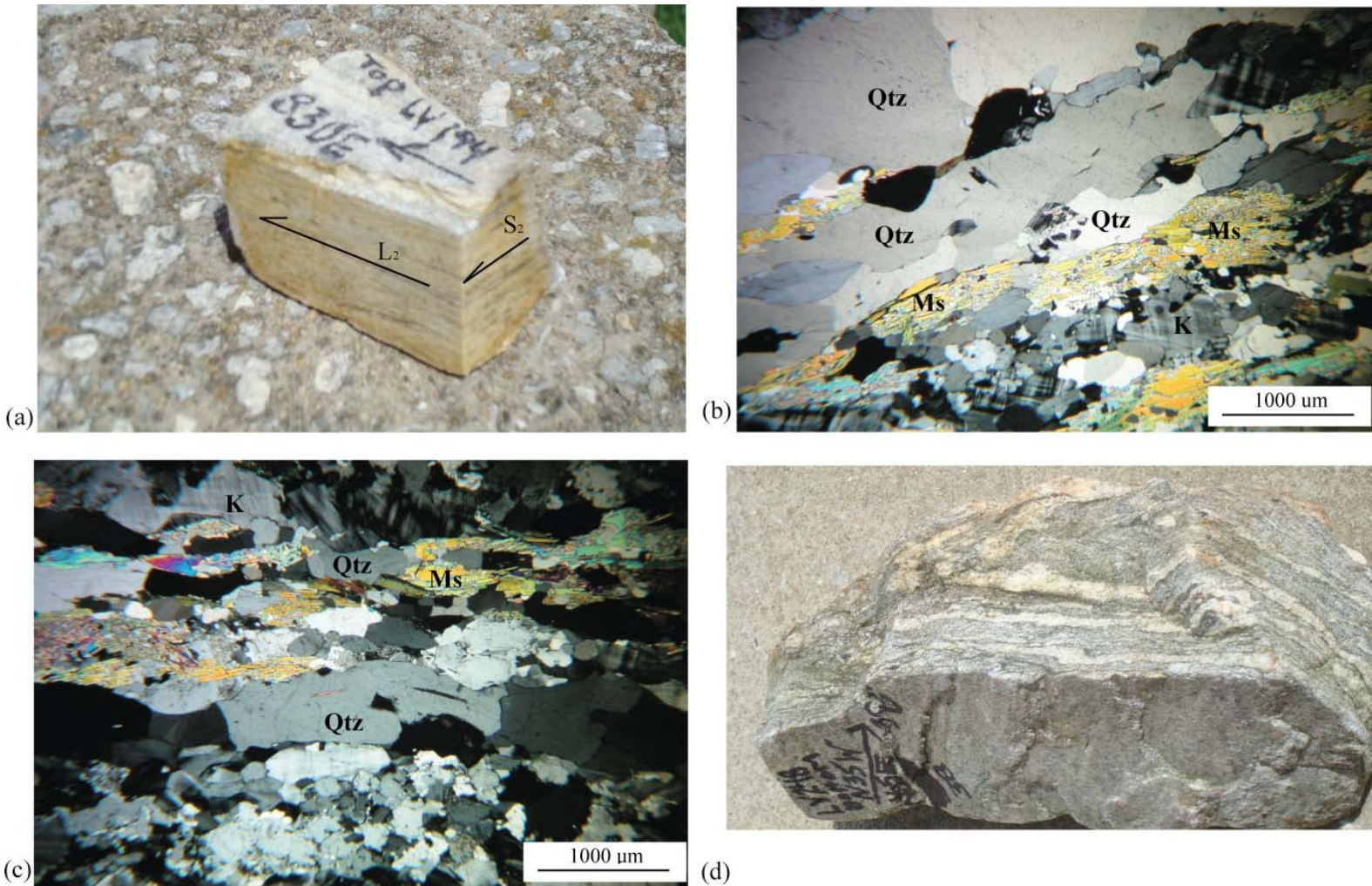


Figure 4–8. (a) S_2 foliations and L_2 lineation intersection in quartzofeldspathic gneissic interlayer in Cat Square terrane sillimanite schist, station LV 194 off NC state route 1102 near intersection with Camp Creek. Figures 4-8b and 4-8c are from same location. Dominant mineral lineation is defined by platy muscovite and elongated quartz. (b) Photomicrograph of Figure 4-8a cut parallel to foliation, oblique to mineral lineation. Foliation is defined by coarse quartz ribbons, interspersed in fine-grained strongly aligned, quartz, feldspar, and muscovite groundmass. (c) Photomicrograph of Figure 4-8a cut parallel to lineation oblique to foliation. (d) L_2 lineation and F_2 fold axis in Cat Square terrane metagraywacke, showing parallelism of isoclinal fold axis and mineral stretching lineation. Sample collected from station LV 248 in small tributary north of Camp Creek near Burke Chapel, North Carolina. Mineral abbreviations: Qtz = quartz, K = alkali-feldspar, and Ms = muscovite.

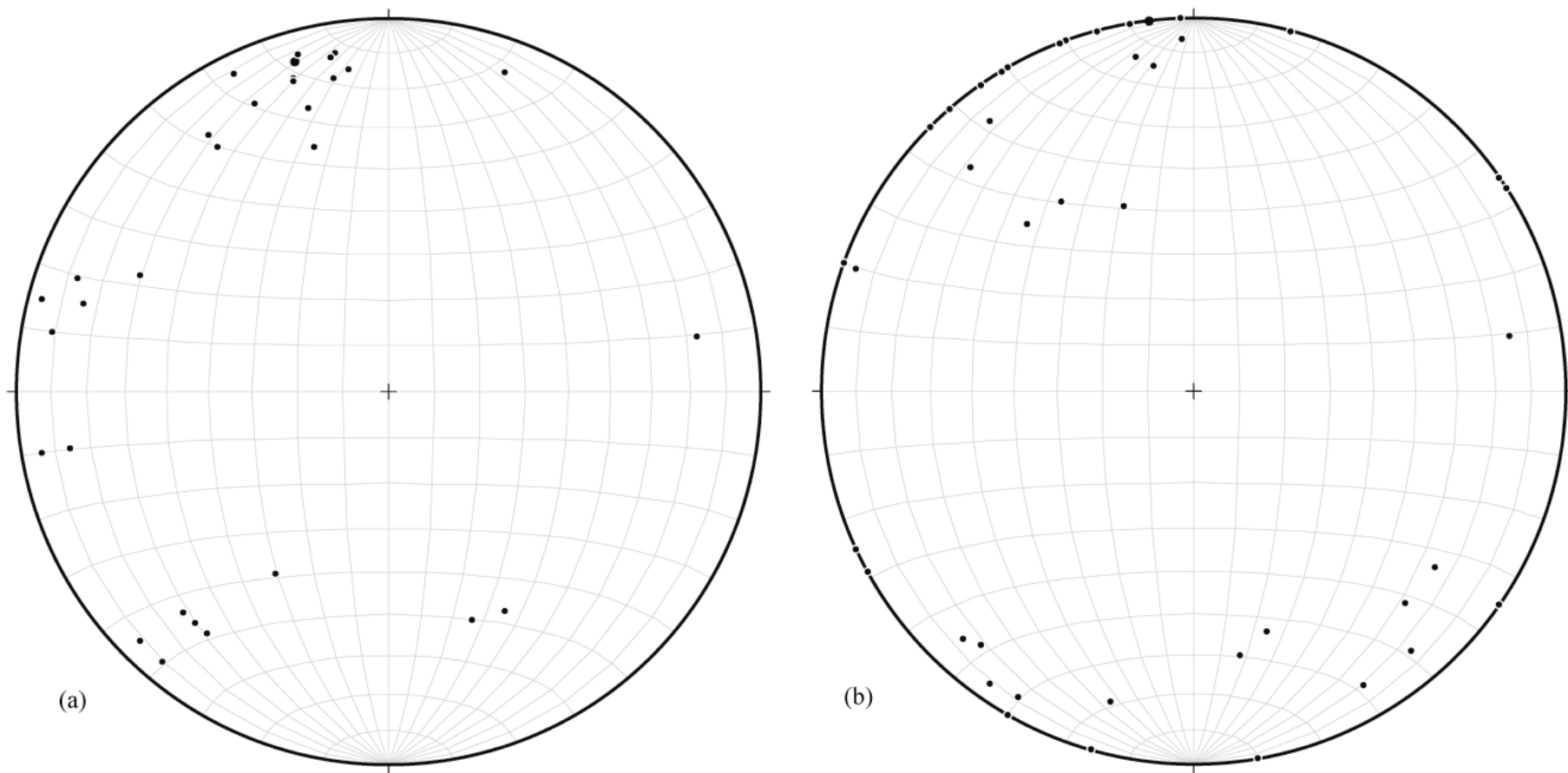


Figure 4–9. (a) Equal-area stereoplot of trend and plunge of L_2 mineral stretching lineations. $n=31$. (b) Equal-area stereoplot of trend and plunge of F_2 fold axes. $n=47$.

Folds

Mesoscale F_2 folds exist as reclined to recumbent, open to tight, upright and overturned, synforms and antiforms (Fig. 4–8d, 4–10a, 4–10b, 4–10c, and 4–10d). A scatter plot of 47 F_2 fold axes indicates the presence of three dominant F_2 fold axis orientations; a northwest, southwest, and southeast (Fig. 4–9b). F_2 fold axes parallel dominant L_2 mineral lineations (Fig. 4–8d, 4–11a, 4–11b, and 4–11c), suggesting they formed coeval with peak deformational and metamorphic conditions, and the presence of sheath folding (Fig. 4–8d and 4–11c).

Measurements of overturned F_2 fold axial planes show a dominant eastward vergence (Fig. 4–8d) of which a large component of these orientations are related to later folding during the D_4 and D_5 events. A north-northwest map-scale sheath fold recognized by Byars (2010) south of the study area trends into the middle portions of my map area (Plate 1).

Faults

Ductile thrusting is a major component of Neoacadian orogenesis, resulting in the emplacement of western Inner Piedmont Tumblebug Creek, Walhalla, Six Mile-Sugarloaf Mountain, Mill Spring, Marion, and the eastern Inner Piedmont Brindle Creek thrust sheet. Recognition of the Brindle Creek fault surrounding the Newton window marks the largest known internal exposure of footwall rocks in the eastern Inner Piedmont. In the vicinity of the central-western Newton window, the Brindle Creek fault trends north-south and displays a moderate westward dip, juxtaposing rocks of the Cat Square terrane against rocks of the lower Tallulah Falls Formation. North of the study area the Brindle Creek fault abruptly changes orientation to a northeasterly trend (Goldsmith et al., 1988). The sinuous trend of the Brindle Creek fault in my study area is related to post emplacement deformation (Plate 1). In outcrop exposure the fault is marked by a sharp truncation of moderately dipping foliations on either side of the fault zone

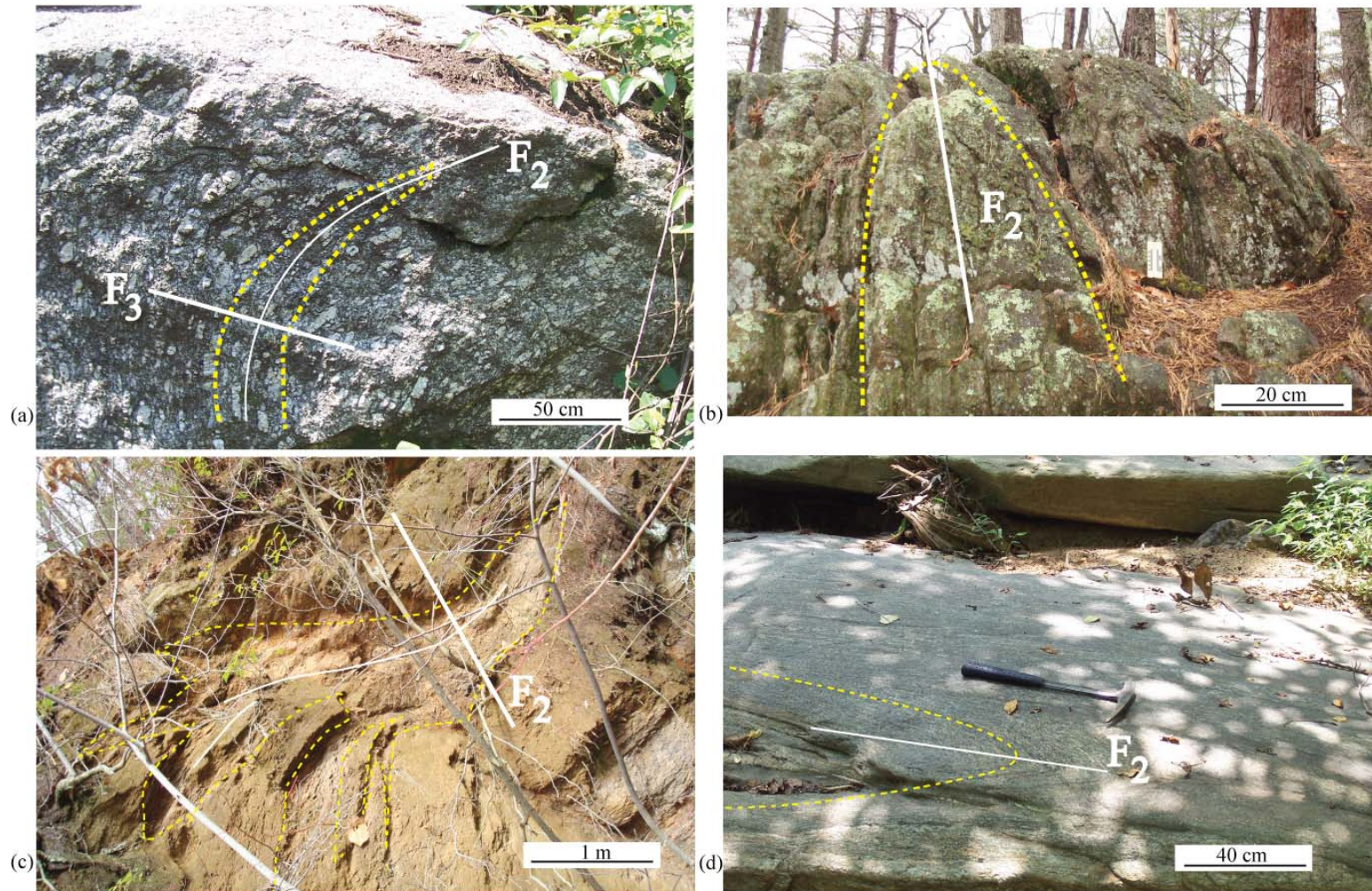


Figure 4–10. (a) Foliated Devonian Walker Top pluton at station R 89 showing refolded isoclinal F_2 fold axis, refolded into F_3 open fold. Yellow dashes follow fold trace. Station is located in small tributary east of Cow Branch Creek southwest of Plateau, North Carolina. (b) Tight fold in Cat Square terrane sillimanite schist at station LV 24 on top of Baker Mountain, southwest of Hickory, North Carolina (c) Station LV 76 on top of Baker Mountain; foliated quartz-feldspar-muscovite pegmatite margin interfingering Cat Square terrane sillimanite schist, displaying an open fold across contact. Pegmatite margin outlined by yellow dashed line. (d) North-plunging antiformal F_2 fold axis at station R 217 displaying east-verging foliations in lower Tallulah Falls Formation granitic gneiss interlayer. Fold outlined with yellow dashes. Station is located in headwaters of Haas Creek near Blackburn, North Carolina.

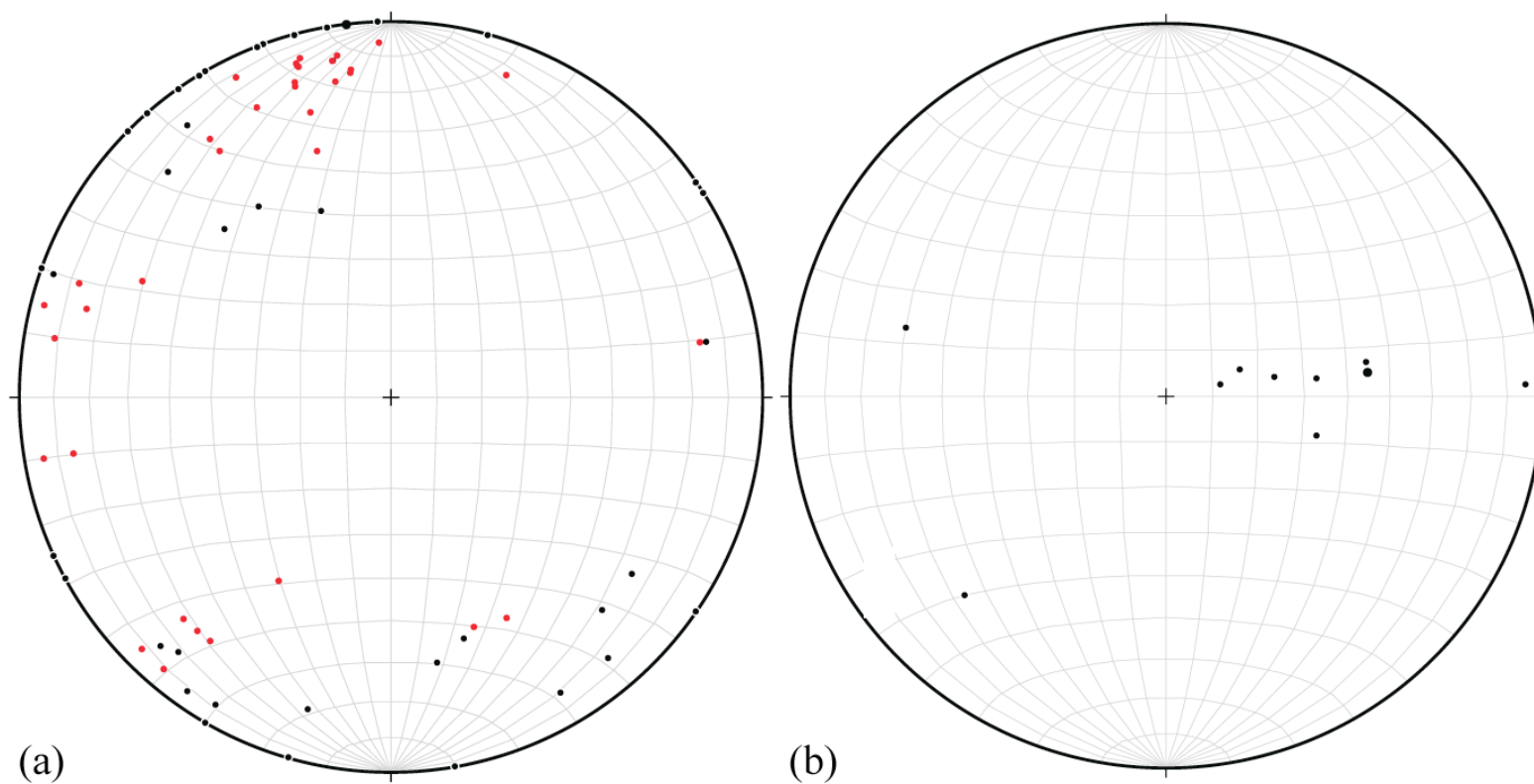


Figure 4-11. (a) Composite scatter plots of L_2 mineral lineations and F_2 fold axes. Black points represent fold axes; red points represent mineral lineations. $n=78$. (b) Scatter plot of inclined F_2 fold axial surfaces showing a predominance of eastward vergence. $n=10$.

(Fig 4–12a and 4–12b). Weathered leucocratic stringers (Fig 4–12c and 4–12d) recognized in a borrow pit may be remnants of mylonitic fabric in lower Tallulah Falls footwall rocks. In addition S-C mylonitic foliations define the Brindle Creek fault in other areas of the study area (Fig. 4–4a). In areas where the Brindle Creek fault is covered, it is delineated by the transition from sillimanite schist to migmatitic biotite gneiss and amphibolite/hornblende gneiss. South of the study area Byars (2010) identified mylonitic textures associated with the contact, and truncations of hanging-wall plutons of the Devonian Walker Top Granite. Similar orientations of foliations exist on both sides of the Brindle Creek fault, suggesting faulting occurred coeval with S₂ foliation formation. Internal mylonitic textures and S-C fabrics exist in outcrops nearest the Brindle Creek fault. In addition, outcrop-scale shear zones and mylonitic textures are commonly found in the internal portions of the Brindle Creek thrust sheet and Newton window, suggesting shearing occurred across a broad zone.

D₃ and D₄ Deformation

Events occurring after the high temperature peak of the Neocadian orogeny, transitioning into the early Alleghanian orogeny, are reserved for the D₃ deformational episode. D₃ events reflect early Alleghanian ductile folding of earlier D₂ structures, such as the Brindle Creek fault, into isoclinal, recumbent folds. Features from the D₃ events formed under conditions less than the peak of the Neocadian orogeny (Mersch et al., 2005). Byars (2010) noted the outcrop pattern of the Brindle Creek fault is likely related to F₃ tight to open folding. D₄ features exist as late Alleghanian open folding. These features refolded previous structures into broad, long-wavelength regional synforms and antiforms. Long-wavelength folding resulted in the formation of the Newton antiform. The emplacement of ductile Inner Piedmont thrust sheets had ceased by this time; temperatures decreased across the Inner Piedmont, resulting in single

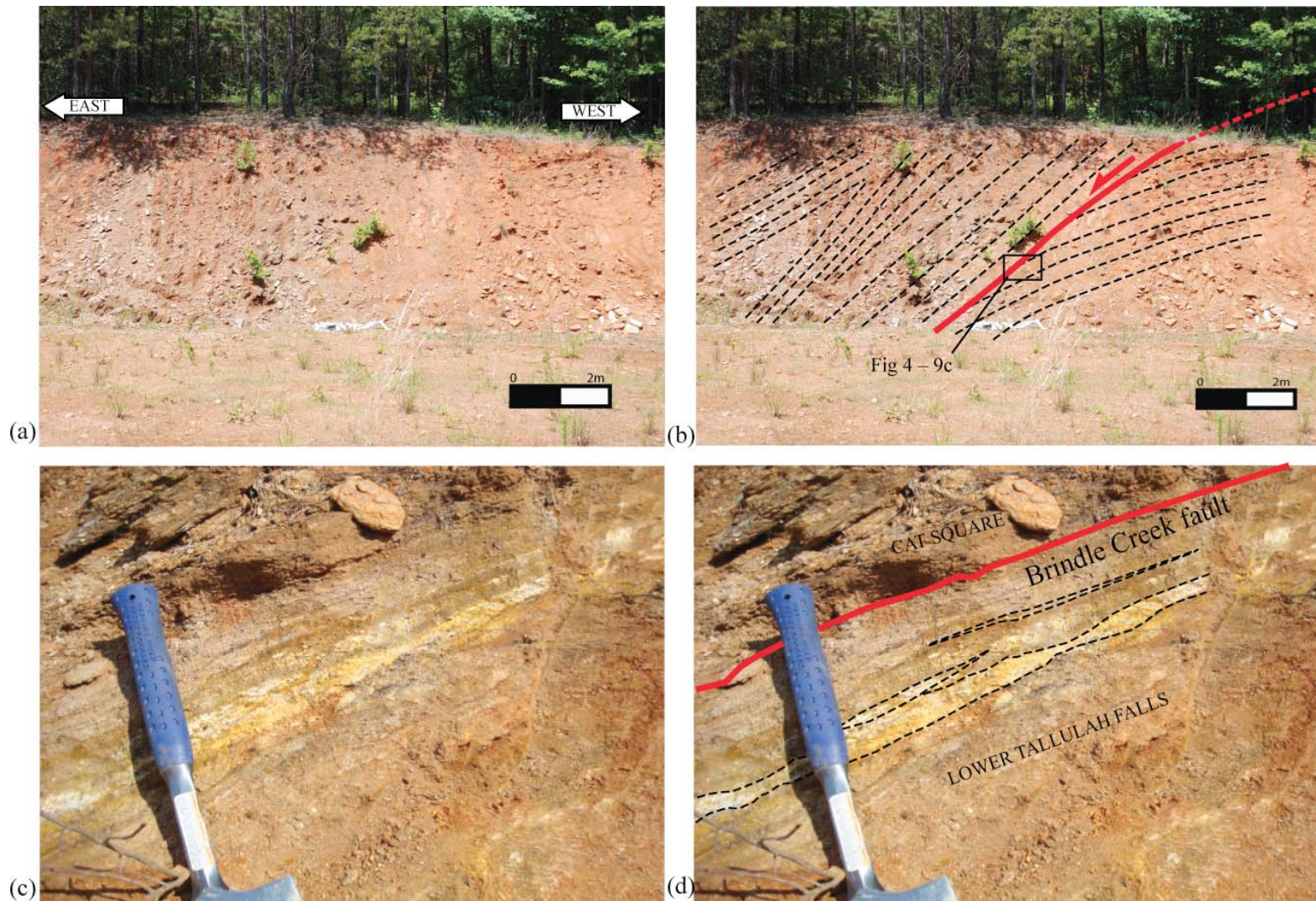


Figure 4-12. (a) West-facing Brindle Creek thrust fault in borrow pit, station R204, near Reepsville, North Carolina. (b) Moderately to steeply dipping hanging wall rocks in the left-hand portion of the photo are truncated against shallowly dipping saprolitic lower Tallulah Falls formation biotite/amphibolite gneiss. Black dashed lines represent form lines from measurements of planes of foliation. Notice the presence of hanging wall Z-folds corresponding to the western limb of the Newton antiform. Picture was taken facing due north, parallel to foliation strike. (c) Truncation of Cat Square terrane sillimanite schist (top left corner) by Brindle Creek fault against lower Tallulah Falls Formation biotite/amphibolite gneiss. (d) Leucocratic stringers (outlined with black dashes) represent relict mylonitic fabric. Hammer for scale. Red line indicates location of Brindle Creek fault.

thrust sheets becoming rigid as composite Blue Ridge and Inner Piedmont thrust sheets cooled. Likewise, major crustal faults such as the Brevard fault zone and the central Piedmont suture were reactivated during D₄. During this time the rigid Blue Ridge-Inner Piedmont megathrusts advanced cratonward at the peak of Alleghanian mountain building (Hatcher, 2002).

D₅ and D₆ Deformation

The D₅ and D₆ deformational events reflect brittle upper crustal deformational conditions associated with Mesozoic extension and Cenozoic uplift. D₅ features of the Inner Piedmont include siliceous Triassic-Jurassic cataclasite (Fig. 2–16) and diabase dikes, and jointing. Diabase dikes crosscutting the map area intruded ~199 Ma (Hames et al., 2000) forming two regional sets: north-south and a northwest-southeast. Diabase dikes present in the map area trend northwest-southeast (~N45°W; Fig. 4–13) and crosscut foliated metamorphic country rocks. An isolated linear body of siliceous cataclasite is present in the Longview quadrangle (Fig. 4–13; Plate I). This feature is traceable for a short distance northeast from a roadside outcrop before terminating into Paleozoic country rock to the northeast. This feature consists of multiply broken and annealed fragments of angular quartz (Fig. 2–17c and Fig. 2–17d) of varying size. Garihan et al. (1993) noted Mesozoic diabase dikes crosscut many large prominent brittle faults in the North Carolina Inner Piedmont. Alternatively, diabase dikes are cut by these faults suggesting the faulting occurred during the Mesozoic.

MAP PATTERNS

Outcrop patterns of lithologic contacts display the intricate relationships between deformation and time (Figure 4–13; Plate I). Interfingering of lithologic contacts (Fig. 4–13) may in small part be due to deposition of protolith sedimentary rocks, but largely is related to extensive protracted deformation, as indicated by north to northwest-trending outcrop pattern,

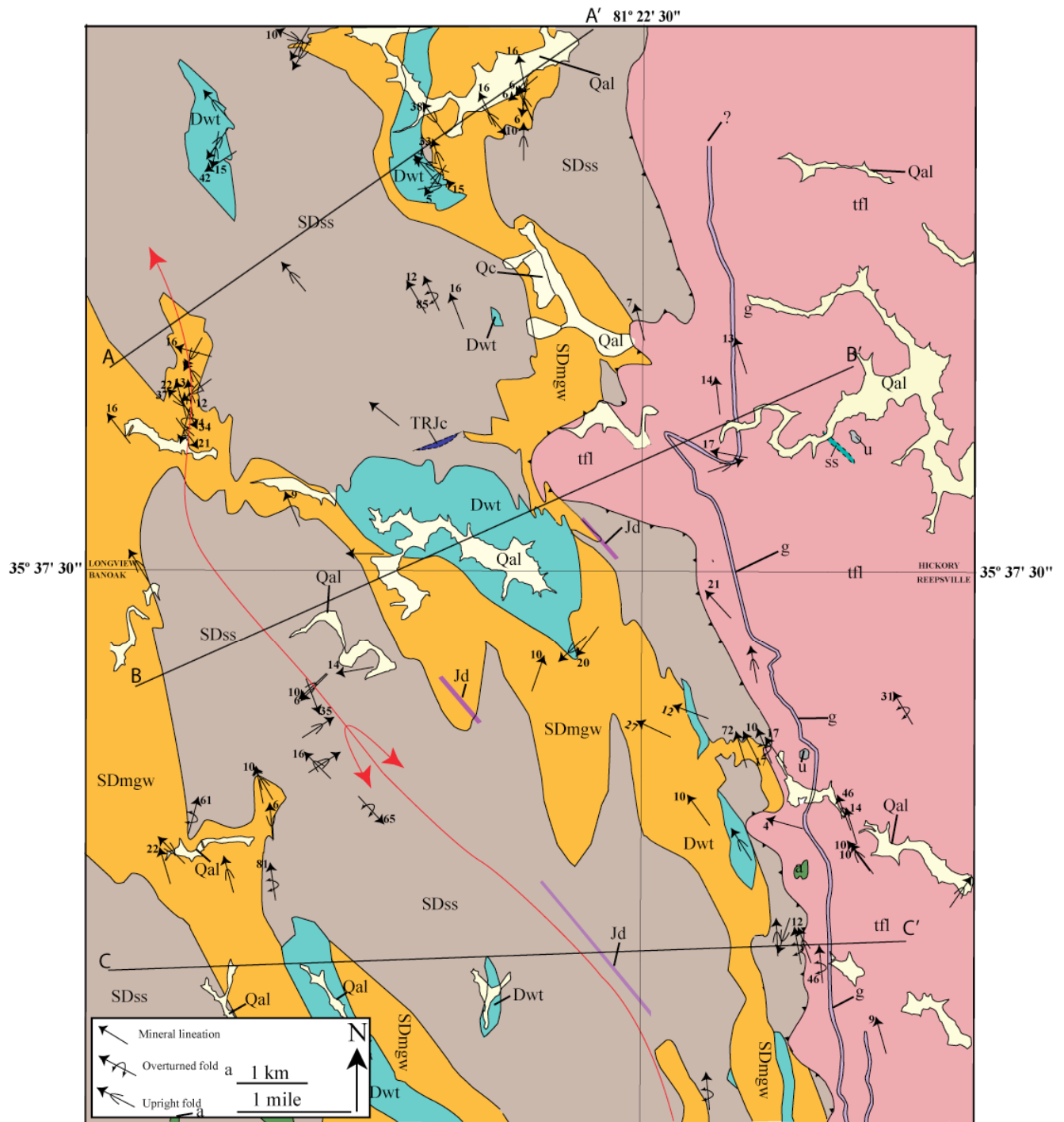


Figure 4-13. Simplified geologic map with cross-section lines corresponding to Figure 4-14, with L₂ mineral lineations, F₂ fold axes, and sheath fold axes. Cat Square terrane: SDss=Siluro-Devonian sillimanite schist, SDmgw=Siluro-Devonian metagraywacke, Dwt=Devonian Walker Top Granite, tfl=lower Tallulah Falls metagraywacke/amphibolite gneiss, ss=lower Tallulah Falls sillimanite/mica schist, a=amphibolite, u=soapstone/altered ultramafic rock, g=gondite, TRJc=Triassic- Jurassic cataclasite, Jd=Jurassic diabase dike, Qc=Quaternary colluvium, Qal =Quaternary alluvial material. Red line=regional antiformal sheath fold axis.

curved mineral lineation patterns, a curved map-scale sheath fold axis, and refolded folds (Fig. 4–13). The axis of a northwest-plunging, tongue-shaped, map-scale sheath fold trends northwest through the study area, is cored by sillimanite schist, and outlined by metagraywacke. It was first recognized by Byars (2010) to the south of this study area (Fig. 4–13). Linear Devonian Walker Top plutons trend into the southern portions of the map area and likely intruded as lens shaped plutons or tabular sills. Progressive deformation created the long tubular shape of these plutons. Alternatively, isolated “boudins” of Devonian Walker Top Granite occur around the margins of sheath folds, possibly reflecting the contrast in strength of granitoids versus surrounding metasedimentary units during progressive deformation (Merschat et al., 2005). The concordance of these plutons with surrounding country rock indicates deformation persisted after emplacement. North-south-striking foliations occur in the southern portions of the study as they begin to trend northwest to southeast. Coaxial mineral stretching lineations and F_2 fold axes follow the same north to northwest curvature of foliations, suggesting they are genetically related, and formed simultaneously (Fig. 4–13).

CROSS SECTIONS INTERPRETATION

Three E-W cross sections were constructed to graphically interpret map patterns, foliations, and down-plunge projections of detailed map geometries gathered throughout the study area (Figs. 4–14 and 4–15). The Brindle Creek fault dips to the west $\sim 43^\circ$. Foliation orientations/intersections indicate the scale of folding throughout the study area; particularly demonstrating the coaxial relationship between isoclinal F_2 folding, sheath folding, and the dominant S_2 foliation. The superposition of later Alleghanian folding is best represented by west-facing fold axial surfaces and eastward vergence. The map-scale sheath fold, cored by sillimanite schist, trends through the western portions of cross sections B-B' and C-C'; the tongue-shaped

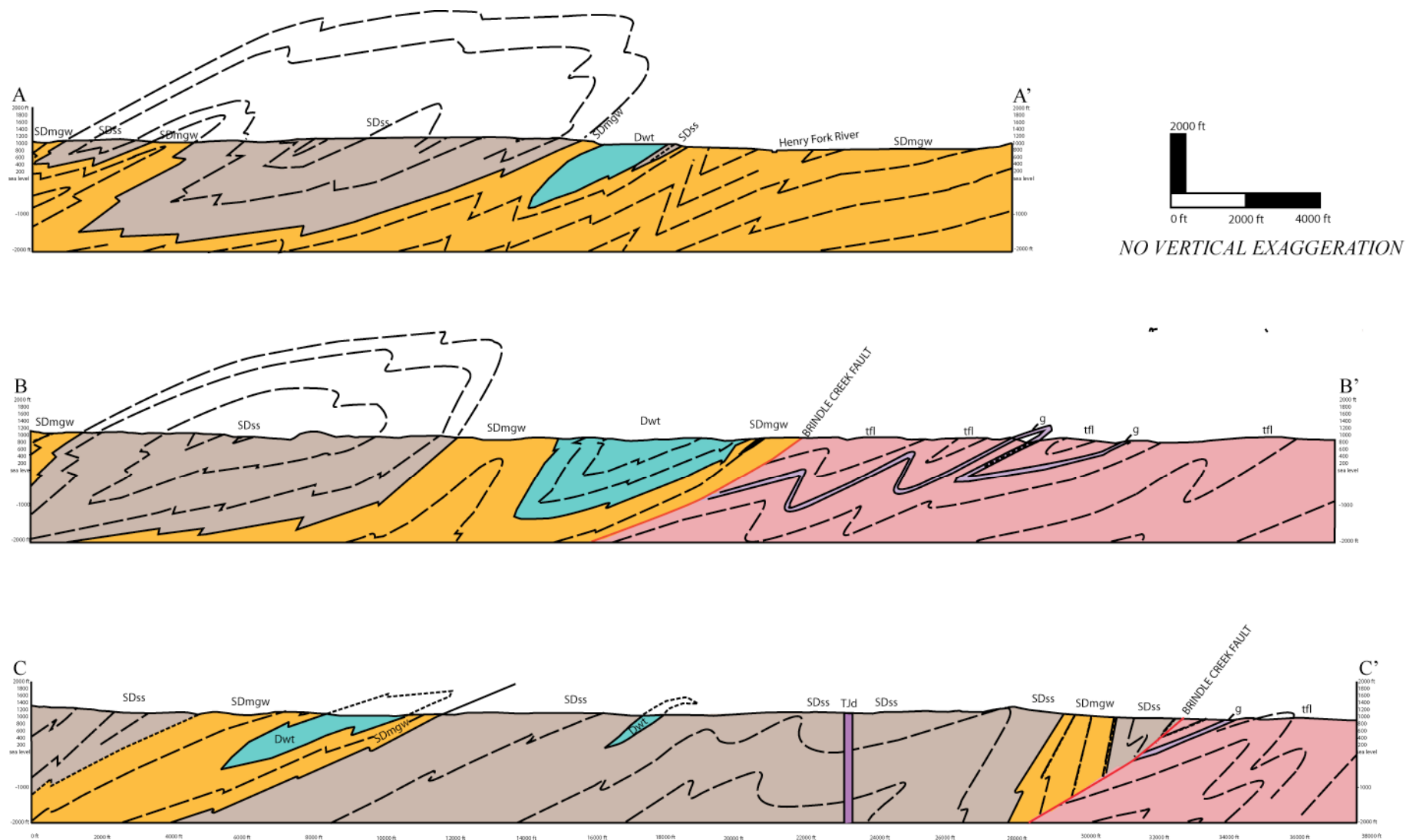


Figure 4–14. Cross sections across the map area located on Figure 4–13. Dashed lines are form lines drawn parallel to surface measurements of foliations and fold axes. tfl= lower Tallulah Falls metagraywacke/amphibolite gneiss, SDss=Silurian Devonian sillimanite schist, SDmgw=Silurian Devonian metagraywacke, Dwt=Devonian Walker Top Granite, Tjd = Triassic-Jurassic diabase dike, g=gondite.

body of sillimanite is encapsulated by metagraywacke surrounded by disjointed Devonian Walker Top plutons at its margins. The disjointing of plutons suggests a rheological contrast existed between deforming Devonian Walker Top plutons and surrounding metasediments.

WESTERN NEWTON WINDOW KINEMATIC OVERVIEW

Previous research has provided a wealth of data regarding deformation, metamorphism, and timing of key events in the southern Appalachian Mountains. A recent synthesis by Merschat et al. (2005) described the Inner Piedmont as a southwest-directed, ductile extruded channel, flowing under heterogeneous conditions beneath the overriding Carolina superterrane (Merschat et al., 2005). They concluded that shallow-dipping foliations (Figs. 4–15a and 4–15b) and the arcuate pattern of mineral lineations, first observed by Goldsmith (1981), define a counterclockwise flow pattern across the Inner Piedmont (Figs. 4–15c and 4–15d). Using regional map relationships of sheath fold axes, arcuate pattern of mineral stretching lineations, and F_2 fold axes they established that the northwest-trending Inner Piedmont features are rooted to the east beneath the Carolina superterrane, trend north to northwest across the core, and are deflected to the southwest along the Brevard fault zone. Channel flow occurred beneath the overriding Carolina superterrane under transpressional conditions, resulting in counterclockwise rotation of the underlying Inner Piedmont rocks. Similar evidence exists in the study area that is consistent with the interpretation of Merschat et al. (2005) (Fig. 4–16). Patterns of subhorizontal mineral lineations and F_2 fold axes in the study area indicate north to northwesterly transport and originate from the south southeast, towards the Kings Mountain belt and Carolina superterrane (Figs. 4–16, 4–17a, 4–17b, and 4–17c). By comparison, the L_2 mineral lineation pattern of the study area follows the same north-northwesterly trend, similar to other mineral stretching lineations recognized in the eastern portion of the eastern Inner Piedmont (Figs. 4–13 and 4–16),

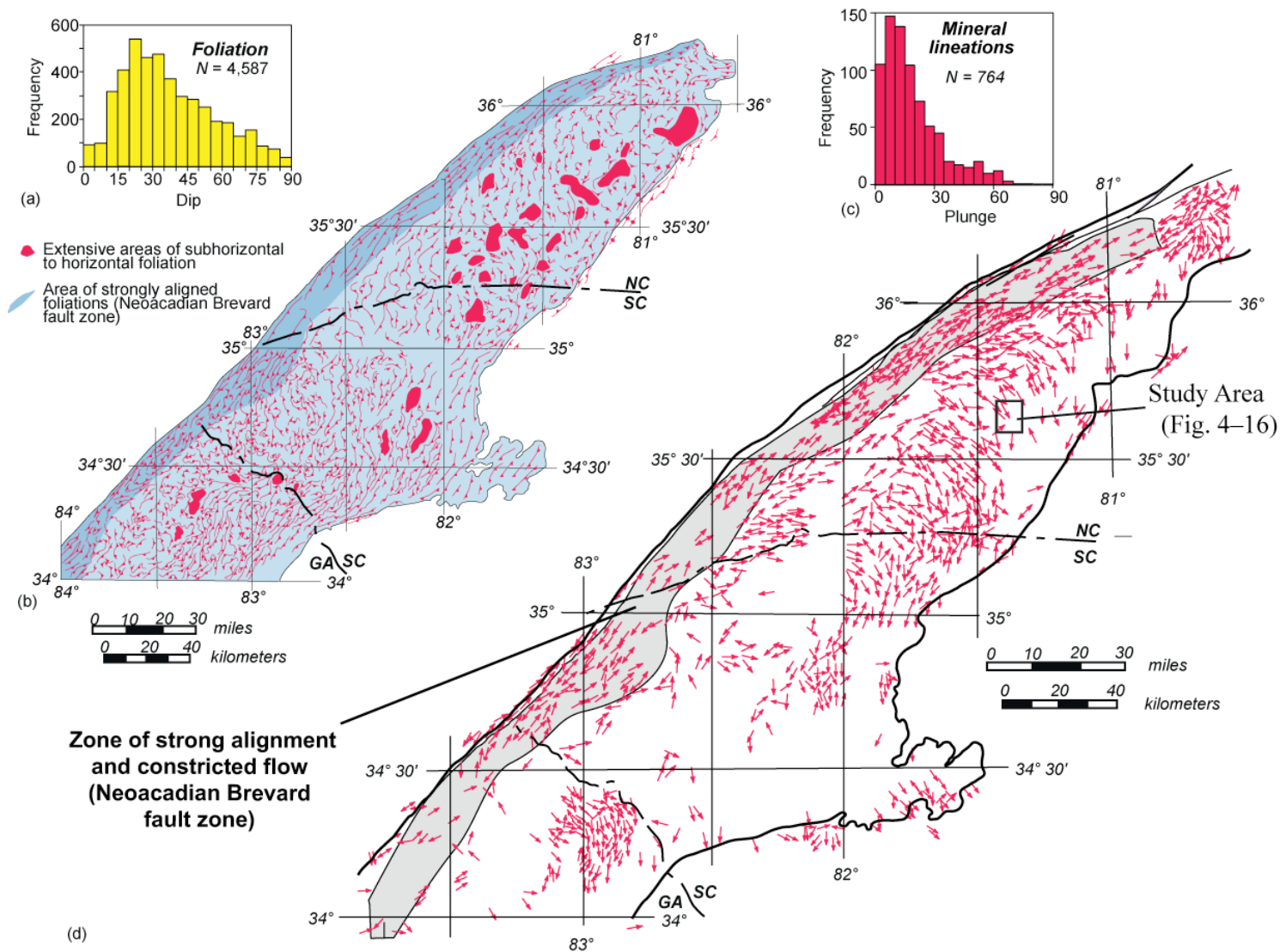


Figure 4-15. Pattern of dominant S_2 foliations and L_2 lineations in the northern Inner Piedmont. (a) Histogram of 4587 dip measurements of foliation in the northern Inner Piedmont. (b) Form-line map of S_2 foliations in the northern Inner Piedmont. Form lines are parallel to strike; teeth on trend line indicate dip direction. (c) Histogram of 764 mineral lineations in the northern Inner Piedmont. Note the dominance of gentle plunge. (d) Distribution of measured lineations. Arrowheads point down plunge. Black box indicates location of study area, corresponding to Figure 4-16. Figure modified from Hatcher (2001).

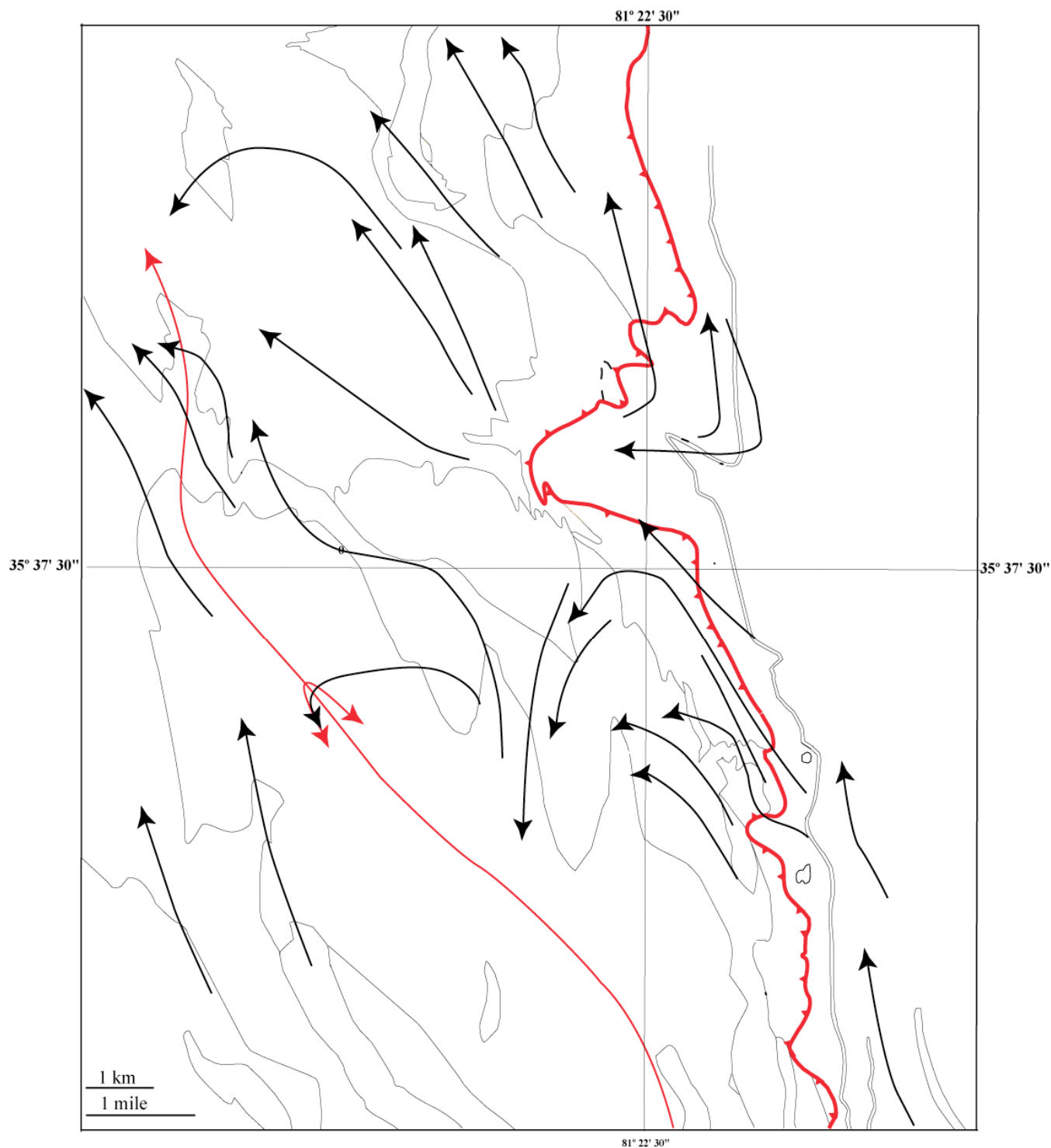


Figure 4–16. L₂ lineation map outlined on Figure 4–15c showing north-northwesterly trend of gentle-plunging lineations in the study area. Lineations show strong alignment near the Brindle Creek fault. Lineations disperse to the northwest and west in the internal portions of the Brindle Creek thrust sheet. Solid red line =map scale sheath fold, Solid black lines=contacts. Dashed red line=Brindle Creek fault, Black arrows=flow lines projected from L₂ mineral lineation.

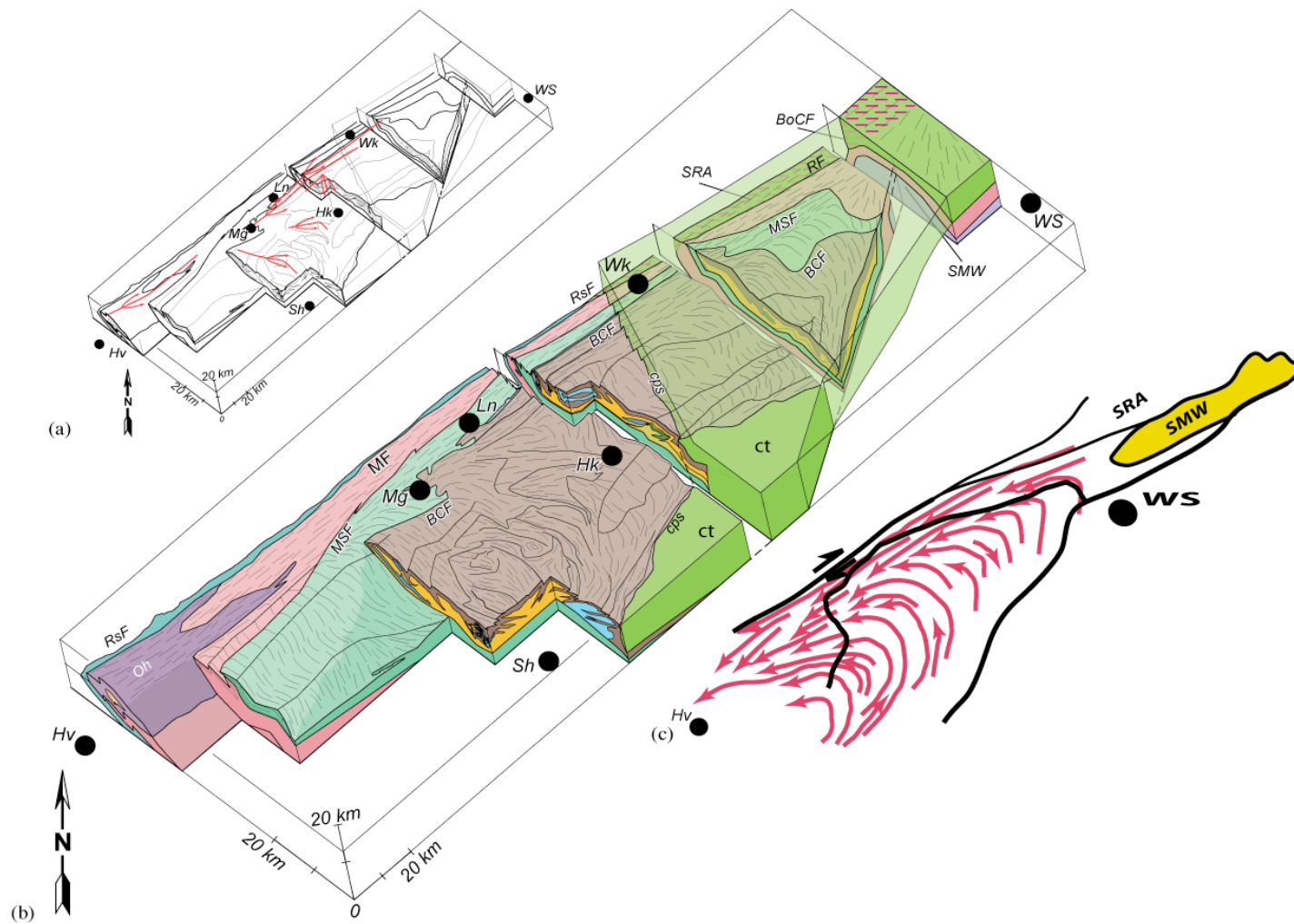


Figure 4-17. (a) 3D block diagram depicting the structure of part of the northern IP from near Hendersonville, NC to the Sauratown Mountains window. Red lines are map-scale sheath folds. Vertical exaggeration in (a) and (b) 1.3:1:1 (X:Y:Z). Towns: Hk-Hickory; Hv-Hendersonville; Ln-Lenoir; Mg-Morganton; Sh-Shelby; Wk-Wilkesboro; WS-Winston-Salem. (b) More detailed 3D block diagram of area in (a) showing major tectonic units. Trends on block surface drawn from lineations. BCF-Brindle Creek fault; BoCF-Bowens Creek fault; cps-Central Piedmont suture; ct-Carolina terrane; MSF-Mill Spring fault; MF-Marion fault; Oh-Henderson Gneiss; RF-Ridgeway fault; RsF-Rosman fault; SMW-Sauratown Mountains window; SRA-Smith River allochthon. Town abbreviations same as in (a). (c) Flow model for the northern Inner Piedmont based on detailed geologic mapping and lineation data of the kind displayed in Figure 4-16. WS-Winston-Salem. Hv-Hendersonville. Figure from Mersch et al. (2005).

defining a counterclockwise arcuate pattern. Shallow to moderate west-dipping foliations occur throughout the study area defining six structural domains. Two dominant domains, IX and X, show a strong parallelism to the Brindle Creek fault, and contain parts of a northwest-plunging map-scale sheath fold (Figs. 4–5 and 4–14). Likewise, tongue-shaped map patterns consisting domain IX and X mesofabrics indicate the presence of this feature. Disjointed outliers of mylonitic Devonian Walker Top indicate deformation occurred syn-to post kinematically during sheath fold formation following the emplacement of anatectic melts.

In conclusion, high temperature structures of the central portion of the western Newton window formed under noncoaxial ductile flow, resulting in the formation of major sheath folds, parallel fold axes, and mineral lineations, similar to other areas of the Inner Piedmont. Mineral stretching lineations formed during the Neoacadian thermal maximum, and track a counterclockwise flow path, indicating oblique deflection under transpressional conditions coinciding with accretion of Carolina (Hatcher, 2002; Merschat et al., 2005; Hatcher and Merschat, 2006) (Figs. 4–18a, 4–18b, and 4–18c). Early Alleghanian folding occurred under moderate temperature conditions, resulting in open to tight folding of previous high temperature structures. Late Alleghanian regional folding coincided with the emplacement of the Blue Ridge/Inner Piedmont megathrusts, and the formation of the Newton antiform. Depth of crustal deformation changes from mid-crustal conditions to upper crustal, brittle conditions, Mesozoic diabase intrusion and the formation of siliceous cataclasite occurred during the breakup of Pangea, crosscutting previous orogenic features. Cenozoic uplift and unroofing resulted in regional joint formation and exposure of high temperature features once contained deep in the crust.

CHAPTER 5

CONCLUSIONS

1. The Newton window exposes a distinct assemblage of hornblende-biotite gneiss, amphibolite, and ultramafic rocks. Geochronologic investigations and detailed field mapping determined the Newton antiform exposes rocks of the lower Tallulah Falls member of the Ashe-Tallulah Falls Formation. The lowest member of this tectonostratigraphy is the only unit present in the Newton window. Framing the Newton window are Cat Square terrane metasedimentary rocks, anatectic melts, and plutons such as the Walker Top orthogneiss, in the Brindle Creek thrust sheet. Four rock types occurring in the lower Tallulah Falls Formation are mapped inside the Newton window, hornblende-biotite gneiss, gondite, amphibolite, and ultramafics. The Cat Square terrane sillimanite schist is a major ridge former and holds up the higher topography of the study area. Rocks rich in biotite such as the Cat Square terrane metagraywacke and lower Tallulah Falls Formation rocks form topographically low areas.

2. Regional metamorphism occurred during the Neocadian orogeny, resulting in the production of high-temperature minerals. Sillimanite occurs across the Brindle Creek fault, suggesting rocks in each terrane were metamorphosed during the same period of time under similar conditions. Common metamorphic accessory minerals in both terranes include garnet, biotite, muscovite, plagioclase, and K-feldspar.

3. X-ray maps of garnet used for temperature and pressure estimates indicate the presence of diffusion along grain boundaries. Electron microprobe analyses of Cat Square terrane core and rim garnet-biotite and garnet-plagioclase pairs from a regional sheath fold indicates an average temperature and pressure of 620° C, 3.6 kbar and 710° C, 6.1 kbar, respectively. Temperature and pressure estimates from the lower Tallulah Falls Formation core and rim analyses yield conditions of 570° C, 4.1 kbar and 660° C, 5.9 kbar, respectively. The maximum burial depth for both Cat Square and Tugalo terrane rocks is ~20 km. The range in metamorphic age dates, 365 Ma to 330 Ma, suggests subduction and accretion occurred at a rate of 1 kilometer per 1.75 million years.

4. Rocks of the western Newton window were deformed under high-grade regionally metamorphic conditions ductile deformation during the Neoacadian orogeny. Evidence of early low-temperature features were destroyed by progressive high-temperature and pressure deformation, although evidence of S_1 foliations is present in boudins in the lower Tallulah Falls rocks occurring inside the Newton window. The high temperature structures of the central portion of the western Newton window formed under noncoaxial ductile flow, resulting in the formation of major sheath folds, parallel fold axes, and mineral lineations, similar to other areas of the Inner Piedmont. Mineral stretching lineations formed during the Neoacadian thermal maximum, and track a counterclockwise flow path, indicating oblique deflection under transpressional conditions coinciding with accretion of Carolina Superterrane. Early Alleghanian folding occurred under moderate temperature conditions, resulting in open to tight folding of previously high temperature structures. Late Alleghanian regional folding coincided with the emplacement of the Blue Ridge/Inner Piedmont megathrust sheet and the formation of the Newton antiform. Depth of crustal deformation changes from mid-crustal conditions to upper crustal brittle conditions.

5. Mesozoic diabase dike intrusion and the formation of siliceous cataclasite occurred during the breakup of Pangea, crosscutting earlier orogenic features. Cenozoic uplift and erosion exposed high temperature features once contained deep in the crust.

REFERENCES CITED

- Albee, A.L., 1965, Phase equilibria in three assemblages of kyanite-zone pelitic schist, Lincoln Mountains Quadrangle, central Vermont: *Journal of Petrology*, vol. 6, p. 246-301.
- Berman, R. G., 1990, Mixing properties of Ca-Mg-Fe-Mn in garnets: *American Mineralogist*, v. 75, p. 328-334.
- Berquist, P. J., Fisher, C. M., Miller, C. F., Wooden, J. L., Fullagar, P. D., and Loewy, S. L., 2005, Geochemistry and U-Pb zircon geochronology of Blue Ridge basement, western North Carolina and eastern Tennessee: Implications for tectonic assembly, *in* Hatcher, R. D., Jr., and Mersch, A. J., eds., *Blue Ridge geology geotraverse east of the Great Smoky Mountains National Park, western North Carolina*: Carolina Geological Society Guidebook, p. 33-43.
- Bier, S. E., 2001, *Geology of the southeastern South Mountains, North Carolina* [M. S.thesis]: Knoxville, University of Tennessee, 162 p.
- Bier, S. E., Bream, B. R., and Giorgis, S. D., 2002, Inner Piedmont stratigraphy, metamorphism, and deformation in the Marion-South Mountains area, North Carolina, *in* Hatcher, R. D., Jr., and Bream, B. R., eds., *Inner Piedmont geology in the South Mountains-Blue Ridge Foothills and the southwestern Brushy Mountains, central-western North Carolina*: North Carolina Geological Survey, Carolina Geological Society annual field trip guidebook, p. 65-99.
- Bream, B. R., 1999, Structure and stratigraphic relationships of ortho- and paragneisses southwest of Marion, North Carolina [M. S. thesis]: Knoxville, University of Tennessee, 155 p.
- Bream, B. R., 2002, The southern Appalachian Inner Piedmont: New perspectives based on recent detailed geologic mapping, Nd isotopic evidence, and zircon geochronology, *in* Hatcher, R. D., Jr., and Bream, B. R., eds., *Inner Piedmont geology in the South Mountains-Blue Ridge Foothills and the southwestern Brushy Mountains, central-western North Carolina*: Carolina Geological Society Guidebook, p. 45-63.
- Bream, B. R., 2003, Tectonic implications of geochronology and geochemistry of para- and orthogneisses from the southern Appalachian crystalline core [Ph. D. dissertation]: Knoxville, University of Tennessee, 296 p.
- Bream, B. R., Hatcher, R. D., Jr., Miller, C. F., and Fullagar, P. D., 2001, Geochemistry and provenance of Inner Piedmont paragneisses, NC and SC: Evidence for an internal terrane boundary?: *Geological Society of America Abstracts with Programs*, v. 33, no. 2, p. 65.
- Bream, B. R., Hatcher, R. D., Jr., Miller, C. F., and Fullagar, P. D., 2004, Detrital zircon ages and Nd isotopic data from the southern Appalachian crystalline core, GA-SC-NC-TN: New provenance constraints for Laurentian margin paragneisses, *in* Tollo, R. P., Corriveau, L., McLelland, J., and Bartholomew, M. J., eds., *Proterozoic evolution of the Grenville orogen in North America*: Geological Society of America Memoir 197, p. 459-475.
- Bryant, B., and Reed, J. C., Jr., 1970, *Geology of the Grandfather Mountain window and vicinity, North Carolina and Tennessee*: U.S. Geological Survey Professional Paper 615, 190 p.
- Butler, J. R., 1991, Metamorphism, *in* Horton, J. W., Jr., and Zullo, V. A., eds., *The geology of the Carolinas*: Carolina Geological Society Fiftieth Anniversary Volume: Knoxville, University of Tennessee Press, p. 127-141.
- Byars, H. E., Mersch, A. J., Hatcher, R. D., Jr., Wooden, J. L., 2008, Timing and implications for the emplacement of the Paleozoic Vale (Cat Square) charnockite and Walker Top Granite, eastern Inner Piedmont, North Carolina: *Geological Society of America Abstracts with Programs*, v. 40, no. 4, p. 18.
- Byars, H. E., 2010, Tectonic evolution of the west-central portion of the Newton window, North Carolina Inner Piedmont: timing and implications for the emplacement of the Paleozoic Vale charnockite, Walker Top granite, and mafic complexes [M.S. thesis]: Knoxville, University of Tennessee, 248 p.
- Carpenter, R. H., 1970, Metamorphic history of the Blue Ridge Province of Tennessee and North Carolina: *Geological Society of America Bulletin*, v. 81, p. 749-762.
- Carrigan, C. W., Bream, B. R., Miller, C. F., and Hatcher, R. D., Jr., 2001, Ion microprobe analyses of zircon rims from the eastern Blue Ridge and Inner Piedmont, NC-SC-GA: Implications for the timing of Paleozoic metamorphism in the southern Appalachians: *Geological Society of America Abstracts with Programs*, v. 33, no. 2, p. 7.

- Carrigan, C. W., Miller, C. F., Fullagar, P. D., Bream, B. R., Hatcher, R. D., Jr., and Coath, C. D., 2003, Ion microprobe age and geochemistry of southern Appalachian basement, with implications for Proterozoic and Paleozoic reconstructions: *Precambrian Research*, v. 120, p. 1-36.
- Chatterjee, N. D., and Johannes, W., 1974, Thermal stability and standard thermodynamic properties of synthetic 2M1 muscovite, $\text{KAl}_2\text{AlSi}_3\text{O}_{10}(\text{OH})_2$: *Contributions to Mineralogy and Petrology*, v. 48, p. 89-114.
- Connelly, J. B., and Dallmeyer, R. D., 1993, Polymetamorphic evolution of the western Blue Ridge province: Evidence from $^{40}\text{Ar}/^{39}\text{Ar}$ whole-rock slate/phyllite and muscovite ages: *American Journal of Science*, v. 293, p. 322-359.
- Corrie, S. L., and Kohn, M. J., 2007, Resolving the timing of orogenesis in the western Blue Ridge, southern Appalachians, via *in situ* ID-TIMS monazite geochronology: *Geology*, v. 35, p. 627-630.
- Dallmeyer, R. D., 1988, Late Paleozoic tectonothermal evolution of the western Piedmont and eastern Blue Ridge, Georgia: Controls on the chronology of terrane accretion and transport in the southern Appalachian orogen: *Geological Society of America Bulletin*, v. 100, p. 702-713.
- Dallmeyer, R. D., Wright, J. E., Secor, D. T., Jr., and Snoke, A. W., 1986, Character of the Alleghanian orogeny in the southern Appalachians: Part II. Geochronological constraints on the tectonothermal evolution of the eastern Piedmont in South Carolina: *Geological Society of America Bulletin*, v. 96, p. 1329-1344, doi: 10.1130/0016-7606(1986)97<1329:COTAOI>2.0CO;2
- Davis, T. L., 1993, Geology of the Columbus Promontory, western Piedmont, North Carolina, southern Appalachians, in Hatcher, R. D., Jr., and Davis, T. L., eds., *Studies of Inner Piedmont geology with a focus on the Columbus Promontory*: Carolina Geological Society Guidebook, North Carolina Geological Survey, p. 17-43.
- Davis, T. L., Hatcher, R. D., Jr., Liu, A., and Tabor, J. R., 1991, Southern Appalachian western Inner Piedmont: A progressive crustal-scale shear zone: *Geological Society of America Abstracts with Programs*, v. 23, p. 138.
- Dennis, A. J., 2007, Cat Square basin, Catskill clastic wedge: Silurian-Devonian orogenic events in the central Appalachians and the crystalline southern Appalachians, in Sears, J. W., Harms, T. A., and Evenchick, C. A., eds., *Whence the Mountains? Inquiries into the evolution of orogenic systems: A volume in honor of Raymond A. Price*: Geological Society of America Special Paper, 433, p. 313-329.
- Dennis, A. J., and Wright, J. E., 1997a, New U-Pb monazite ages for the Inner Piedmont of South Carolina: *Geological Society of America Abstracts with Programs*, v. 29, no. 3, p. 12.
- Dennis, A. J., and Wright, J. E., 1997b, The Carolina terrane in northwestern South Carolina, USA: Late Precambrian-Cambrian deformation and metamorphism in a peri-Gondwanan oceanic arc: *Tectonics*, v. 16, no. 3, p. 460-473, doi: 10.1029/97TC00449
- Eckert, J. O., Jr., Hatcher, R. D., Jr., and Mohr, D. W., 1989, The Wayah granulite-facies metamorphic core, southwestern North Carolina: High-grade culmination of Taconic metamorphism in the southern Blue Ridge: *Geological Society of America Bulletin*, v. 101, p. 1434-1447, doi: 10.1130/0016-7806(1989)101<1434:TWGFMC>2.3CO;2.
- Espenshade, G. H., Rankin, D. W., Shaw, K. W., and Neuman, R. B., 1975, Geologic map of the east half of the Winston-Salem quadrangle, North Carolina-Virginia: U.S. Geological Survey Map I-709-B, scale 1:250,000.
- Ferry, J. M., and Spear, F. S., 1978, Experimental calibration of the partitioning of Fe and Mg between biotite and garnet: *Contributions to Metamorphic Petrology*, vol. 66, p. 113-117.
- Garihan, J. M., Preddy, M. S., and Ransom, W. A., 1993, Summary of mid-Mesozoic brittle faulting in the Inner Piedmont and nearby Charlotte belt of the Carolinas, in Hatcher, R. D., Jr., and Davis, T. L., eds., *Studies of Inner Piedmont geology with a focus on the Columbus Promontory*: North Carolina Geological Survey, Carolina Geological Society Guidebook, p. 55-65.
- Gatewood, M. P., 2007, Structure and tectonics of the northeastern Inner Piedmont from detailed geologic mapping, geochronologic, geochemical, and petrologic studies with macro-, meso-, and microstructural analyses of ductile fault zones [M.S thesis]: Knoxville, University of Tennessee, 279 p.

- Giorgis, S. D., 1999, Inner Piedmont geology of the northwestern South Mountains near Morganton, North Carolina [M.S. thesis]: Knoxville, University of Tennessee, 191 p.
- Giorgis, S. D., Mapes, R. W., and Bream, B. R., 2002, The Walker Top Granite: Acadian granitoid or eastern Inner Piedmont basement?, *in* Hatcher, R. D., Jr., and Bream, B. R., eds., Inner Piedmont geology in the South Mountains-Blue Ridge Foothills and the southwestern Brushy Mountains, central-western North Carolina: Carolina Geological Society Guidebook, p. 33-44.
- Goldberg, S. A., and Dallmeyer, R. D., 1997, Chronology of Paleozoic metamorphism and deformation in the Blue Ridge thrust complex, North Carolina and Tennessee: *American Journal of Science*, v. 297, p. 488-526.
- Goldsmith, R., 1981, Structural patterns in the Inner Piedmont of the Charlotte and Winston-Salem 2-degree quadrangles, North Carolina and South Carolina, *in* Horton, J. W., and Milton, D. W., eds., Geological investigations of the Kings Mountain belt and adjacent areas in the Carolinas. Carolina Geological Society Field Trip Guidebook, p. 19-27, <http://carolinageologicalsociety.org/cgsguide.htm>.
- Goldsmith, R., Milton, D. J., and Horton, J. W., Jr., 1988, Geologic map of the Charlotte 1-degree x 2-degree quadrangle, North Carolina and South Carolina: U.S. Geological Survey Map I-1251-E, scale 1:250,000.
- Griffin, V. S., Jr., 1969, Migmatitic Inner Piedmont belt of northwestern South Carolina: *South Carolina Division of Geology Geologic Notes*, v. 13, p. 87-104.
- Griffin, V. S., Jr., 1971, The Inner Piedmont belt of the southern crystalline Appalachians: *Geological Society of America Bulletin*, v. 82, p. 1885-1898.
- Griffin, V. S., Jr., 1974, Analysis of the Piedmont in northwest South Carolina: *Geological Society of America Bulletin*, v. 85, p. 1123-1138.
- Hadley, J. B., and Goldsmith, R., 1963, Geology of the eastern Great Smoky Mountains, North Carolina: U.S. Geological Survey Professional Paper 349-B, 118 p.
- Hadley, J. B., and Nelson, A. E., 1971, Geologic map of the Knoxville quadrangle, North Carolina, Tennessee, and South Carolina: U.S. Geological Survey Miscellaneous Geologic Investigations Map I-654, scale 1:250,000.
- Hames, W. E., Renne, P. R., and Ruppel, C., 2000, New evidence for geologically instantaneous emplacement of the earliest Jurassic Central Atlantic magmatic province basalts on the North American margin: *Geology*, v. 28, no. 9, p. 859-862.
- Hatcher, R. D., Jr., 1972, Developmental model for the southern Appalachians: *Geological Society of America Bulletin*, v. 82, p. 2735-2760.
- Hatcher, R. D., Jr., 1974, Introduction to the tectonic history of northeast Georgia: *Georgia Geological Society Guidebook* 13-A, 59 p.
- Hatcher, R. D., Jr., 1993, Perspective on the tectonics of the Inner Piedmont, southern Appalachians, *in* Hatcher, R. D., Jr., and Davis, T. L., eds., Studies of Inner Piedmont geology with a focus on the Columbus Promontory: Carolina Geological Society Guidebook, North Carolina Geological Survey, p. 17-43.
- Hatcher, R. D., Jr., 2001, Rheological partitioning during multiple reactivation of the Paleozoic Brevard fault zone, southern Appalachians, USA, *in* Holdsworth, R. E., Strachan, R. A., MacLoughlin, J. F., and Knipe, R. J., eds., The nature and tectonic significance of fault zone weakening: *Geological Society of London Special Publication*, 186, p. 255-269.
- Hatcher, R. D., Jr., 2002, The Alleghanian (Appalachian) orogeny, a product of zipper tectonics: Rotational transpressive continent-continent collision and closing of ancient oceans along irregular margins, *in* Catalan, J. R. M., Hatcher, R. D., Jr., Arenas, R., and Garcia, F. D., eds., Variscan-Appalachian dynamics: The building of the late Paleozoic basement: *Geological Society of America Special Paper* 394, p. 199-208.
- Hatcher, R. D., Jr., 2004, Southern Appalachian crustal transect: Day 2, The Neoacadian metamorphic core, large ductile thrust sheets, and a multiply reactivated crustal scale shear zone, *in* Mersch, A. J., and Hatcher, R. D., Jr., eds., Trans Appalachian Internides Geotraverse: 17th International Basement Tectonics Association Field Trip Guidebook, p. 29-60.

- Hatcher, R. D., Jr., and Goldberg, S. A., 1991, The Blue Ridge geologic province, *in* Horton, J. W., Jr., and Zullo, V. A., eds., *The Geology of the Carolinas*, Carolina Geological Society 50th Anniversary Volume: Knoxville, The University of Tennessee Press, p. 11–35.
- Hatcher, R. D., Jr., and Hooper, R. J., 1992, Evolution of crystalline thrust sheets in the internal parts of mountain chains, *in* McClay, K. R., ed., *Thrust Tectonics*: London, Chapman and Hall, p. 217-234.
- Hatcher, R. D., Jr., and Merschat, A. J., 2006, The Appalachian Inner Piedmont: An exhumed strike-parallel, tectonically forced orogenic channel, *in* Law, R. D., Searle, M., and Godin, L., eds., *Channel flow, ductile extrusion and exhumation of lower-mid crust in continental collision zones*: London, Geological Society of London Special Publication 268, p. 517-540.
- Hatcher, R. D., Jr., Bream, B. R., and Merschat, A. J., 2007, Tectonic map of the southern and central Appalachians: A tale of three orogens and a complete Wilson cycle, *in* Hatcher, R. D., Jr., Carlson, M. P., McBride, J. H., and Martínez Catalán, J. R., eds., *4-D Framework of Continental Crust*: Geological Society of America Memoir 200, p. 595-632.
- Higgins, M. W., Crawford, T. J., Atkins, R. L., and Crawford, R. F., 2003, Geologic map of the Atlanta 30' x 60' quadrangle, Georgia: U.S. Geological Survey, Geologic Investigations Series Map I-2602, scale 1:100,000.
- Hill, J. C., 1999, Geology of the Marion East quadrangle, North Carolina, and the stratigraphy of the Tallulah Falls formation Chauga belt [M.S. thesis], Knoxville, University of Tennessee, 168 p.
- Hibbard, J. P., Tracy, R. J., and Henika, W. S., 2003, Smith River allochthon: A southern Appalachian peri-Gondwanan terrane emplaced directly on Laurentia?: *Geology*, v. 31, p. 215-218.
- Holdaway, M. J., 1971, Stability of andalusite and the aluminum silicate phase diagram: *American Journal of Science*, v. 297, p. 97-131.
- Holdaway, M. J., and Lee, S. M., 1977, Fe-Mg cordierite stability in high-grade pelitic rocks based on experimental, theoretical, and natural observation: *Contributions to Mineralogy and Petrology*, v. 63, p. 175-198.
- Hodges, K. V., and Spear, F. S., 1982, Geothermometry, geobarometry, and the Al_2SiO_5 triple point at Mt. Moosilauke, New Hampshire: *American Mineralogist*, v. 67, p. 1118-1134.
- Hopson, J. L., and Hatcher, R. D., Jr., 1988, Structural and stratigraphic setting of the Alto allochthon, NE Georgia: *Geological Society of America Bulletin*, v. 100, p. 339-350.
- Hopson, J. L., Hatcher, R. D., Jr., and Stieve, A. L., 1989, Geology of the eastern Blue Ridge, northeastern Georgia and the adjacent Carolinas, *in* Fritz, W. J., Hatcher, R. D., Jr., and Hopson, J. L., eds., *Geology of the eastern Blue Ridge of northeast Georgia and the adjacent Carolinas*: Georgia Geological Society Guidebooks, v. 9, p. 1-40.
- Kalbas, J. L., 2003, Geology of part of the southwestern Brushy Mountains, Inner Piedmont [M. S. thesis]: Knoxville, University of Tennessee, 206 p.
- Kalbas, J. L., Bream, B. R., Hatcher, R. D., Jr., and Maybin, A. H., 2002, Evidence for mafic Ordovician magmatism in the Brushy Mountains, western Inner Piedmont of North Carolina: *Geological Society of America Abstracts with Programs*, v. 34, no. 2, p. 119.
- Kish, S. A., 1997, The Cat Square charnockite—a Paleozoic charnockite in the Inner Piedmont of North Carolina: *Geological Society of America Abstracts with Programs*, v. 29, no. 3, p. 28.
- Luth, W. D., Jahns, R. H., and Tuttle, O. F., 1964, The granite system at pressures of 4 to 10 kilobars: *Journal of Geophysical Research*, v. 69, p. 759-773.
- Mapes, R. W., 2002, Geochemistry and geochronology of mid-Paleozoic granitic plutonism in the southern Appalachian Piedmont terrane, North Carolina-South Carolina-Georgia [M.S. thesis]: Nashville, Vanderbilt University, 150 p.
- Mapes, R. W., Maybin, A. H., III, Miller, C. F., Fullagar, P. D., and Bream, B. R., 2002, Geochronology and geochemistry of mid Paleozoic granitic magmatism, central and eastern Inner Piedmont, North Carolina and South Carolina: *Geological Society of America Abstracts with Programs*, v. 34, p. A-94.

- McSween, H. Y., Jr., and Harvey, R. P., 1997, Concord Plutonic Suite: Pre-Acadian gabbro-syenite intrusion in the southern Appalachians, *in* Sinha, A. K., Whalen, J. B., and Hogan, J. P., eds., *The nature of magmatism in the Appalachian orogen*: Boulder, Colorado, Geological Society of America Memoir 197, p. 221-234.
- McSween, H. Y., Jr., Sando, T. W., Clark, S. R., Harden, J. T., and Strange, E. A., 1984, The gabbro-metagabbro association of the southern Appalachian Piedmont: *American Journal of Science*, v. 284, p. 437-461.
- McSween, H. Y., Jr., Speer, J. A., and Fullagar, P. D., 1991, Plutonic rocks, *in* Horton, J. W., Jr., and Zullo, V. A., eds., *The Geology of the Carolinas, Carolina Geological Society Fiftieth Anniversary Volume*: Knoxville, University of Tennessee Press, p. 109-126.
- Merschat, A. J., 2003, Inner Piedmont tectonics in the southwestern Brushy Mountains, North Carolina: Field and laboratory data revealing 3-D crustal flow and sillimanite I and II metamorphism [M.S. thesis]: Knoxville, University of Tennessee, 198 p.
- Merschat, A. J., 2009, Assembling the Blue Ridge and Inner Piedmont: Insights into the nature and timing of terrane accretion in the southern Appalachian orogen from geologic mapping, stratigraphy, kinematic analysis, petrology, geochemistry, and modern geochronology [Ph.D. dissertation]: Knoxville, University of Tennessee, 455 p.
- Merschat, A. J., Hatcher, R. D., Jr., and Davis, T. L., 2005a, The northern Inner Piedmont, southern Appalachians, USA: Kinematics of transpression and SW-directed mid-crustal flow: *Journal of Structural Geology*, v. 27, p. 1252-1281.
- Merschat, A. J., Gatewood, M. P., Fisher, C. M., Miller, C. F., Hatcher, R. D., Jr., Wooden, J. L., and Stahr, D. W., III, 2005b, The Newton antiform, NC: A previously unrecognized window through the allochthonous Inner Piedmont thrust stack: *Geological Society of America Abstracts with Programs*, v. 37, no. 7, p. 20.
- Merschat, A. J., Bream, B. R., Hatcher, R. D., Jr., Miller, C. F., Wooden, J. L., 2007, Provenance and timing of crust formation in the southern Appalachian crystalline core: evidence from detrital zircon studies: *Geological Society of America Abstracts with Programs*, v. 39, no. 6, p. 341.
- Merschat, A. J., and Hatcher, R. D., Jr., 2007, The Cat Square terrane: Possible Siluro-Devonian remnant ocean basin in the Inner Piedmont, southern Appalachians, USA, *in* Hatcher, R. D., Jr., Carlson, M. P., McBride, J. H., and Martínez Catalán, J. R., eds., *4-D Framework of Continental Crust*: Geological Society of America Memoir 200, p. 553-565.
- Merschat, A. J., Hatcher, R. D., Jr., Byars, H. B., and Gilliam, W. G., 2008, Inner Piedmont geotraverse from the Brushy Mountains to Lincolnton, North Carolina: Architecture of the Cat Square and Tugaloo terrane: *Geological Society of America Southeastern Meeting Field Trip Guidebook*, 62 p.
- Merschat, A. J., and Kalbas, J. L., 2002, Geology of the southwestern Brushy Mountains, North Carolina Inner Piedmont: A summary and synthesis of recent studies, *in* Hatcher, R. D., Jr., and Bream, B. R., eds., *Inner Piedmont geology in the South Mountains-Blue Ridge Foothills and the southwestern Brushy Mountains, central-western North Carolina*: Carolina Geological Society Guidebook, p. 101-126.
- Merschat, C. E., and Wiener, L. S., 1988, Geology of the Sandymush and Canton quadrangles, North Carolina: *North Carolina Geological Survey Bulletin* 90, 66 p.
- Miller, B. V., Fetter, A. H., and Stewart, K. G., 2006, Plutonism in three orogenic pulses, eastern Blue Ridge province, southern Appalachians: *Geological Society of America Bulletin*, v. 118, p. 171-184.
- Mirante, D. C., and Patino-Douce, A. E., 2000, Melting and migmatization in the southern Appalachian Inner Piedmont of northeast Georgia; the Athens gneiss: *Geological Society of America Abstracts with Programs*, v. 33, no. 7, p. 297.
- Moecher, D. P., Samson, S. D., and Miller, C. F., 2004, Precise time and conditions of peak Taconian granulite facies metamorphism in the southern Appalachian orogen, USA, with implications for zircon behavior during crustal melting events: *Journal of Geology*, v. 112, p. 289-304, doi: 10.1086/382760.
- Nelson, A. E., Horton, J. W., and Clarke, J. W., 1998, Geologic map of the Greenville 1° x 2° quadrangle, Georgia, South Carolina, and North Carolina: U.S. Geological Survey Map I-2175, scale 1:250,000.

- Osberg, P. H., Tull, J. F., Robinson, P., Hon, R., and Butler, J. R., 1989, The Acadian orogen, Chapter 4, *in* Hatcher, R. D., Jr., Thomas, W. A., and Viele, G. W., eds., *The Appalachian-Ouachita orogen in the United States*: Boulder, Colorado, Geological Society of America, *The Geology of North America*, v. F-2, p. 179-232.
- Overstreet, W. C., Yates, R. G., and Griffiths, W. R., 1963, *Geology of the Shelby quadrangle, North Carolina*: U.S. Geological Survey Map I-384, scale 1:62,500.
- Ownby, S. E., Miller, C. F., Berquist, P. J., Carrigan, C. W., Wooden, J. L., and Fullagar, P. D., 2004, U-Pb geochronology and geochemistry of a portion of the Mars Hill terrane, North Carolina-Tennessee: Constraints on origin, history, and tectonic assembly, *in* Tollo, R. P., Corriveau, L., McLelland, J., and Bartholomew, M. J., eds., *Proterozoic evolution of the Grenville orogen in North America*: Boulder, Colorado, Geological Society of America Memoir 197, p. 609-632.
- Pigage, L. C., and Greenwood, H. J., 1982, Internally consistent estimates of pressure and temperature: The staurolite problem: *American Journal of Science*, v. 282, p. 943-969.
- Quinn, M. J., 1991, Two lithotectonic boundaries in western North Carolina: Geologic interpretation of a region surrounding Sylva, Jackson County [unpublished M.S. thesis]: Knoxville, University of Tennessee, 223 p.
- Rankin, D. W., Espenshade, G. J., and Neuman, R. B., 1972, *Geologic map of the west half of the Winston-Salem quadrangle, North Carolina, Virginia, and Tennessee*: U.S. Geological Survey Map I-709-A, scale 1:250,000. 1252-1281.
- Reed, J. C., Jr., and Bryant, B., 1964, Evidence for strike-slip faulting along the Brevard zone in North Carolina: *Geological Society of America*, v. 75. p. 1177-1196.
- Settles, D. J., 2002, Defining the Hayesville-Soque River and Allatoona faults and an Ordovician arc assemblage within the central Blue Ridge northwest of Dahlonega, Georgia [unpublished M.S. thesis]: Knoxville, University of Tennessee, 148 p.
- Spear, F. S., 1993, *Metamorphic phase equilibria and pressure-temperature-time paths*: Chelsea, Michigan, Book Crafters, Inc., 799 p.
- Streckeisen, A. L., 1976, To each plutonic rock its proper name: *Earth Science Reviews*, v. 12, p. 1-33.
- Tull, J. F., and Holm, C. S., 2005, Structural evolution of a major Appalachian salient-recess junction: Consequences of oblique collisional convergence across a continental margin transform fault: *Geological Society of America Bulletin*, v. 117, p. 482-499.
- Williams, S. T., 2000, Structure, stratigraphy, and migmatization in the southwestern South Mountains, North Carolina [M.S. thesis]: Knoxville, University of Tennessee, 111 p.
- Wilson, C. G., 2006, Origin and tectonic evolution of the southern Appalachian Neocadian crystalline core: Evidence from the geology of the Gilreath 7.5-minute quadrangle, North Carolina [M.S. thesis]: Knoxville, University of Tennessee, 219 p.
- Yanagihara, G. M., 1994, Structure, stratigraphy, and metamorphism of a part of the Columbus Promontory, western Inner Piedmont, North Carolina [M. S. thesis]: Knoxville, University of Tennessee, 214 p.

APPENDIX I

QUAD	STATION	FOLIATION		LINEATION		FOLD AXIS	
		strike	dip	trend	plunge	trend	plunge
BANOAK	1	N 25 W	44 SW				
BANOAK	2	N 24 W	21 SW				
BANOAK	3A	N 8 W	21 SW				
BANOAK	3B	N 8 W	45 W				
BANOAK	3C	N 9 W	46 W				
BANOAK	3D	N 9 W	8 E			N 9 W	12
BANOAK	3E	N 9 W	25 W				
BANOAK	4	N 39 W	37 W				
BANOAK	5	N 42 W	37 SW				
BANOAK	6	N 35 W	49 W				
BANOAK	7	N 6 W	67 W				
BANOAK	8						
BANOAK	9	N 21 W	44 SW				
BANOAK	10	N 30 W	57 SE				
BANOAK	11	N 55 E	36 SE				
BANOAK	12	N 24 W	35 SW				
BANOAK	13	N 83 E	36 SE				
BANOAK	13B	N 10 E	24 W				
BANOAK	14	N 55 E	14 SE			S 43 W	17 SW
BANOAK	14B	N 10 W	17 SW				
BANOAK	15	N 20 E	37 SW	N 20 E	10		
BANOAK	16	N 17 W	43 SW				
BANOAK	17	N 8 W	17 SW				
BANOAK	18	N 10 W	43 SW				
BANOAK	19	N 10 W	37 SW				
BANOAK	20	N 43 W	14 SE				
BANOAK	21					S 25 W	17
BANOAK	22	N 25 W	24 SW				
BANOAK	23	N 32 W	20 SW				
BANOAK	24	N 32 W	17 N				
BANOAK	25	N 80 W	17 S				
BANOAK	26	N 14 W	35 W				
BANOAK	27	N 37 W	23 W	S 37 W	20		
BANOAK	28	N 26 W	14 W				

QUAD	STATION	FOLIATION	LINEATION	FOLD AXIS
BANOAK	29	N 5 W	14 W	
BANOAK	30	N 19 W	31 SW	
BANOAK	31	N 10 W	24 SW	
BANOAK	32	N 5 W	17 SW	
BANOAK	33	N 30 W	17 SW	
BANOAK	34	N 29 W	20 SW	
BANOAK	35	N 37 W	48 SW	
BANOAK	36	N 6 W	34 SW	
BANOAK	37	N 6 W	30 SW	
BANOAK	38	N 15 W	27 SW	
BANOAK	39	N 5 W	31 SW	
BANOAK	40	N 10 W	14 SW	
BANOAK	41	N 12 E	17 SW	
BANOAK	42	N 31 W	17 SW	
BANOAK	43	N 37 W	17 SW	
BANOAK	44	N 11 W	21 SW	
BANOAK	45	N 21 W	37 SW	
BANOAK	46	N 10 E	23 SW	
BANOAK	47	N 13 E	21 SW	
BANOAK	48	N 21 W	17 SW	
BANOAK	49	N 20 W	21 SW	
BANOAK	50	N 15 E	21 SW	
BANOAK	51	N 13 W	34 SW	
BANOAK	52	N 5 W	21 SW	
BANOAK	53	N 7 W	23 SW	
BANOAK	54	N 20 W	17 SW	
BANOAK	55	N 35 W	17 SW	
BANOAK	56	N 7 W	10 SW	
BANOAK	57	N 21 W	32 SW	
BANOAK	58	N 21 W	47 SW	
BANOAK	59	N27W	65 SW	
BANOAK	60	N 17 W	41 SW	
BANOAK	61	N 23 W	40 W	
BANOAK	62	N 30 W	52 SW	

QUAD	STATION	FOLIATION		LINEATION		FOLD AXIS	
BANOAK	63	N 24 W	31 SW				
BANOAK	64	N 80 E	45 S				
BANOAK	65	N 80 E	50 S	S 20 E	35		
BANOAK	66	N 80 E	57 S				
BANOAK	67	N 47 W	30 S			S 40 E	10
BANOAK	68	N 70 W	37 S	S 45 W	6		
BANOAK	69	N 61 W	41 S				
BANOAK	70	N 70 W	67 S				
BANOAK	71	N 70 W	32 SW				
BANOAK	72	N 63 W	50 SW				
BANOAK	73	N 70 W	61 SW				
BANOAK	74	N 80 W	57 SW				
BANOAK	75	N 80 W	51 SW				
BANOAK	76	N 53 W	41 SW				
BANOAK	77	N 57 W	38 SW				
BANOAK	78	N 41 W	21 SW				
BANOAK	79	N 37 W	21 SW				
BANOAK	80	N 17 W	34 SW	S 80 W	14		
BANOAK	81	N 20 W	17 SW				
BANOAK	82	N 15 W	20 SW				
BANOAK	83	N 37 W	31 SW				
BANOAK	84	N 60 W	47 SW				
BANOAK	85	N 65 W	50 SW				
BANOAK	86	N 60 W	54 SW				
BANOAK	87	N 77W	29 S				
BANOAK	88	N 45 E	67 E				
BANOAK	89	0	0				
BANOAK	90	N 5 E	7 W				
BANOAK	91	N 37 W	55 NE				
BANOAK	92					N 2 W	6
BANOAK	93	N 34 W	79 SW				
BANOAK	94	N 40 E	24 SE				
BANOAK	95	N 36 E	54 SE				
BANOAK	96	N 57 W	33 SW				

QUAD	STATION	FOLIATION		LINEATION	FOLD AXIS	
BANOAK	97				N 30 W	
BANOAK	98	N 31 W	44 SW		N 2 W	
BANOAK	99	N 45 E	51 SE		N 15 E	
BANOAK	100	N 10 E	44 SW			
BANOAK	101	N 10 E	24 SW			
BANOAK	102	N 5 E	15 SW			
BANOAK	103	N 70 E	31 SW			
BANOAK	104	N 67 E	57 SE			
BANOAK	105				N 57 E	41
BANOAK	106	N 80 E	37 N			
BANOAK	107	N 55 E	29 S		N 55 E	
BANOAK	108	N 55 W	41 SW			
BANOAK	109	N 61 W	57 SW			
BANOAK	110				N 45 W	16
BANOAK	111	N 42 W	32 W			
BANOAK	112	N 31 W	27 W			
BANOAK	113	N 5 W	41 SW			
BANOAK	114	N 7 W	19 W			
BANOAK	115	N 21 W	15 SW			
BANOAK	116	N 53 W	41 SW			
BANOAK	117	N 60 W	31 SW			
BANOAK	118	N 70 W	47 S			
BANOAK	119	N 41 W	21 SW			
BANOAK	120	N 79 W	31 SW			
BANOAK	121	N 60 W	31 SW			
BANOAK	122	N 41 W	17 SW			
BANOAK	123				S 45 E	21
BANOAK	124	N 41 W	11 SW			
BANOAK	125	N 49 W	21 SW			
BANOAK	126	N 41 W	31 SW			
BANOAK	127	N 7 W	37 SW			
BANOAK	128			N 35 W		
BANOAK	129	N 21 W	41 SW			
BANOAK	130	N 35 W	47 SW			

QUAD	STATION	FOLIATION	LINEATION	FOLD AXIS
BANOAK	131	N 70 W	21 SW	
BANOAK	132	N 21 W	34 SW	
BANOAK	133	N 37 W	36 SW	
BANOAK	134	N 44 W	19 SW	
BANOAK	135	N 40 W	17 SW	
BANOAK	136	N 10 W	17 SW	
BANOAK	137	N 81 E	17 NW	
BANOAK	138		N 34 W	
BANOAK	139	N 21 E	17 N	
BANOAK	140	N 31 W	21 SW	
BANOAK	141	N 61 W	34 SW	
BANOAK	142	N 17 E	16 N	
BANOAK	143	N 27 W	19 W	
BANOAK	144	N 15 W	61 SW	
BANOAK	145		N 65 E	
BANOAK	146	N 21 W	34 SW	
BANOAK	147	N 21 W	61 SW	
BANOAK	148	N 14 W	22 SW	
BANOAK	149	N 5 E	24 SW	
BANOAK	149b			S 11 W
BANOAK	149c	N 16 E	19 SE	
BANOAK	150	N 10 W	44 SW	
BANOAK	151	N 22 W	17 W	
BANOAK	152	N 3 W	32 W	
BANOAK	153	N 14 W	63 NE	
BANOAK	154	N 24 W	34 SW	
BANOAK	155	N 23 W	24 W	
BANOAK	156	N 11 W	31 SW	
BANOAK	157	N 19 W	21 W	
BANOAK	158	N 10 W	25 SW	
BANOAK	159	N 23 W	31 SW	
BANOAK	160	N 32 W	37 SW	
BANOAK	161	N 31 W	21 SW	
BANOAK	162	N 21 W	27 SW	

QUAD	STATION	FOLIATION		LINEATION		FOLD AXIS
BANOAK	163	N 80 W	19 SW	N 17 W	22	
BANOAK	164	N 35 W	34 SW			
BANOAK	165	N 10 W	37 SW			
BANOAK	166	N 17 W	39 SW			
BANOAK	167	N 34 W	19 SW			
BANOAK	168	N 37 W	61 SW			
BANOAK	169	N 10 W	34 SW			
BANOAK	170	N 17 W	38 SW			
BANOAK	171	N 14 W	35 SW			
BANOAK	172	N 14 W	27 SW			
BANOAK	173	N 35 W	21 SW			
BANOAK	174	N 59 W	34 SW			
BANOAK	175	N 8 W	21 SW			
BANOAK	176	N 42 W	34 SW			
BANOAK	177	N 10 W	37 SW			
BANOAK	178	N 35 W	39 SW			
BANOAK	179	N 42 W	19 SW			
BANOAK	180	N 37 W	23 SW			
BANOAK	181	N 10 W	21 SW			
BANOAK	182	N 13 E	23 N			
BANOAK	183	N 27 W	44 SW			
BANOAK	184	N 10 W	31 W			
BANOAK	185	N 35 W	17 W			
BANOAK	186	N 42 W	24 W			
BANOAK	187	N 22 W	26 SW			
BANOAK	188	N 84 W	31 SW			
BANOAK	189	N 18 W	22 SW			
BANOAK	190	N 35 W	17 W			
BANOAK	191	N 29 W	21 W			
BANOAK	192	N 21 W	61 SW			
BANOAK	193	N 64 E	23 S			
BANOAK	194	N 61 W	19 SW			
BANOAK	195	N 41 W	21 SW			
BANOAK	196	N 14 W	33 SW			

QUAD	STATION	FOLIATION		LINEATION		FOLD AXIS
BANOAK	197	N 10 W	61 W			
BANOAK	198	N 15 W	22 SW			
BANOAK	199	N 15 W	64 SW			
BANOAK	200	N 4 W	90			
BANOAK	201	N 32 W	34 SW			
BANOAK	202	N 36 W	41 SW			
BANOAK	203	N 34 W	48 SW			
BANOAK	204	N 10 W	24 E			
BANOAK	205	N 14 W	31 SW			
BANOAK	206	N 17 W	27 SW			
BANOAK	207	N 22 W	34 SW			
BANOAK	208	N 44 W	28 NE			
BANOAK	209	N 3 W	44 SW			
BANOAK	210	N 30 W	22 SW			
BANOAK	211	N 36 W	41 SW			
BANOAK	212	N 21 W	22 SW			
BANOAK	213	N 33 E	14 SE			
BANOAK	214	N 45 W	60 SW			
BANOAK	215	N 23 W	31 NE			
BANOAK	216	N 9 W	85 SW			
BANOAK	217	N 15 W	69 SW			
BANOAK	218	N 47 W	51 SW			
BANOAK	219	N 42 E	19 SE			
BANOAK	220	N 72 W	19 SW			
BANOAK	221	N 45 W	31 SW			
BANOAK	222	N 21 W	43 SW			
BANOAK	223	N 45 E	12 SE			
BANOAK	224	N 37 W	34 NE			
BANOAK	225	N 21 W	36 SW			
BANOAK	226					N 70 W
BANOAK	227	N 62 W	56 SW			
REEPSVILLE	1	N 8 W	41 W			
REEPSVILLE	2	N 8 W	25 W			
REEPSVILLE	3	N 26 W	37 W	N 16 W	9 SW	

QUAD	STATION	FOLIATION		LINEATION	FOLD AXIS
REEPSVILLE	4	N 14 E	41 W		
REEPSVILLE	5	N 4 E	27 W		
REEPSVILLE	6	N 9 E	27 W		
REEPSVILLE	7	N 16 W	55 W		
REEPSVILLE	8	N 31 E	71 N		
REEPSVILLE	9	N 6 E	41 W		
REEPSVILLE	10	N 80 E	10 N		
REEPSVILLE	11	N 11 W	37 E		
REEPSVILLE	12	N 14 W	44 W		
REEPSVILLE	13	N 4 W	43 W		
REEPSVILLE	14	N 15 E	73 W		
REEPSVILLE	15	N 8 W	27 W		
REEPSVILLE	16	N 1 W	15W		
REEPSVILLE	17	N 6 W	41 W		
REEPSVILLE	18	N 7 W	74 W		
REEPSVILLE	19a	N 7 W	4 W		N 7 W
REEPSVILLE	19b	N 8 W	47 W		
REEPSVILLE	20	N 20 W	62 W		
REEPSVILLE	21	N 21 W	69 W		
REEPSVILLE	22	N 80 W	71 S		
REEPSVILLE	23	N 10 W	64 W		
REEPSVILLE	24	N 1 W	54 W		
REEPSVILLE	25	N 30 W	34 E		N 30 W
REEPSVILLE	26	N 15 W	14 W		
REEPSVILLE	27a	N 26 E	32 E		
REEPSVILLE	27b	N 25 E	37 E		
REEPSVILLE	27c	N 40 E	61 S		
REEPSVILLE	27d	N 21 E	26 E		
REEPSVILLE	27e	N 9 E	26 E	N 9 W	
REEPSVILLE	27f	N 14 E	21 E		
REEPSVILLE	28	N 3 W	90		
REEPSVILLE	29	N 10 W	90		
REEPSVILLE	30	N 21 W	49 E		
REEPSVILLE	31	N 90 E	56 N		

QUAD	STATION	FOLIATION		LINEATION	FOLD AXIS	
REEPSVILLE	32	N 2 W	77 W			
REEPSVILLE	33	N 1 E	62 W			
REEPSVILLE	34	N 32 W	57 W			
REEPSVILLE	35	N 30 W	78 W			
REEPSVILLE	36a	N 37 W	69 W			
REEPSVILLE	36b	N 10 W	5 W			
REEPSVILLE	36C	N 48 W	54 W			
REEPSVILLE	37a	N 7 W	49 W		S 16 W	
REEPSVILLE	37b	N 90 W	9 S			
REEPSVILLE	38	N 24 W	87 W			
REEPSVILLE	39	N 50 W	79 E			
REEPSVILLE	40	N 10 W	54 W			
REEPSVILLE	41	N 12 W	72 W			
REEPSVILLE	42	N 4 W	62 W			
REEPSVILLE	43	N 35 W	38 W			
REEPSVILLE	44a	N 15 W	90			
REEPSVILLE	44b				N 2 W	12
REEPSVILLE	44c	N 12 W	86 E			
REEPSVILLE	45	N 8 W	52 W			
REEPSVILLE	46	N 12 E	49 W			
REEPSVILLE	47	N 20 E	40 W			
REEPSVILLE	48a	N 17 E	61 W			
REEPSVILLE	48b				N 20 W	
REEPSVILLE	48c	N 3 E	74 E			
REEPSVILLE	49	N 37 W	30 W			
REEPSVILLE	50	N10W	59 SW			
REEPSVILLE	51	N10W	49 SW			
REEPSVILLE	52	N7W	47 SW			
REEPSVILLE	53	NO DATA AVAILABLE				
REEPSVILLE	54	N20W	37 SW			
REEPSVILLE	55	N10W	19 SW			
REEPSVILLE	56	N9W	21 SW			
REEPSVILLE	57	N10W	21 SW			
REEPSVILLE	58	N10W	15 SW			

QUAD	STATION	FOLIATION	LINEATION	FOLD AXIS
REEPSVILLE	59	10W	20 SW	
REEPSVILLE	60	N7W	25 SW	
REEPSVILLE	61	N3E	15 SW	
REEPSVILLE	62	N30E	21 SW	
REEPSVILLE	63	N33E	21 SW	
REEPSVILLE	64	N5W	65 SW	
REEPSVILLE	65	N3W	64W	
REEPSVILLE	66	N10W	37 SW	
REEPSVILLE	67	N10W	59 SW	
REEPSVILLE	68	N19E	20 S E	
REEPSVILLE	69	N10W	51 SW	
REEPSVILLE	70	N10W	60 SW	
REEPSVILLE	71	N10E	71 SW	
REEPSVILLE	72	N21W	61 SW	
REEPSVILLE	73	N20W	59 SW	
REEPSVILLE	74	N15W	45 SW	
REEPSVILLE	75	N20W	18 SW	
REEPSVILLE	76	N20W	15 SW	
REEPSVILLE	77	N10W	10 SW	
REEPSVILLE	78	N15W	10 SW	
REEPSVILLE	79	N15W	14 SW	
REEPSVILLE	80	N20E	61 SW	
REEPSVILLE	81	N10E	25 SW	
REEPSVILLE	82	N2W	29 SW	
REEPSVILLE	83	N80W	59 N E	
REEPSVILLE	84	N4W	30 SW	
REEPSVILLE	85	N15W	44 SW	
REEPSVILLE	86	N15W	34 SW	
REEPSVILLE	87	N20W	47 N E	
REEPSVILLE	88	N14W	35 SW	
REEPSVILLE	89	N23W	27 SW	
REEPSVILLE	90	N3W	36 SW	
REEPSVILLE	91	N15W	17 SW	
REEPSVILLE	92	SAMPLE COLLECTED		

QUAD	STATION	FOLIATION	LINEATION	FOLD AXIS
REEPSVILLE	93	SAMPLE COLLECTED		
REEPSVILLE	94	N6E	80 NW	
REEPSVILLE	95	N6E	8 E	
REEPSVILLE	96	N6E	76W	
REEPSVILLE	97	SAMPLE COLLECTED		
REEPSVILLE	98	N6W	29W	
REEPSVILLE	99	N50W	31 SW	
REEPSVILLE	100	N15W	31 SW	
REEPSVILLE	101	N17W	30 SW	
REEPSVILLE	102	N15W	37 SW	
REEPSVILLE	103	N31W	41 SW	
REEPSVILLE	104	N31W	41 SW	
REEPSVILLE	105	N37W	41W	
REEPSVILLE	106	N26W	24 E	
REEPSVILLE	107	N12W	14 SW	
REEPSVILLE	108	N15W	15 SW	
REEPSVILLE	109	N20W	18 SW	
REEPSVILLE	110	N17W	15 SW	
REEPSVILLE	111	N14W	15 SW	
REEPSVILLE	112	N5W	58 SW	
REEPSVILLE	113	N28W	58 SW	
REEPSVILLE	114	N18E	47 SW	
REEPSVILLE	115	N10E	21 SW	
REEPSVILLE	116	N10E	27 SW	
REEPSVILLE	117	N10W	47 SW	
REEPSVILLE	118	N60W	16 SW	
REEPSVILLE	119	N10W	47 SW	
REEPSVILLE	120	N17W	27 SW	
REEPSVILLE	121	N18W	72 SW	
REEPSVILLE	122	N10W	57 SW	
REEPSVILLE	123	N18W	27 SW	
REEPSVILLE	124	N20W	18 SW	
REEPSVILLE	125	N20		
REEPSVILLE	126	N20W	37 SW	

QUAD	STATION	FOLIATION	LINEATION	FOLD AXIS
REEPSVILLE	127	N20W	31 SW	
REEPSVILLE	128	N58E	27 NW	
REEPSVILLE	129	N12W	7 SW	
REEPSVILLE	130			
REEPSVILLE	131	N30E	41 N E	
REEPSVILLE	132	N10W	29 SW	
REEPSVILLE	133	N5W	17 SW	
REEPSVILLE	134	N10W	21 S E	
REEPSVILLE	135	N20W	34 SW	
REEPSVILLE	136	N15W	37 SW	
REEPSVILLE	137	N80W	67 N	
REEPSVILLE	138	N85W	17 N	
REEPSVILLE	139	0	0	
REEPSVILLE	140	N50W	67 SW	
REEPSVILLE	141	N15W	17 SW	
REEPSVILLE	142	N50W	90	
REEPSVILLE	143	N25W	37 SW	
REEPSVILLE	144	N50W	90	
REEPSVILLE	145	N30W	27W	
REEPSVILLE	146	N32W	30 SW	
REEPSVILLE	147	N41W	47 SW	
REEPSVILLE	148	N57W	59 N E	
REEPSVILLE	149	N27W	87 SW	
REEPSVILLE	150	N50W	47 SW	
REEPSVILLE	151	N75W	36 SW	
REEPSVILLE	152	N8W	66 SW	
REEPSVILLE	153	N47W	17 SW	
REEPSVILLE	154	N17W	18 SW	
REEPSVILLE	155	N23W	21 SW	
REEPSVILLE	156	N31W	27 SW	
REEPSVILLE	157	N35W	21 SW	
REEPSVILLE	158	N36W	25 SW	
REEPSVILLE	159	N53W	24 SW	
REEPSVILLE	160	N4W	47 SW	

QUAD	STATION	FOLIATION		LINEATION		FOLD AXIS
REEPSVILLE	161	N13E	61 S E	N21W	10	
REEPSVILLE	162	N56W	17 N E			
REEPSVILLE	163	N50W	23 SW			
REEPSVILLE	164	N27W	32 SW			
REEPSVILLE	165	N23W	45 SW			
REEPSVILLE	166	N37W	51 SW			
REEPSVILLE	167	N10W	24W			
REEPSVILLE	168	N26W	31 SW			
REEPSVILLE	169	N17W	31 SW			
REEPSVILLE	170	N21W	17 SW			
REEPSVILLE	171	N7W	37 SW			
REEPSVILLE	172	N24W	19 SW			
REEPSVILLE	173	N48E	19 NW			
REEPSVILLE	174	N47W	19 SW	N37W	10	
REEPSVILLE	175					
REEPSVILLE	176	N41W	37 N E			
REEPSVILLE	177	N10W	37 N E			
REEPSVILLE	178	N10W	10 E			
REEPSVILLE	179	N8W	17 SW			
REEPSVILLE	180	N7E	19 S E			
REEPSVILLE	181	N10W	19 SW			
REEPSVILLE	182	N16W	25W			
REEPSVILLE	183	N17E	21 SW			
REEPSVILLE	184	N5W	21 SW			
REEPSVILLE	185	N31W	37 SW			
REEPSVILLE	186	N21W	28 SW			
REEPSVILLE	187	N10W	21 SW	N17W	14	
REEPSVILLE	188	N10W	21 SW			
REEPSVILLE	189	N7W	24 SW			
REEPSVILLE	190	N47W	21 SW			
REEPSVILLE	191	N71E	24 S E			
REEPSVILLE	192	N21W	46 SW			
REEPSVILLE	193	N37W	21 SW			
REEPSVILLE	194	N10W	21 SW			

QUAD	STATION	FOLIATION	LINEATION	FOLD AXIS
REEPSVILLE	195	N21W	32 SW	
REEPSVILLE	196	N18W	17 SW	
REEPSVILLE	197	N13W	22 SW	
REEPSVILLE	198	N7W	34 SW	
REEPSVILLE	199	N1E	31 SW	
REEPSVILLE	200	N31W	19 SW	
REEPSVILLE	201	N17E	21 SW	
REEPSVILLE	202	N10W	61 SW	N 35 W 21
REEPSVILLE	203	N10W	21 SW	
REEPSVILLE	204	N21W	53 SW	
REEPSVILLE	205	N25W	47 SW	
REEPSVILLE	206	N29W	39 SW	
REEPSVILLE	207			
REEPSVILLE	208	N13W	21 SW	
REEPSVILLE	209	N1W	17 SW	
REEPSVILLE	210	N21W	62 SW	
REEPSVILLE	211	N34W	61 SW	
REEPSVILLE	212	N17W	27 SW	
REEPSVILLE	213	N10W	31 SW	
REEPSVILLE	214	N35W	31 W	
REEPSVILLE	215	N21W	13 SW	
HICKORY	1	N 40 W	55 SW	
HICKORY	2	N 40 W	55 SW	
HICKORY	3	N 7 E	19 W	
HICKORY	4	N 10 W	22 W	N 7 W 14
HICKORY	5	N 21 W	17 W	
HICKORY	6	N 17 W	21W	
HICKORY	7	N 18 W	20 W	
HICKORY	8	N 60 W	24 SW	
HICKORY	9	N 33 W	27 W	
HICKORY	10	N 37 W	21 W	
HICKORY	11	N 29 W	20 W	
HICKORY	12	N 25 W	20 W	
HICKORY	13a	N 10 W	26 W	

QUAD	STATION	FOLIATION		LINEATION	FOLD AXIS
HICKORY	13b	N 10 W	7 W		
HICKORY	14	N 15 W	78 W		
HICKORY	15	N 55 W	17 W		
HICKORY	16	N 55W	21 W		
HICKORY	17	N 56 W	17 W		
HICKORY	18	N 75 W	43 W		
HICKORY	19	N 65 W	17 W		
HICKORY	20	N 15 W	24 W		
HICKORY	21	N 55 W	21 W		
HICKORY	22	N 47 W	24 W		
HICKORY	23	N 35 W	27 W		
HICKORY	24	N 5 E	21 W	N 15 W	
HICKORY	25	N 35 W	24 W		
HICKORY	26	N 27 W	17 W		
HICKORY	27	N 25 W	21 W		
HICKORY	28	N 80 W	17 S		
HICKORY	29	N 42 W	7 W		
HICKORY	30	N 46 W	6 E		
HICKORY	31	N 45 W	17 W		
HICKORY	32	N 45 W	34 W		
HICKORY	33	N 45 W	42 W		
HICKORY	34	N 37 W	35 W		
HICKORY	35	N 3 E	7 W		
HICKORY	36	N 75 W	31 W		
HICKORY	37	N 70 W	17 W		
HICKORY	38	N 70 W	15 W		
HICKORY	39	N 70 W	15 S		
HICKORY	40	0	0		
HICKORY	41	N 65 E	35 E	N 80 W	17
HICKORY	41b	N 80 W	27 S		
HICKORY	42	N 72 W	34 S		
HICKORY	43	N 67 W	29 S		
HICKORY	44	N 47 W	36 W		
HICKORY	45	N 47 W	37 W		

QUAD	STATION	FOLIATION	LINEATION	FOLD AXIS
HICKORY	46	N 10 W	17 W	
HICKORY	47	N 5 W	23 W	
HICKORY	48	N 10 E	27 W	
HICKORY	49	N 10 E	17 W	
HICKORY	50	N 25 E	21 W	
HICKORY	51	N 21 E	30 W	
HICKORY	52	N 25 E	21 W	
HICKORY	53	N 20 E	21 W	
HICKORY	54	N 11 E	17 W	
HICKORY	55	N 11 W	41 W	N 17 W
HICKORY	56	N 14 W	21 W	13
HICKORY	57	N 6 W	17 W	
HICKORY	58	N 12 E	31 NW	
HICKORY	59	N 14 W	24 W	
HICKORY	60	N 21 W	31 W	
HICKORY	61	N 16 W	64 W	
HICKORY	62	N 35 W	19 SW	
HICKORY	63	N 37 W	61 W	
HICKORY	64	N 28 W	24 W	
HICKORY	65	N 32 W	37 W	
HICKORY	66	N 16 W	21 W	N 32 W
LONGVIEW	1			
LONGVIEW	2	N 55 W	42 W	
LONGVIEW	3	N 29 W	69 N	
LONGVIEW	4	N 80 W	81 N	
LONGVIEW	5	N 65 W	73 N	
LONGVIEW	6	N 24 W	56 W	
LONGVIEW	7	N 64 W	52 S	
LONGVIEW	8	N 75 W	6 S	
LONGVIEW	9	N 71 W	41 N	
LONGVIEW	10	N 80 W	59 N	
LONGVIEW	11	N 77 W	63 N	
LONGVIEW	12	N 60 W	12 S	
LONGVIEW	13	N 62 W	12 S	

QUAD	STATION	FOLIATION		LINEATION	FOLD AXIS
LONGVIEW	14	N 47 W	16 W		
LONGVIEW	15a	N 1 W	73 E		
LONGVIEW	15b	N 59 E	57 S		
LONGVIEW	16	N 80 W	90		
LONGVIEW	17	N 35 W	90		
LONGVIEW	18	N 10 W	65 E		
LONGVIEW	19	N 42 W	13 W		
LONGVIEW	20	N 19 E	12 E		
LONGVIEW	21a	N 32 W	39 N		
LONGVIEW	22a	N 12 W	7 W		
LONGVIEW	22b				S 7 E
LONGVIEW	22c	N1W	13 E		
LONGVIEW	23	N 90 E	90		
LONGVIEW	24	N 35 W	90		
LONGVIEW	25	N 90 E	84 S		
LONGVIEW	26	N 60 W	61 S	N 60 W	
LONGVIEW	27	N 32 W	14 N		
LONGVIEW	28	N 80 E	57 N		
LONGVIEW	29				
LONGVIEW	30	N 36 W	27 N		
LONGVIEW	31	N 32 W	4 N		
LONGVIEW	32	N 72 W	12 S		
LONGVIEW	33	N 31 W	36 S		
LONGVIEW	34	N 10 W	29 S		
LONGVIEW	35	N 14 W	37 W		
LONGVIEW	36	N 75 W	23 S		
LONGVIEW	37	N 27 E	14 N		
LONGVIEW	38	N 33 W	14 S		
LONGVIEW	39	N 72 W	47 N		
LONGVIEW	40a	N 53 E	18 N		
LONGVIEW	40b	N 62 W	31 S		
LONGVIEW	41	N 58 E	12 S		
LONGVIEW	42	N 37 W	63 W		
LONGVIEW	43	N 52 W	37 W		

QUAD	STATION	FOLIATION		LINEATION	FOLD AXIS	
LONGVIEW	44	N 47 W	46 W			
LONGVIEW	45	N 33 W	34 W			
LONGVIEW	46	N 57 W	24 S			
LONGVIEW	47	N 26 W	44 W			
LONGVIEW	48	N 22 E	67 W			
LONGVIEW	49	N 22 W	68 E			
LONGVIEW	50	N 36 W	72 W			
LONGVIEW	51	N 72 W	49 N			
LONGVIEW	52	N 57 E	87 N			
LONGVIEW	53	N 53 W	47 W			
LONGVIEW	54	N 42 W	36 W			
LONGVIEW	55	N 55 W	37 W			
LONGVIEW	56	N 57 W	82 W			
LONGVIEW	57	N 47 W	82 S			
LONGVIEW	58a	N 37 W	74 W			
LONGVIEW	58b				N 32 W	59
LONGVIEW	58c	N 40 W	87 S			
LONGVIEW	59	N 70 W	74 S			
LONGVIEW	60	N 20 W	27 W			
LONGVIEW	61	N 10 W	81 E			
LONGVIEW	62	N 65 W	51 N			
LONGVIEW	63	N 64 W	27 S			
LONGVIEW	64	N 82 W	52 S			
LONGVIEW	65	N 16 W	44 W			
LONGVIEW	66	N 10 W	66 E			
LONGVIEW	67	N 62 W	81 S			
LONGVIEW	68	N 69 W	17 S	N 80 W		
LONGVIEW	69	N 67 W	47 S			
LONGVIEW	70	N 82 W	33 S			
LONGVIEW	71	N 52 W	54 W			
LONGVIEW	72	N 54 W	57 S			
LONGVIEW	73	N 60 W	41 W			
LONGVIEW	74	N 6 W	67 E			
LONGVIEW	75	N 80 W	49 S			

QUAD	STATION	FOLIATION	LINEATION	FOLD AXIS
LONGVIEW	76	N 56 W	51 S	
LONGVIEW	77	N 52 W	64 S	
LONGVIEW	78	N 80 W	21 S	
LONGVIEW	79	N 80 W	27 S	
LONGVIEW	80	N 72 W	47 S	
LONGVIEW	81	N 47 W	54 W	
LONGVIEW	82	N 82 W	47 S	
LONGVIEW	83	N 40 W	37 W	
LONGVIEW	84a	N 64 E	21 S	
LONGVIEW	84b	N 80 E	37 N	
LONGVIEW	84c			N 55 E
LONGVIEW	84d	N 69 W	58 E	
LONGVIEW	84e	N 45 W	19 E	
LONGVIEW	85	N 80 W	37 N	
LONGVIEW	86	N 44 W	37 W	
LONGVIEW	87	N 10 E	19 E	
LONGVIEW	88	N 21 W	16 E	
LONGVIEW	89	N 16 W	10 E	
LONGVIEW	90	N 21 W	22 W	
LONGVIEW	91	N 16 W	23 N	N 15 W 7
LONGVIEW	92	N 47 W	37 W	
LONGVIEW	93	N 27 W	37 W	
LONGVIEW	94a	N 35 W	50 SW	
LONGVIEW	94b	N 10 E	17 NW	
LONGVIEW	94c	N 21 E	47 SE	
LONGVIEW	95	N 35 W	22 SW	
LONGVIEW	96	N 47 W	27 SW	
LONGVIEW	97	N 3 W	54 W	
LONGVIEW	98	N 47 W	36 SW	
LONGVIEW	99	N 10 E	71 NW	
LONGVIEW	100	N 6 E	59 NW	
LONGVIEW	101	N 80 W	60 N	
LONGVIEW	102	N 80 W	37 S	
LONGVIEW	103	N 71 W	17 S	

QUAD	STATION	FOLIATION		LINEATION	FOLD AXIS
LONGVIEW	104	N 7 E	17 SW		
LONGVIEW	105	N 10 W	17 NE		
LONGVIEW	106	N 22 W	89 SW		
LONGVIEW	107	N 37 W	59 SW		
LONGVIEW	108	N 57 W	36 SW		
LONGVIEW	109	N 6 W	14 W		
LONGVIEW	110	N 35 E	54 NE	N 21 W	9
LONGVIEW	111	N 37 E	28 N		
LONGVIEW	112	N 50 W	27 SW		
LONGVIEW	113	N 52 W	57 SW		
LONGVIEW	114	N 5 W	17 SW		
LONGVIEW	115	N 7 W	20 SW		
LONGVIEW	116	N 15 W	21 SW		
LONGVIEW	117	N 17 W	23 SW		
LONGVIEW	118	N 21 W	27 SW		
LONGVIEW	119	N 23 W	25 SW		
LONGVIEW	120	N 25 W	19 SW		
LONGVIEW	121	N 50 W	13 NE		
LONGVIEW	122	N 41 W	7 SW		
LONGVIEW	123	N 30 E	16 NW		
LONGVIEW	124	N 29 E	20 NW		
LONGVIEW	125	N 25 E	20 NW		
LONGVIEW	126	N 6 W	31 SW		
LONGVIEW	127	N 45 W	27 NE		
LONGVIEW	128	N 45 W	27 NE		
LONGVIEW	129	N 10 E	55 SW		
LONGVIEW	130	N 10 E	47 W		
LONGVIEW	131	N 21 E	47 W		
LONGVIEW	132	N 11 E	47 W		
LONGVIEW	133	N 10 W	31 SW		
LONGVIEW	134	N 17 W	21 SW		
LONGVIEW	135	N 37 W	27 SW		
LONGVIEW	136	N 61 W	57 SW		
LONGVIEW	137	N 80 W	40 SW		

QUAD	STATION	FOLIATION	LINEATION	FOLD AXIS
LONGVIEW	138	N 57 W	43 SW	
LONGVIEW	139	N 60 W	43 SW	
LONGVIEW	140	N 47 W	40 SW	
LONGVIEW	141	N 35 W	41 SW	
LONGVIEW	142	N 35 W	41 SW	
LONGVIEW	143	N 35 W	37 SW	
LONGVIEW	144	N 27 W	37 SW	
LONGVIEW	145	N 30 W	31 SW	
LONGVIEW	146	N 31 E	23 SE	
LONGVIEW	147	N 31 W	17 SW	
LONGVIEW	148	N 50 W	41 SW	
LONGVIEW	149	N 5 W	13 W	
LONGVIEW	150	N 23 W	47 W	
LONGVIEW	151	N 50 W	31 W	
LONGVIEW	152	N 10 W	41 W	
LONGVIEW	153	N 50 W	67 SW	
LONGVIEW	154	N 40 W	67 SW	
LONGVIEW	155	N 21 W	37 SW	
LONGVIEW	156	N 35 W	46 SW	
LONGVIEW	157	N 70 W	50 SW	
LONGVIEW	158	N 60 W	45 SW	
LONGVIEW	159	N 58 W	24 SW	
LONGVIEW	160	N 5 W	61 E	
LONGVIEW	161	N 26 W	40 SW	
LONGVIEW	162	N 31 W	34 SW	
LONGVIEW	163	N 35 W	24 SW	
LONGVIEW	164	N 10 W	7 E	
LONGVIEW	165a	N 15 W	87 E	N 45 W
LONGVIEW	165b	N 25 W	21 W	
LONGVIEW	166	N 17 E	25 SW	
LONGVIEW	167	N 80 E	15 S	
LONGVIEW	168	N 60 E	24 SW	
LONGVIEW	169			S 35 W 5
LONGVIEW	170			N 80 E 15

QUAD	STATION	FOLIATION		LINEATION		FOLD AXIS	
LONGVIEW	171	N 81 W	7 N				
LONGVIEW	172	N 55 E	24 NW				
LONGVIEW	173	N 61 E	4 SE				
LONGVIEW	174	N 80 E	21 NW				
LONGVIEW	175	N 75 W	51 S				
LONGVIEW	176	N 27 W	51 S				
LONGVIEW	177					S 54 E	21
LONGVIEW	178					S 15 W	15
LONGVIEW	179			S 28 E	34		
LONGVIEW	180	N 60 W	46 SW				
LONGVIEW	181	N 80 E	61 S				
LONGVIEW	182						
LONGVIEW	183	N 10 W	34 SW	N 16 W	22		
LONGVIEW	184					N 45 W	37
LONGVIEW	185	N 21 W	17 SW				
LONGVIEW	186	N 21 E	17 NW				
LONGVIEW	187					N 7 W	13
LONGVIEW	188					S 40 W	12
LONGVIEW	189	N 10 E	19 SW				
LONGVIEW	190						
LONGVIEW	191					S 10 E	29
LONGVIEW	192	N 37 W	47 SW				
LONGVIEW	193	N 44 W	37 SW				
LONGVIEW	194	N 20 W	29 NE				
LONGVIEW	195	N 37 W	29 NE				
LONGVIEW	196	N 40 E	35 SE				
LONGVIEW	197a	N 47 W	21 SW				
LONGVIEW	197b	N 5 E	34 SW				
LONGVIEW	198	N 70 W	61 SW				
LONGVIEW	199	N 64 W	27 SW				
LONGVIEW	200	N 47 W	41 SW				
LONGVIEW	201	N 54 W	27 SW				
LONGVIEW	202	N 50 W	14 NE				
LONGVIEW	203	N 4 E	42				

QUAD	STATION	FOLIATION		LINEATION		FOLD AXIS	
LONGVIEW	204	N 6 E	39				
LONGVIEW	205	N 60 W	26 SW	N 25 W	6		
LONGVIEW	206	N 62 W	21 SW				
LONGVIEW	207	N 60 W	21 SW				
LONGVIEW	208	N 21 E	16 SW				
LONGVIEW	209	N 44 W	14 SW				
LONGVIEW	210	N 80 W	16 SW	S 80 W	16		
LONGVIEW	211	N 80 W	4 SW				
LONGVIEW	212	N 65 E	45 NW				
LONGVIEW	213	N 75 E	30 N				
LONGVIEW	214	N 10 W	17 NE				
LONGVIEW	215	N 80 W	23 N	N 10 W	10		
LONGVIEW	216					S 30 W	6
LONGVIEW	217	N 80 W	61 N				
LONGVIEW	218	N 41 W	27 SW				
LONGVIEW	219	N 29 W	27 SW				
LONGVIEW	220	N 80 W	21 N				
LONGVIEW	221	N 80 W	41 S				
LONGVIEW	222					S 30 E	10
LONGVIEW	223	N 45 W	21 SW				
LONGVIEW	224	N 55 W	51 NE				
LONGVIEW	225	N 36 W	44 NE				
LONGVIEW	226	N 47 W	17 NE				
LONGVIEW	227	N 80 W	55 N				
LONGVIEW	228					N 70 W	4
LONGVIEW	229	N 30 W	37 NE				
LONGVIEW	230	N 19 W	35 NE				
LONGVIEW	231	N 15 W	17 NE				
LONGVIEW	232	N 21 W	25 NW				
LONGVIEW	233					S 17 E	33
LONGVIEW	234	N 17 E	19 NW				
LONGVIEW	235	N 17 E	21 SE				
LONGVIEW	236	N 5 E	55 W				
LONGVIEW	237	N 25 W	61 NW				

QUAD	STATION	FOLIATION		LINEATION	FOLD AXIS	
LONGVIEW	238	N 65 E	20 NW			
LONGVIEW	239	N 80 W	7 N			
LONGVIEW	240	N 55 E	49 S			
LONGVIEW	241	N 85 W	10 W			
LONGVIEW	242	N 80 W	17 S			
LONGVIEW	243	N 65 W	31 SW			
LONGVIEW	244	N 20 W	17 SW			
LONGVIEW	245	N 42 W	33 NE			
LONGVIEW	246	N 80 W	21 N			
LONGVIEW	247	N 70 E	21 N			
LONGVIEW	248	N 65 E	38 NW		N 35 W	38
LONGVIEW	249	N 32 E	41 NW			
LONGVIEW	250	N 21 W	71 SW			
LONGVIEW	251	N 80 W	17 N			
LONGVIEW	252	N 43 W	17 S			
LONGVIEW	253	N 21 E	24 SE			
LONGVIEW	254	N 10 E	17 N			
LONGVIEW	255	N 47 W	17 W			
LONGVIEW	256	N 17 W	27 W		N 25 W	8
LONGVIEW	257	N 45 E	19 N			
LONGVIEW	258	N 61 E	14 SE			
LONGVIEW	259	N 35 E	21 S			
LONGVIEW	260	N 17 W	21 W			
LONGVIEW	261	N 18 W	34 SW			
LONGVIEW	262	N 47 W	27 S			
LONGVIEW	263	N 51 E	17 S			
LONGVIEW	264	N 75 E	21 N			
LONGVIEW	265	N 80 E	11 S			
LONGVIEW	266	N 71 E	15 S			
LONGVIEW	267	N 10 W	17 SW			
LONGVIEW	268	N 56 E	61 S			
LONGVIEW	269	N 30 W	21 NE			
LONGVIEW	270	N 10 W	36 NE			
LONGVIEW	271	N 10 W	61 SW			

QUAD	STATION	FOLIATION		LINEATION	FOLD AXIS	
LONGVIEW	272	N 10 W	41 SW			
LONGVIEW	273	N 37 W	61 SW			
LONGVIEW	274	N 31 E	27 N			
LONGVIEW	275	N 50 E	17 N			
LONGVIEW	276	N 48 E	33 N			
LONGVIEW	277	N 75 W	19 S			
LONGVIEW	278	N 80 E	61 N			
LONGVIEW	279	N 66 W	27 S			
LONGVIEW	280	N 71 E	37 N			
LONGVIEW	281	N 47 W	21 W		N 74 W	16
LONGVIEW	282				S 61 W	
LONGVIEW	283	N 61 E	38 SE			
LONGVIEW	284	N 31 E	47 SE			
LONGVIEW	285	N 41 E	22 N			
LONGVIEW	286	N 35 W	61 SW			
LONGVIEW	287	N 44 W	27 W			
LONGVIEW	288	N 21 W	43 E			
LONGVIEW	289	N 10 W	43 E			
LONGVIEW	290	N 80 W	16 N			
LONGVIEW	291				N 31 W	0
LONGVIEW	292	N 45 W	16 SW			
LONGVIEW	293	N 37 W	40 SW			
LONGVIEW	294	N 61 W	37 SW			
LONGVIEW	295				N 35 W	19
LONGVIEW	296	N 35 E	21 S			
LONGVIEW	297	N 10 E	21 SW			
LONGVIEW	298	N 35 W	61 SW			
LONGVIEW	299	N 35 W	61 W			
LONGVIEW	300	N 21 W	31 SW			
LONGVIEW	301	N 10 W	21 SW			
LONGVIEW	302	N 40 W	17 SW			
LONGVIEW	303	N 39 W	41 SW			
LONGVIEW	304	N 35 W	21 SW			
LONGVIEW	305	N 10 W	61 SW			

QUAD	STATION	FOLIATION		LINEATION		FOLD AXIS	
LONGVIEW	306	N 40 W	61 SW				
LONGVIEW	307	N 36 W	39 SW				
LONGVIEW	308	N 23 W	31 SW				
LONGVIEW	309	N 27 W	64 SW				
LONGVIEW	310	N 14 W	53 SW				
LONGVIEW	311	N 17 W	35 SW				
LONGVIEW	312	N 7 W	55 SW				
LONGVIEW	313	N 12 W	41 SW				
LONGVIEW	314	N 60 W	42 SW	S 32 W	42		
LONGVIEW	315	N 21 W	37 SW				
LONGVIEW	316	N 37 W	21 SW				
LONGVIEW	317					S 10 E	15
LONGVIEW	318	N 80 W	21 SW				
LONGVIEW	319	N 65 E	27 E	N 41 E			
LONGVIEW	320	N 65 E	21 SE				
LONGVIEW	321					S 55 E	10
LONGVIEW	322	N 20 W	37 NE				
LONGVIEW	323	N 44 W	31 SW				
LONGVIEW	324	N 21 W	31 SW				
LONGVIEW	325	N 37 E	21 SE				
LONGVIEW	326	N 20 W	61 SW				
LONGVIEW	327	N 17 W	27 SW				
LONGVIEW	328	N 22 W	61 SW				
LONGVIEW	329	N 31 W	34 SW				
LONGVIEW	330	N 17 W	21 SW				
LONGVIEW	331	N 37 W	14 SW				
LONGVIEW	332	N 22 W	27 SW				
LONGVIEW	333	N 15 W	27 SW				
LONGVIEW	334	N 10 W	21 SW				
LONGVIEW	335	N 10 E	17 SE				
LONGVIEW	336	N 23 W	44 SW				
LONGVIEW	337	N 11 W	61 SW				
LONGVIEW	338	N 3 E	21 W				
LONGVIEW	339	N 7 W	5 W				

QUAD	STATION	FOLIATION		LINEATION	FOLD AXIS	
LONGVIEW	340	N 77 W	21 SW			
LONGVIEW	341	N 14 W	23 W			
LONGVIEW	342	N 80 E	43 N			
LONGVIEW	343	N 21 E	17 S			
LONGVIEW	344	N 37 W	23 S			
LONGVIEW	345					
LONGVIEW	346	N 17 W	32 SE			
LONGVIEW	347	N 17 W	22 SE			
LONGVIEW	348	N 7 E	27 NW			
LONGVIEW	349	N 37 E	27 NW			
LONGVIEW	350	N 43 W	37 NE			
LONGVIEW	351	N 21 W	46 NE			
LONGVIEW	352	N 3 W	31 W			
LONGVIEW	353	N 21 W	17 SW			
LONGVIEW	354	N 31 W	18 SW			
LONGVIEW	355	N 14 W	23 SW			
LONGVIEW	356	N 26 W	37 SW			
LONGVIEW	357	N 32 W	41 SW			
LONGVIEW	358	N 17 W	52 SW			
LONGVIEW	358b	N 55 E	21 N			
LONGVIEW	359	N 60 W	25 NE			
LONGVIEW	360				N 65 W	10
LONGVIEW	361	N 64 W	32 SW			
LONGVIEW	362	N 70 E	16 N			
LONGVIEW	363	N 55 W	15 NE			
LONGVIEW	364	N 31 E	21 SE			
LONGVIEW	365				S 30 W	
LONGVIEW	366	N 61 W	21 SW			
LONGVIEW	367				S 30 W	
LONGVIEW	368	N 20 E	14 SE			
LONGVIEW	369					
LONGVIEW	370					
LONGVIEW	371					
LONGVIEW	372	N 80 W	24 SW			

QUAD	STATION	FOLIATION	LINEATION	FOLD AXIS
LONGVIEW	373	N 74 W	26 SW	
LONGVIEW	374	N 76 W	21 S	
LONGVIEW	375	N 75 W	31 S	
LONGVIEW	376	N 67 W	35 SW	
LONGVIEW	377	N 51 W	23 SW	
LONGVIEW	378	N 61 W	23 SW	
LONGVIEW	379	N 47 W	23 SW	
LONGVIEW	380	N 25 W	16 SW	
LONGVIEW	381	N 41 W	16 SW	
LONGVIEW	382	N 17 W	21 SW	
LONGVIEW	383	N 21 W	35 SW	
LONGVIEW	384	N 17 W	22 SW	
LONGVIEW	385	N 23 E	16 SE	
LONGVIEW	386	N 24 W	37 SW	
LONGVIEW	387	N 21 W	37 SW	
LONGVIEW	388	N 21 W	16 SW	
LONGVIEW	389	N 64 W	43 SW	
LONGVIEW	390	N 42 W	16 SW	
LONGVIEW	391	N 16 W	32 SW	
LONGVIEW	392		N 41 W	
LONGVIEW	393		N 43 W	3
LONGVIEW	394	N 79 W	31 SW	
LONGVIEW	395	N 51 W	36 SW	
LONGVIEW	396	N 26 W	21 SW	
LONGVIEW	397	N 80 W	42 SW	
LONGVIEW	398	N 32 W	19 SW	
LONGVIEW	399	N 21 W	34 SW	
LONGVIEW	400	N 44 W	31 SW	
LONGVIEW	401	N 16 W	44 SW	
LONGVIEW	402	N 14 E	17 SE	
LONGVIEW	403	N 21 E	24 SW	
LONGVIEW	404	N 44 W	17 SW	
LONGVIEW	405	N 34 W	34 SW	
LONGVIEW	406	N 23 W	41 SW	

QUAD	STATION	FOLIATION	LINEATION	FOLD AXIS
LONGVIEW	407	N 3 W	14 W	
LONGVIEW	408	N 21 W	62 W	
LONGVIEW	409	N 13 W	19 W	
LONGVIEW	410	N 13 W	33 W	
LONGVIEW	411	N 31 W	37 W	
LONGVIEW	412	N 22 W	31 W	
LONGVIEW	413	N 31 W	23 W	
LONGVIEW	414	N 24 E	17 SE	
LONGVIEW	415	N 37 W	21 W	
LONGVIEW	416	N 42 W	19 W	
LONGVIEW	417	N 80 E	21 S	
LONGVIEW	418	N 47 W	33 W	
LONGVIEW	419	N 37 W	14 W	
LONGVIEW	420	N 66 W	44 W	
LONGVIEW	421	N 17 W	19 W	
LONGVIEW	422	N 63 W	33 W	
LONGVIEW	423	N 41 W	22 W	
LONGVIEW	424	N 21 W	41 SW	
LONGVIEW	425	N 18 W	19 SW	
LONGVIEW	426	N 31 W	17 SW	
LONGVIEW	427	N 10 W	21 W	
LONGVIEW	428	N 31 W	73 SW	
LONGVIEW	429	N 37 W	14 W	
LONGVIEW	430	N 37 W	71 SW	
LONGVIEW	431	N 41 W	22 SW	
LONGVIEW	432	N 38 W	32 NE	
LONGVIEW	433	N 64 W	53 SW	

VITA

William Gilliam was born March 21st, 1981 in Winchester, Kentucky. He developed an interest in geology while visiting his grandfather in the coalfields of eastern Kentucky. Unbeknownst to him this interest would manifest in later years while attending introductory geology at Morehead State University. While at MSU he developed a passion for mapping, structural geology, and tectonics. He followed this passion to the University of Tennessee and embarked on a mapping based, structural geology related thesis. Aside from geology he likes to spend time on his mountain bike or dirt bike in the woods with his wife Lyndci. William is forever grateful to his mentors who nurtured his passion for geology through the years, and his grandfather for carrying his rocks

